

Doctoral Dissertation

**Realistic modelling of complex systems of
biological agents: epidemiology of HIV on
complex sexual networks and collective
motion of hierarchical herds**

Bence Ferdinandy

Doctoral School of Physics

head of school: Prof. Dr. Tamás Tél

Statistical physics, biological physics and physics of quantum systems program

head of program: Prof. Dr. Jenő Kúrti



Supervisor:

Tamás Vicsek

Professor of Physics

Department of Biological Physics

Faculty of Science

EÖTVÖS LORÁND UNIVERSITY

2017

With regard to the difficulty which we have described in connection with definitions and numbers, what is the cause of the unification? **In all things which have a plurality of parts, and which are not a total aggregate but a whole of some sort distinct from the parts, there is some cause;** inasmuch as even in bodies sometimes contact is the cause of their unity, and sometimes viscosity or some other such quality. But a definition is one account, not by connection, like the Iliad, but because it is a definition of one thing.

Aristotle, *Metaphysics*, VIII, 1045a

The whole is more, than the sum of its parts.

Popular paraphrasing of the above.

Contents

Preface	vi
1 Introduction	1
2 Methodology	3
2.1 Complex systems	3
2.2 Modelling of complex systems	6
2.2.1 Agent-based modelling	7
3 Study 1: Epidemiology of HIV on complex sexual networks	10
3.1 Background literature	11
3.1.1 Complex networks	11
3.1.2 Epidemiology	18
3.1.3 Introduction to HIV and AIDS	21
3.1.4 Motivation	24
3.2 Our model	24
3.2.1 Basic model	24
3.2.2 Mechanisms of interference	27
3.3 Results	31
3.3.1 Network properties with single strain infection	31
3.3.2 Default scenario	34
3.3.3 Inhibition of superinfection dominates first comer advantage	36
3.3.4 Short head start or fast population turnover reduce first comer advantage	40
3.3.5 Case study: The expansion of HIV-1 subtype A in Uganda . .	41
3.4 Discussion	43
3.5 Summary	50

4 Study 2: Collective motion of hierarchical herds	51
4.1 Background literature	52
4.1.1 Collective motion	52
4.1.2 The language of collective motion	52
4.1.3 Evidence	53
4.1.4 Simple two dimensional model of collective motion	54
4.1.5 Collective motion of tissue cells	56
4.1.6 Coordinated stopping	58
4.1.7 Connection to network and control theory	60
4.1.8 Leadership	61
4.1.9 Motivation	62
4.2 Our model	64
4.2.1 Formal model description	65
4.2.2 Parameters	70
4.3 Results	71
4.3.1 Cohesiveness of the herd	71
4.3.2 Group size distribution	75
4.3.3 Dimension scales	78
4.4 Discussion	79
4.5 Summary	82
5 Conclusion	84
Publications	86
Bibliography	87

List of Figures

3.1	Rewiring in the Watts-Strogatz network model.	14
3.2	Small world properties of the Watts-Strogatz model.	15
3.3	The global prevalence of HIV	23
3.4	New infections and deaths by HIV	23
3.5	Worldwide prevalence of HIV-1 group M subtypes and CRF	25
3.6	Contact degree distribution of males	31
3.7	Contact degree distribution of females	32
3.8	Effects of infection on population.	33
3.9	Prevalence of resident and invader strain in various scenarios.	35
3.10	Comparison of competition scenarios	37
3.11	The contribution of superinfection events and acute-stage transmissions to the spread of the invader strain.	39
3.12	The effect of multiple acute infections on the competition of HIV strains	40
3.13	First comer advantage in growth phase.	42
3.14	The effect of population turnover	43
4.1	SVM trajectories	55
4.2	Collective motion of cells	57
4.3	Landing forces overview	59
4.4	Landing results	59
4.5	Model overview	66
4.6	Snapshot of the force \mathbf{F}_{com}	69
4.7	Ordering of the model	73
4.8	Switching from translational to rotational ordered movement.	74
4.9	Rotation and translation with CoM boundary	74
4.10	”Fights” among leaders	75

4.11	Pair-correlation of the herd	76
4.12	Group stability	77
4.13	Group size distribution of the model and the real herd	78

List of Tables

3.1	Properties of several real world graphs.	13
3.2	Parameters used for the simulation of the HIV infection model.	30
4.1	Collective motion model parameters	72
4.2	Order parameters of the collective motion model.	76

Preface

I am rather unsure when and where I decided I would pursue a doctorate in physics, and even less so, when and where I decided to pursue anything at all in physics. Most of my relatives that I personally know are medical doctors, so although in the end I evaded the nudge to continue the family tradition and took up physics (I kind of struck a deal at home to take an extra maturity exam in biology, to keep all avenues open), my choosing of the Eötvös Loránd University was highly motivated by its biophysics specialization and its many possibilities for interdisciplinary studies. So much so that I took up biology for some time, which turned out to be interesting, but the courses and I did not have the same thing in mind, so we parted ways.

Early on I decided to delve into research – undoubtedly the influence of my father, scientist and businessman –, which was when I stumbled upon the works of Tamás Vicsek, professor at the Department of Biological Physics. Professor Vicsek agreed to be my supervisor for a student project, marking the starting point of the long and arduous process of him teaching me the ways of a scientist, culminating almost nine years later in this dissertation. It was he who showed me, that our everyday environment, visible without sophisticated machinery, still holds plenty of excitement for a physicist and that trying to tackle biological problems with the armament of a physicist is more than fascinating. And thus was born the broader topic of my PhD.

Out of all the things I have had a chance to dabble in Professor Vicsek's group, the collective motion of animals was what caught my attention the most, as half of this dissertation attests to. In the last two years, I've been an assistant research fellow in another great group at the Eötvös Loránd University, working with Professor Ádám Miklósi at the Department of Ethology on the observation of actual animals and not just the theoretical modelling of them. I hope that in the near future I may be able to combine these two efforts, and put some more hard data behind my models.

I wish to mention some people, without whom this dissertation could never have

been finished. First of all, of course Tamás Vicsek, for guiding me all these years, even though I didn't always listen. I thank the co-authors of the papers comprising the bulk of the present work, Katalin Ozogány, Enys Mones and Viktor Müller, and the people at the Department of Biological Physics for helping me out in various ways. A heartfelt thank you goes to Ádám Miklósi and the Department of Ethology for providing an opportunity to keep working on my PhD these last two years. Also to the friends and fellow PhD students who were a tremendous help in finishing and polishing. And of course the biggest thank you goes to my family, who had my back all these years.

1

Introduction

The most successful stories of science in the 20th century were all reductionist in essence, both in physics and in biology. The discovery of the atom, then the nuclei, the particles of the Standard Model or the advent of the genetic code and molecular biology were all trying to take apart systems into smaller and smaller parts. But at the end of the century, a new, more holistic science started to gain popularity: that of complex systems. An underlying assumption of complexity sciences is that complexity has universal rules independent of the actual system, and thus one does not study the constituents of the complex system, rather, the emergent phenomena that exist only at the level of the system. Of course, even if one subscribes to Kuhn's view of the scientific progress, predecessors of the science of complexity can be found in statistical physics, systems theory and some other disciplines. As it is with many fields of science, the rise of computing power facilitated the paradigm change. As we will see later, complexity science is *hard*, since the eponymous systems are, well, complex, with many constituent parts and many interactions between them which very quickly make pen-and-paper approaches severely limited. Complexity science

is more a collection of methods to tackle such problems rather than the study of specific systems. Its principles of looking for system-wide properties that emerge from the interactions of the constituents make it applicable in many fields, with this inherent interdisciplinarity making it rather successful, and also very popular. Popularity also has its drawbacks, however. Compared to, say, quantum mechanics and special relativity, the jargon of complexity science is quite accessible, leading to debates about the scientific status of research running under the name of complexity science in areas not traditionally close to hard science.

When writing this dissertation, I had two goals in mind. First and obviously, I had to show how I have contributed to science while I was in doctoral school and secondly, that mayhap it will be of some use for a student wishing for orientation in the subjects of complex systems and agent-based modelling. In Chapter 2 I will present an overview of complex systems in general and try to show why they are interesting. Then I will cover aspects of the modelling of complex systems with the focus on the agent-based modelling method, with both practical and philosophical issues in mind. In Chapters 3 and 4 two papers will be covered in which agent-based modelling is employed, and are my aforementioned contributions and requirements for the doctoral degree. In both cases, I will try to emphasise the rationale behind choices in the agent-based methodology to further my second goal. Since the two fields (epidemiology of HIV on sexual networks and collective motion of hierarchical herds) are quite far apart, both chapters will cover the necessary background to appreciate the choices in modelling the systems. Common characteristic of both systems are that they are rather specific and the models try to closely follow this, passing some "reality tests" and that they both have distinct types of agents, which of course, complicate matters. I hope that these two examples will be able to demonstrate how general the methods of complex system modelling are, being able to address very different question in very different systems.

2

Methodology

2.1 Complex systems

The definition of what a complex system and complexity science exactly are is not very straightforward, as there are several definitions circulating in the literature [1]. A common idea to mention about complex systems is the paraphrased quotation from Aristotle's *Metaphysics*: "The whole is more, than the sum of its parts." Although the out-of-context quotation's implications are slightly misleading (see the epigraph), it does capture a general picture: a complex system cannot be understood via study of its components; it has to be studied as a whole, with the interactions of the components playing an important role in creating something entirely new. Along these lines some authors emphasize self-organisation and emergent behaviour as the hallmarks of complexity [2].

Péter Érdi offers a more detailed definition by contrasting a complex system with a simple system [3]. He defines simple systems as having (some or all) of the following properties:

- single cause and single effect,
- small change in cause implies small change in effect,
- predictability,

and, in a contrast, complex systems as having (some or all) these:

- circular causality, feedback loops, logical paradoxes (self-referential paradoxes) and strange loops (self-similarity),
- small change in cause implies dramatic change in effect,
- emergence and unpredictability.

Another important aspect of complexity, is that complex systems are very often - although far from always - hierarchical. The physical internet is made up of individual computers and routers on one level, but autonomous systems (this is a technical term, they are officially numbered) act on another level; a large herd may consist of smaller groups; a human body is made of organs, which in turn are made of cells; a university is made up of faculties, which are made up of departments, etc. In a complex system it might not be trivial to determine the relevant constituents as all tiers of the hierarchy may be equally important.

As we can see, Érdi's definition is ambiguous and has some elements of chaos theory in it. The ambiguity of the definition of complexity is not helped by the fact, that there are some concepts of complexity that are incongruent with the above idea. For example, computational complexity deals with how difficult a computational problem is for a computer to solve it, in terms of required resources. The Kolmogorov complexity (or as also called, algorithmic information content) is the measure of complexity of strings, defined by the length of the shortest algorithm that outputs the given string. Following this definition one would find the random string to be the most complex entity, which is clearly not what we had in mind [4].

The student of complexity may also be hampered when trying to find his or her way around in complexity science by "complexity" sometimes being used metaphorically in the social sciences, with jargon referenced, but, from a natural sciences perspective, in a questionably scientific manner [5], [6]. Actually, there is special issue of an otherwise business oriented journal [7], which is rather reminiscent of the attempted peace-treaty of the "Science Wars", the book "One Culture?" [8].

Before moving on, it is worth noting that the complex/(non-complex) simple dichotomy is not the same as the complicated/(not-complicated) simple dichotomy.

Indeed, a (non-complex) simple system could be complicated and a complex system could be not-complicated. For example, a mechanical watch is quite complicated, but its very essence is to be predictable. On the other hand, non-complicated interaction rules between very non-complicated constituents can lead to non-trivial emergent behaviour as is the case with the simple collective motion of self-propelled particles (see Section 4.1).

When one starts to list examples of complex systems most will come from biology or from some specific part of human life. Wikipedia, for one, lists the following examples: "*Examples of complex systems are Earth's global climate, organisms, the human brain, social and economic organizations (like cities), an ecosystem, a living cell, and ultimately the entire universe.*", another online search hit gives four examples from society (markets, organisations, language, internet), six from biology (cells, organs, immune system, organisms, populations, ecosystems), and only four from physics (turbulence, weather, percolation, sandpile). No wonder, that many physicists turn to the study of systems derived from biology, or society. Of course, perhaps greater public interest and the feeling of a need to better understand ourselves and our immediate environment is also a drive (I would argue that a modern human's most immediate environment is definitely other modern humans).

But why are there so many complex systems out there? One of the things that make complex systems so interesting from a scientific point of view, is that it seems that self-organization into complex systems is something like a law of nature, that occurs everywhere, and that these complex systems seem to follow very similar laws in their behaviour despite sometimes having very different constituents. Although no definite answer can be given, we do have some hints. The biosphere is one of the largest and most complex complex system that we know about. The state-of-the-art scientific consensus is that from the start of life on Earth, the process of biological evolution has pushed this system to increasingly greater complexity, starting from single-celled life forms to the present variety of multi-celled complex life forms, of which at least one (humanity), is capable of creating even more complexity as a result of its technological and social evolution (let us not dwell on the question of how exactly unique is *Homo sapiens* in the animal kingdom in this regard). A very recent article [9] provides some theoretical background on how evolution could be thermodynamically driven. In short, the authors show that a many-particle system under a dissipative external drive (as the biosphere is driven by the radiation of the Sun) evolves along the trajectory in its phase space that maximises dissipation (and thus

absorption) of energy. If the system consists of self-replicators (the energy absorption is tied into a positive feedback loop), this will lead to the proliferation of the most adapted self-replicator, in a manner strikingly similar to that outlined in Darwinian theory of evolution.

The methods of modelling (and simulating) complex systems have a lot in common, even when the systems in question markedly differ. In the following section, I will overview some general features of complex system modelling and in the later chapters investigate how they can be applied to two different research questions about two different systems: a network of human sexual contacts and a hierarchical system of self-propelled particles. Both consist of many agents of different types in non-trivial interactions that change over time, leading to complex dynamics.

2.2 Modelling of complex systems

The advent of the computer age has given a tremendous boost to the modelling of complex systems. A model of a complex system - typically differential equations in the pen-and-paper era - generally does not have an analytical solution, unless significant approximations (e.g mean field) are made. Although having an analytical solution to a problem makes one feel easier about our understanding the topic, computer simulation of models has become an invaluable tool, since given enough computing power, we can now simulate arbitrary complex systems using a computer.

Obviously, the "law of conservation of difficulty" - a frequently-heard phrase during my undergraduate studies, that turned out to be true more times than I would have wished for - holds here as well. A complete analytical solution will cover the entire parameter space of the problem with a precision that is limited only by the theory and the precision of input parameters. Although checking the validity of an analytical model is also plagued by philosophical issues, using numerical simulations to acquire solutions of models introduces even more problems [10]. Numerical solutions are prone to errors from discretization, numerical instabilities and possible errors introduced by pseudo-random number generators. Benchmarking against partial analytical solutions may yield some piece of mind, but, in general, there is no sure way to guarantee veracity. Also, during simulation of our model we are forced into a subset of the parameter space, as limited by the available computational power, making complete exploration of a model technically impossible.

In fact, the topic of the epistemological issues related to science's quest for truth

is rather bleak and, if read about too much, can cause a young researcher to despair. Yet, as the colloquial saying goes: it works [...]. Nevertheless, the fact that the basis of hard sciences do work is quite surprising and not at all self-evident: the ability to formulate mathematical models of phenomena that can then be used to predict new phenomena is both baffling, and one of our greatest blessings as scientists (I would refer the reader to Wigner's famous lecture on this "unreasonable effectiveness" [11]).

Aside from essentially creating models to be simulated in computers, another common property of complex systems models is that they are stochastic in nature. This is not only convenient (since quite often unknown or complicated processes are lumped into some noise acting on the system), but this has a profound connection to statistical physics, where temperature (thermal noise) is the most important parameter of any system.

In the following section I will overview agent-based modelling, a type of modelling paradigm often used in complex system modelling, and will touch upon how some of the aforementioned modelling issues are mitigated.

2.2.1 Agent-based modelling

In general, there are two ways one can go about modelling a complex system, the more traditional dynamical approach or the somewhat newer agent-based approach. The first approach considers the system evolving along some trajectory in its phase space. One constructs differential equations describing this evolution (typically a master equation), which is then numerically integrated. An obvious perk of such an approach is that although analytical solutions are not possible, one can explore the system with approximate analytical solutions, aiding greatly the understanding and bench-marking of the numerical solutions. A caveat is that microscopic information is not available, since one does not track all individual elements of the system during simulation.

Contrasting the dynamical approach is agent-based modelling. In this paradigm each constituent element of the system and each interaction between these elements is simulated individually. This approach has two main advantages: first, microscopic information is tracked during the entire simulation, and second, when the system to be modelled presents clear candidates for agents and their interaction, it is very straightforward to conceptualize the model. Biological and social systems clearly benefit from the latter: it is very easy to see a cell, an animal or an or-

ganisation as an agent. Another, more technical advantage, is that an agent-based model very easily translates to object-oriented computer code, which is quite popular nowadays, and many popular programming languages are tailored to it. The drawback of the agent-based approach, compared to the dynamical approach, is that even approximate analytical solutions are generally not possible to calculate and the concept of agents and their interactions is somewhat prone to the inflation of model parameters, both of which can hinder meaningful understanding of the system through the simulation results.

In a typical setting, we have data about global phenomena in the system we wish to model and candidate entities - whose properties we also have some information about - which we can use as agents. In creating the model, we basically model the entity chosen as an agent, which may or may not have several internal parameters and processes, and we model interaction between agents. Following this, we simulate our model *in silico* and check whether it is able to reproduce the global phenomena, about which we had data.

At this point, we should again consider relevant epistemological questions. What do we learn, when our model does not reproduce the global phenomena, and what do we learn when it does? In the former case, we learn that our model, with the given parameters, is not a good representation of reality, but from a purely theoretical viewpoint, this is not much, given that there are infinite number of models to test. In the latter case, we learn that our current model, with the current parameters, produces behaviour similar to the given system we are using as a reference, but purely theoretically, this does not imply anything about our model's details corresponding to reality's details. So, this all begs the question, "How *does* it work?".

The first issue is, what does it mean if we have a model that reproduces some observed phenomena? Or even a step further back, what do we mean by reproducing observed phenomena? At one extreme, we have what they do in modern computer games or CGI movies: for example, the way to model human facial expressions is to record actual actors and then build the animation around them (even the wording changes, this is not a simulation, it is an animation). On the other extreme, we have the joke about the physicist modelling a chicken: let's take a sphere of a radius of unity in vacuum. So, one must first decide how much of the details one wants to model, and then do the modelling. As we have said, in principle, this should be easy, but in practice, it is surprisingly difficult to create models that both pass Occam's Razor (a frequently used heuristic in science, which roughly says to choose the simpler

of two models, that fit your data, so in other words, try to make simple models) and work sufficiently well. Thus, we assume, that any model that passes the razor and works has a high chance of corresponding to reality in a meaningful way. And, of course we gain another important thing: we have a model, whose internal working we presumably understand, which does something we want and can be used as a template to build artificial systems. With agent-based modelling, this means a very straightforward mapping to some artificial agents, e.g. robots or drones.

The second issue is about problems introduced by the numerical method and possibly the pseudo-random number generators. In agent-based modelling, instead of solving a few equations, we generally deal with hundreds and thousands of agents, each solving their own equations and applying interaction rules, etc. This means that, at any a given time, we have agents in different states interacting with many other agents. If the time resolution of the simulation is fine enough, this means that in practice, simple numerical methods are usually enough to produce a stable solution since the small numerical errors are washed out, especially when using a random noise element in the model.

The third issue to address is exploring the entire parameter space of the problem, which is technically impossible without analytical solutions. So, how do we know whether we have found everything of interest in our model? On one hand, we can't know. On the other hand, our agents are based on some constituent part of the system we are trying to understand, which limits the parameter space worth exploring. Further, many times, meaningful behaviour of the system as a whole can provide guidance about where computational capacity should be focused. Of course, one must do this carefully, since as we have stated, in general there is no guarantee that nothing interesting will be missed.

All in all, agent-based modelling is an easily graspable and versatile method for modelling complex systems, capable of delivering stable solutions.

3

Study 1: Epidemiology of HIV on complex sexual networks

This chapter will present our study titled "HIV competition dynamics over sexual networks: first comer advantage conserves founder effects" [12] as an example of agent-based modelling. The study concerns itself with the modelling of different strains of HIV/AIDS infections competing on a realistic human sexual network. In the next section we will overview the background literature needed to understand the different aspects of the problem and then present our specific motivation in creating the model. The rest of the sections of the chapter will present our work on the problem: the agent-based model we created, the results we obtained, and its discussion.

3.1 Background literature

3.1.1 Complex networks

The study of complex system very often involves the study of complex networks. A network is essentially a graph, and network theory is essentially graph theory, albeit sometimes networks are defined to be some subset of graphs. Generally, since the mathematical literature uses the graph and a good number of applications use the network terminology, the latter appears more often when graphs are used to model some real-world phenomena.

Erdős-Rényi model and real world networks

When tackling the Königsberg bridge problem Euler studied a small graph, but complex networks cannot be handled in the same way, and have to be treated statistically, which leads naturally to the study of random graphs. The Hungarian mathematicians Alfréd Rényi and the somewhat legendary Pál Erdős proposed the first random graph model in 1959 [13].

In its original formulation, the Erdős-Rényi graph is formed by taking N nodes, and randomly placing E edges between them. A slightly different formulation is placing edges between nodes with a probability p instead of fixing their number. It is clear, that if we choose p , so that

$$pN(N - 1)/2 = E \quad (3.1)$$

in the thermodynamic limit of $N \rightarrow \infty$, the two formulations are statistically equivalent. In the first formulation, the number of edges are known exactly, in the second formulations the existence of edges are independent of one-another, making each formulation good in different scenarios. The Erdős-Rényi model was a very important step, but has shortcomings when trying to model real world phenomena. To understand this, first we will introduce some properties of networks. Although there are many more, three properties will be of interest to us: the degree distribution, clustering coefficient and the average shortest path length.

The degree of a node is the number of edges attached to it, thus the degree distribution of a network carries information on how the edges are distributed among the nodes. The clustering coefficient c_i of the node i is defined as the ratio between the number of edges e_i among its nearest neighbours and its maximum possible value

$k_i(k_i - 1)/2$, that is

$$c_i = 2e_i/k_i(k_i - 1). \quad (3.2)$$

Then the clustering coefficient of the network is given by $\langle c_i \rangle$. It gives an indication of how embedded nodes are in a network. The third property we mention is the average shortest path length $\langle l_{ij} \rangle$ in the network, which is a measure of how easy it is to go from one node to the other. The name very much implies the definition: the shortest path length is the minimum number of edges traversed while going from one node to the other.

The degree distribution of the Erdős-Rényi model in the thermodynamic limit is easy to calculate when we take the definition with the probability p . On average the graph will have

$$\langle E \rangle = \frac{1}{2}N(N - 1)p \quad (3.3)$$

edges, and since each edge contributes to the degree of two nodes, the average degree is

$$\langle k \rangle = \frac{2\langle E \rangle}{N} = (N - 1)p \approx Np. \quad (3.4)$$

If $\langle k \rangle < 1$ then the network will be a bunch of small disconnected components, thus usually only the $\langle k \rangle > 1$ regime is investigated.

To arrive at the $P(k)$ degree distribution we notice, that the probability of a node with degree k is equal to the probability that it is connected to k nodes and not connected to the other $N - 1 - k$ nodes, leading us to the binomial distribution in the form of

$$P(k) = \binom{N - 1}{k} p^k (1 - p)^{N - 1 - k}, \quad (3.5)$$

which in the thermodynamic limit with $pN = \langle k \rangle$ can be approximated with the Poisson distribution

$$P(k) = e^{-\langle k \rangle} \frac{\langle k \rangle^k}{k!}. \quad (3.6)$$

The clustering coefficient also yield easily from the independent connection probability, since for a given node the probability that two of its neighbours are also con-

nected is given by the probability p , thus giving

$$\langle c \rangle = p = \frac{\langle k \rangle}{N}. \quad (3.7)$$

The scaling of the average shortest path length $\langle l \rangle$ can be approximated with the following argument. The number of neighbours within a distance of d of a given node can be approximated with $\langle k \rangle^d$. Since this grows exponentially fast when $\langle k \rangle > 1$, if we choose d to be $\langle l \rangle$ we should have approximately all the nodes within this distance, thus $\langle k \rangle^{\langle l \rangle} \approx N$, leading us to

$$\langle l \rangle \propto \frac{\log N}{\log \langle k \rangle}. \quad (3.8)$$

Network	N	$\langle k \rangle$	$\langle l \rangle$	$\langle l \rangle_{\text{rand}}$	$\langle c \rangle$	$\langle c \rangle_{\text{rand}}$
WWW, site level, undir.	153127	35.21	3.1	3.35	0.1078	0.00023
Internet, domain level	3015–6209	3.52–4.11	3.7–3.76	6.36–6.18	0.18–0.3	0.001
Movie actors	225226	61	3.65	2.99	0.79	0.00027
LANL co-authorship	52909	9.7	5.9	4.79	0.43	1.8×10^{-4}
MEDLINE co-authorship	1520251	18.1	4.6	4.91	0.066	1.1×10^{-5}
SPIRES co-authorship	56627	173	4.0	2.12	0.726	0.003
NCSTRL co-authorship	11994	3.59	9.7	7.34	0.496	3×10^{-4}
Math. co-authorship	70975	3.9	9.5	8.2	0.59	5.4×10^{-5}
Neurosci. co-authorship	209293	11.5	6	5.01	0.76	5.5×10^{-5}
<i>E. coli</i> , substrate graph	282	7.35	2.9	3.04	0.32	0.026
<i>E. coli</i> , reaction graph	315	28.3	2.62	1.98	0.59	0.09
Ythan estuary food web	134	8.7	2.43	2.26	0.22	0.06
Silwood Park food web	154	4.75	3.40	3.23	0.15	0.03
Words, co-occurrence	460902	70.13	2.67	3.03	0.437	0.0001
Words, synonyms	22311	13.48	4.5	3.84	0.7	0.0006
Power grid	4941	2.67	18.7	12.4	0.08	0.005
<i>C. elegans</i>	282	14	2.65	2.25	0.28	0.05

Table 3.1: Properties of several read world graphs, adopted from [14], the references to the original data source can be found there.

Numerous real world networks have been measured to calculate the above properties, and although not exclusively, many are very similar regarding these proper-

ties. First, in these real networks the degree distributions are heavy-tailed distributions, meaning that their tails are not exponentially bounded (i.e. there is finite chance of finding nodes with a very large degree). Second, they exhibit the so-called small-world property, the famous "six-degrees of separation". Technically, it means that the average shortest path length scales with the logarithm of the number of nodes ($\langle l \rangle \propto \log N$) while the clustering coefficient $\langle c \rangle$ is not small [15].

The Erdős-Rényi model fails on two accounts with being a model for such real world networks. First, its degree distribution has an exponential cut-off, and second, its clustering coefficient is very small when using the number of edges and nodes from real world examples. Table 3.1 lists several networks with their measured average degree, average shortest path length and clustering coefficient. The latter two are also calculated if the network were randomized (the same number of edges placed randomly among the same number of nodes, i.e. as an Erdős-Rényi graph). It can be clearly seen that the clustering coefficients are much larger, than what an Erdős-Rényi graph would yield.

The Watts-Strogatz model for small-world networks

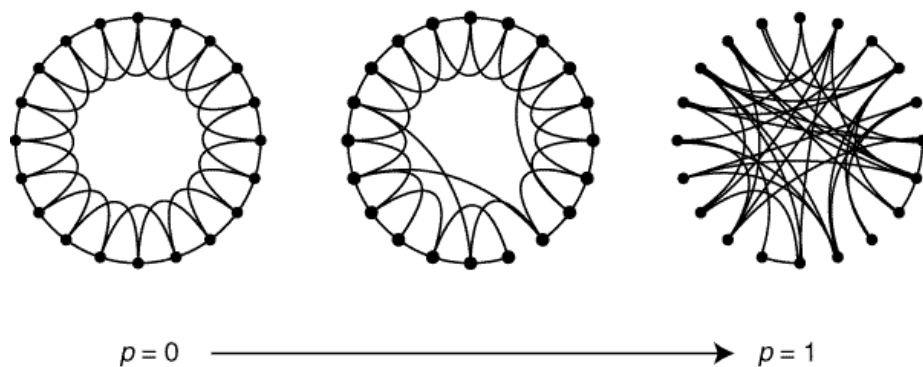


Figure 3.1: Rewiring in the Watts-Strogatz model. Each node is connected to its four nearest neighbours. As p is increased more and more edges are rewired. At $p = 1$ all edges have been rewired. Figure from [16].

To solve the issue of the low clustering coefficient Watts and Strogatz introduced the model named after them, which has a tunable clustering coefficient. The model starts with N nodes in a ring (see Figure 3.1), which are connected to the m nearest neighbours on both sides. Then for each node each edge connected to a counter-

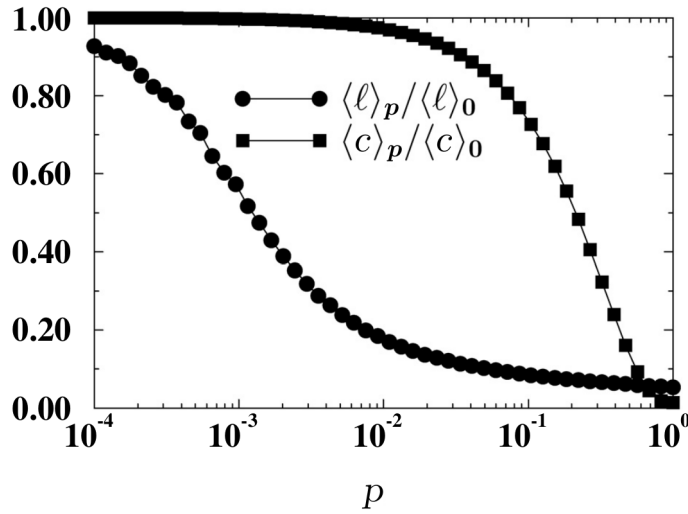


Figure 3.2: The plot shows that as p is increased from 0 to 1 there is a regime where the clustering $\langle c \rangle$ is still large while the average shortest path length $\langle \ell \rangle$ drops rapidly. In this regime the Watts-Strogatz model has small-world properties. Figure from [17].

clockwise (right side) neighbour is rewired with a probability p to a randomly chosen other node. It should be noted that even at $p = 1$ the graph will not be totally random, since half the edges are not rewired even in that case. The degree distribution of the Watts-Strogatz model can be obtained analytically [17] yielding

$$P(k) = \sum_{n=0}^{\min(k-m, m)} \binom{m}{n} (1-p)^n p^{m-n} \frac{(pm)^{k-m-n}}{(k-m-n)!} e^{-pm}, \text{ for } k \geq m. \quad (3.9)$$

As we can see, this still has an exponential cut-off, so the degree distribution is very similar to that of the Erdős-Rényi, but the clustering coefficient and the average shortest path length behaves very differently. When p is zero, the graph has a very large clustering coefficient, but a small average shortest path length. A small increase in p will not effect the clustering, since only a few edges are rewired, but they introduce significant shortcuts within the graph. If we observe Figure 3.2 we will see that there is a large regime of p , where the clustering coefficient is essentially the same as with $p = 0$ yet the mean shortest path length is greatly reduced, which regime is more in line with observations of real world networks, although this model still lacks a heavy-tailed degree distribution.

The Barabási-Albert model

The most famous and ubiquitous heavy-tailed degree distribution is the $P(k) \propto k^{-\gamma}$ power law distribution, describing the so-called scale-free graphs. The name derives from the homogeneous property of such a degree distribution, that is $P(\lambda k) = \lambda^{-\gamma} P(k)$, which means that any rescaling of the degrees will only offset the distribution by a constant factor. A notable feature of the power-law distribution is that on the $[1, \infty[$ interval, it only has a well defined mean if the exponent γ is bigger than two, and a well defined variance if $\gamma > 3$. If one tries to do the actual calculation it should be noted that when talking about power-law degree distribution it is customary to use the continuous k approach, i.e. to treat the degree as a continuous variable and also, that in the continuous approach one must introduce a k_{\min} minimum degree for the integrals to converge. The exponent of many real world networks fall between 2 and 3, although in reality, a network is called scale-free if the power law holds for 3 orders of magnitude, since there is always an upper boundary: either the system size (no node can have more edges than $N - 1$) or some other physical limitation. Thus any reference to a real world network's power-law exponents must be understood to hold between some k_{\min} and k_{\max} values.

If scale-free networks are so common in very different scenarios, we start looking for some universal property that explains it. László Barabási and Réka Albert proposed a mechanism, which can yield power-law networks through preferential attachment of links to nodes that already have many links. The model starts with m_0 nodes and no edges. Then for each step we

1. add a new node, with $m < m_0$ edges
2. connect the other end of the m edges to already present nodes with a probability $k_i / \sum_j k_j$

i.e. the probability of connecting a new edge to an old node is proportional to its degree. Using the continuous k approximation we can show that this mechanism leads to the degree distribution $P(k) \propto k^{-3}$. The derivation goes like this. The probability that the node i acquires a new edge is proportional to its degree as defined by the model

$$P(k_i(t)) = \frac{k_i(t)}{\sum_j k_j(t)}. \quad (3.10)$$

The growth of the degree is governed by the equation

$$\frac{dk_i(t)}{dt} = mP(k_i(t)) \quad (3.11)$$

with the condition that $k_i(i) = m$ as each node is introduced with m edges. Since at each step we add $2m$ to the total number of degrees Equation 3.11 will take the following form:

$$\frac{dk_i(t)}{dt} = \frac{mk_i(t)}{2mt}, \quad (3.12)$$

which yields

$$k_i(t) = m \left(\frac{t}{i} \right)^{1/2}. \quad (3.13)$$

The degree distribution is

$$P(k, t) = \frac{1}{t + m_0} \int_0^t \delta(k - k_i(t)) di = -\frac{1}{t + m_0} \left(\frac{dk_i(t)}{di} \right)^{-1} \Big|_{i=i(k,t)}, \quad (3.14)$$

where δ is the Dirac delta function and $N = t + m_0$. This gives

$$P(k, t) = 2m^2 \frac{t}{t + m_0} k^{-3} \xrightarrow{t \rightarrow \infty} 2m^2 k^{-3}. \quad (3.15)$$

The average shortest path and the clustering coefficient can also be calculated with some approximations, giving short paths but a low clustering coefficient as the system size increases [15]:

$$\langle l \rangle \propto \frac{\log N}{\log \log N}, \quad (3.16)$$

$$\langle c \rangle = \frac{m}{8N} (\ln N^2) \quad (3.17)$$

Generalized random graphs

Although it is good to know that preferential attachment leads to a scale-free behaviour, for modelling purposes we need a tool that can produce power law degree distribution with arbitrary exponents. The method of generalized random graphs is a method to create a graph with a degree distribution of our choice for a given number of nodes. Given N nodes and a $P(k)$ distribution we generate a k_i sequence of N numbers from $P(k)$ and assign these as the desired k_i degrees of each node. For each degree of a node, the node receives a half-edge, then these half-edges are

paired up randomly. Obviously if $\sum_i k_i$ is odd this cannot be done so care must be taken to only generate sequences with an even sum, although in practice, if N and the number of edges are large enough, we can safely discard the last orphan half-edge in an odd case.

We now have a tool to generate networks with power-law degree distributions of given exponents, but is the small-world property present? It can be shown, that the average shortest path lengths scale with the logarithm of the graph size, which is good, but the clustering coefficient goes to zero as N increases, which is less so. Fortunately the situation is not as bad as in case of the Erdős-Rényi graph. The clustering coefficient is very similar to the Erdős-Rényi $\langle c \rangle = \langle k \rangle / N$, but has another factor

$$\langle c \rangle = \frac{\langle k \rangle}{N} \left[\frac{\langle k^2 \rangle - \langle k \rangle^2}{\langle k \rangle^2} \right], \quad (3.18)$$

which can be rather large for the graph sizes of observed networks. For instance, Newman showed that just the power law degree distribution accounts for much of the clustering of the World Wide Web [18].

3.1.2 Epidemiology

SI, SIS and SIR models with full mixing

Epidemiology concerns itself among other things, with question about the spreading of diseases in given populations. Classical epidemiological modelling starts from the assumption of "full mixing", which means that all individuals have equal chance of coming into contact with an infected individual (i.e. mean field approach, or in case of networks the Erdős-Rényi model). This assumption allows for easily solvable differential equation, but can be dropped to use actual contact networks, to introduce more realistic models. Based on the full mixing assumption, there are three simple models of infection spreading, named after the allowed states of individuals in the model. There are three such states: susceptible (S), infected (I) and recovered (R), which are also called compartments, since each individual of the population can be assigned to one of these compartments. A susceptible individual may be infected by an infected individual, becoming an infected individual, while an infected individual may recover from infection and become recovered (R) and immune to further infection. The most basic model is the SI, where only $S \rightarrow I$ can happen (e.g. HIV). In the SIS model, an infected individual may become susceptible again (e.g. flu) and in the SIR model an infected individual may become recovered (e.g. mumps). In the

following let us investigate the properties of these models based on Chapter 9 of [13].

Let us denote the ratio of susceptible, infected and recovered individuals in the population with s , i and r . Based on the full mixing assumption each individual is in contact with $\langle k \rangle$ other individuals. Assuming that in a given dt time an infected individual will infect a susceptible individual with a probability β , then in the $\beta dt \ll 1$ limit the probability for a susceptible individual to get infected is $\beta \langle k \rangle i dt$. Given that the influx of individuals into to infected compartment is proportional to the number of susceptible individuals and $s(t) = 1 - i(t)$ in the SI model, we can write the following differential equation to describe the SI dynamics:

$$\frac{di(t)}{dt} = \beta \langle k \rangle i(t) [1 - i(t)]. \quad (3.19)$$

As can be readily seen from the equation, the SI model leads eventually to all individuals being infected, leaving only the speed of the spreading at question.

The SIS model has a bit more variation to it, since in this case an already infected individual may become healthy and susceptible again. Assuming an infected individual becomes susceptible again with the probability μdt , we can modify the previous equation like thus:

$$\frac{di(t)}{dt} = -\mu i(t) + \beta \langle k \rangle i(t) [1 - i(t)]. \quad (3.20)$$

The SIR model complicates this with a third state. In this case the μdt still denotes the probability of leaving the susceptible state, but now to the recovered and not the susceptible state, further complicating the equations:

$$\frac{ds(t)}{dt} = -\beta \langle k \rangle i(t) [1 - r(t) - i(t)], \quad (3.21)$$

$$\frac{di(t)}{dt} = -\mu i(t) + \beta \langle k \rangle i(t) [1 - r(t) - i(t)], \quad (3.22)$$

$$\frac{dr(t)}{dt} = \mu i(t). \quad (3.23)$$

Note, that both the SIS and the SIR model behave the same when taking the limits of the μ/β ratio. By taking the limit of $\mu \gg \beta$ infected individuals heal faster than they can infect other individuals, leading to the epidemic dying out quickly. In contrast, taking the $\mu \ll \beta$ limit all terms containing μ are negligible leading effectively to the SI model. Next we will explore the behaviour of these models.

The initial condition of an epidemic is a small fraction of infected individuals, i.e. $i \ll 1$ so we need only keep the terms that are first order in i

$$\frac{di(t)}{dt} = \beta\langle k \rangle i(t) \quad (3.24)$$

leading to the solution

$$i(t) \simeq i_0 e^{\beta\langle k \rangle t}, \quad (3.25)$$

for small t -s, where i_0 is the initial ratio of infected individuals. The solution defines the $\tau = (\beta\langle k \rangle)^{-1}$ timescale of the spreading of the epidemic. For the SIS and the SIR models taking the terms that are first-order in i leads to the same equation in both cases:

$$\frac{di(t)}{dt} = -\mu i(t) + \beta\langle k \rangle i(t). \quad (3.26)$$

Similarly as with 3.24 this leads to an exponential solution,

$$i(t) \simeq i_0 e^{t/\tau}, \quad (3.27)$$

albeit with a different timescale:

$$\tau^{-1} = \beta\langle k \rangle - \mu. \quad (3.28)$$

The main difference here is that τ in the SIS and SIR models may be negative, leading to the withering of the epidemic. This allows for the definition of the so-called epidemic threshold as such:

$$\tau^{-1} = \mu(R_0 - 1) > 0, \quad (3.29)$$

where $R_0 = \beta\langle k \rangle / \mu$ is the basic reproductive rate, which has to be larger than 1 for an epidemic to occur.

Infection spreading in graphs

The above equations can be modified to take into account heterogeneity in the underlying contact network. This can become very important when modelling real-life networks and as we will later see, human sexual networks are very heterogeneous. Previously we took the average number of contacts and assumed each individual has that many contacts. Let us relax this assumption and allow each individual to inter-

act with as many individuals as s/he has contact with. To do this we will introduce the quantities s_k , i_k and r_k as the ratio of individuals who are susceptible, infected or recovered respectively, among the individuals with k number of contacts. Assuming the only difference between individuals is their number of contacts and introducing Θ_k , the density of infected individual in the neighbourhood of individuals with k contacts, we arrive at the following SI equation:

$$\frac{di_k(t)}{dt} = \beta[1 - i_k(t)]k\Theta_k(t). \quad (3.30)$$

The SIS and SIR models can likewise be adapted. Without detailing calculations, in this case the timescale previously defined changes to the following:

$$\tau = \frac{\langle k \rangle}{\beta\langle k^2 \rangle - (\mu + \beta)\langle k \rangle}, \quad (3.31)$$

and setting the condition for the spreading of the epidemic (the epidemic threshold) to

$$\frac{\beta}{\mu} \leq \frac{\langle k \rangle}{\langle k^2 \rangle - \langle k \rangle}. \quad (3.32)$$

Note, that in case of $\langle k^2 \rangle / \langle k \rangle \rightarrow \infty$, the epidemic threshold is zero, meaning any kind of infection will spread eventually. As we will see later, human sexual contact networks are modelled with networks where this is the case in the thermodynamic limit.

3.1.3 Introduction to HIV and AIDS

History of HIV

The acronym AIDS stands for Acquired Immune Deficiency Syndrome and is a very recent addition to the various diseases plaguing humanity, which attacks the immune system, and if left untreated, leads to death through secondary infection which would not be able to attack a healthy individual. First diagnosed in the western world in 1981 in the United States of America, initially it was regarded as a disease only affecting homosexuals, since it first started amongst homosexual men. Later it was diagnosed in intravenous drug users and an infant died to due AIDS, rapidly leading to larger awareness. After it also spread to Europe international efforts began to stop it. In 1983 the cause of AIDS was found: Human Immunodeficiency Virus (HIV).

The origin of HIV can be traced back to Central Africa. Monkeys and apes in Africa have been infected with the Simian Immunodeficiency Virus (SIV) for at least 30 millennia before the start of the HIV pandemic, possibly passing over to humans several times, but these strains of HIV presumably died out. There are several types of HIV, but the global pandemic of infections is being driven mainly by the group M lineage of HIV-1, which crossed the species barrier from chimpanzees to humans about 100 years ago, most possible in Léopoldville (today Kinshasa, Democratic Republic of Congo) [19], [20]. By the time it started to spread beyond its epicentre in Central Africa, the virus had already accumulated considerable sequence diversity [20], and distinct divergent clades initiated a series of rapid expansions that gave rise to the subtypes of HIV-1 group M [21], [22].

There are several theories on why over the last 30000 years HIV could only start a pandemic in the 20th century, but they all share a common theme of tying it to the colonization of Africa: rapidly growing cities, destabilized social structures and widespread infections of sexually transmitted diseases. One theory is that the organised medical fight against the sexually transmitted diseases was the direct cause of the spreading of HIV. At that time Léopoldville had 2-4 times as many men as women residents and a considerable part of the women were involved in so-called soft prostitution with several men, leading to a high level of syphilis. The countermeasures to syphilis was the regular vaccination of the population with needles of questionable sterility due to poor economic conditions, spreading HIV very quickly.

On Figures 3.3 and 3.4 we can observe 20 years of the pandemic from 1990 to 2010, showing that although it is still a major issue, the number of new infections and the number of deaths related to HIV is on the decline, thanks to prevention and treatment efforts, but as we shall see later, our results suggest that the future may hold some unpleasant surprises.

Infection and disease

HIV can be transmitted via blood, semen, vaginal secretions and breast milk and attacks a type of immune cell called the CD4⁺ T lymphocytes. It seems that most infections are started by a single virion. In the initial phase of the infection, the acute phase, HIV starts to rapidly multiply and mutate (the latter being one of the major causes that we still do not have a vaccine). During the acute phase the virus concentration is extremely high, while the virulence is also high and the diseased may suffer from various symptoms.

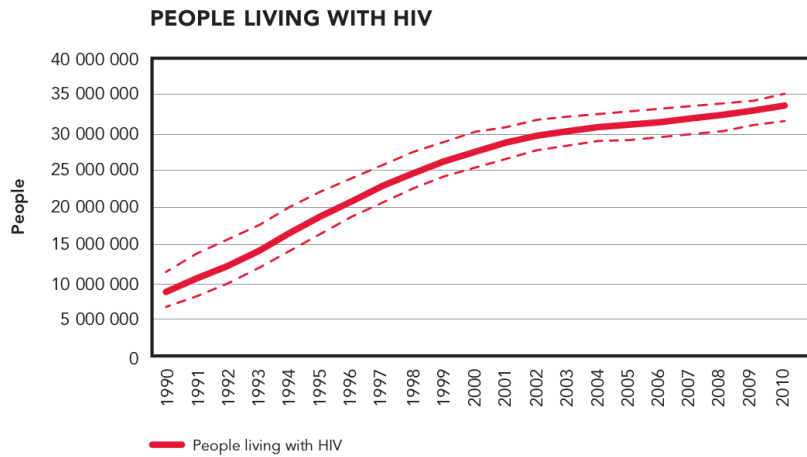


Figure 3.3: The global prevalence of HIV from 1990 to 2010. Figure taken from [23].

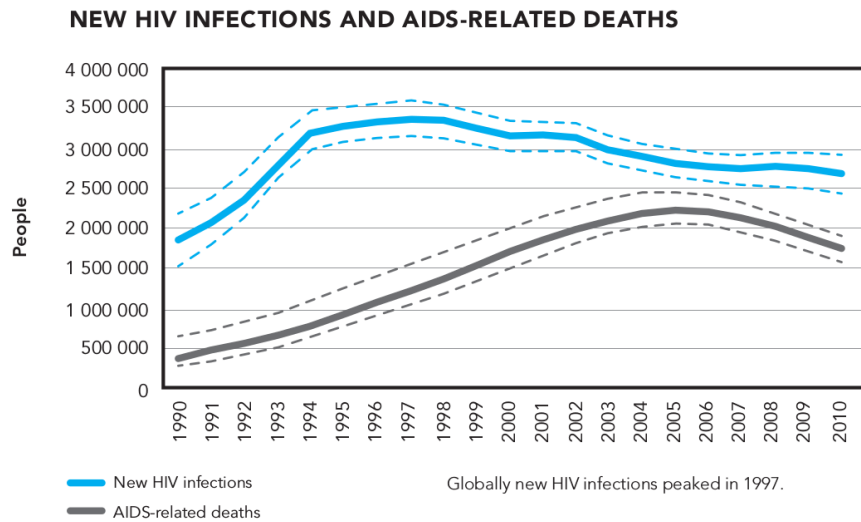


Figure 3.4: The yearly number of new HIV infection and deaths related to HIV. Both the number of new infections and deaths are on a decline. Figure taken from [23].

The acute phase lasts a few months then passes into the chronic phase. In the chronic phase there are no symptoms, the virulence is low, and this may last for years. At the end of the chronic phase the number of T cells drops to such a low level, that AIDS develops. AIDS itself usually does not cause death in itself, but the lack of a normal immune system makes diseases deadly, that a healthy individual would not even notice [24].

3.1.4 Motivation

The global molecular diversity of the pandemic still bears the clear footprint of the strong founder effects that characterized this initial expansion. While diversity is very high near the epicentre of the epidemic in Central Africa, the epidemics of other regions are typically characterized by the dominance of at most a few subtypes or circulating recombinant forms (CRFs) [25], see Figure 3.5. The countries where more than one subtype is prevalent tend to be characterized by parallel, compartmentalized epidemics with distinct subtypes infecting different risk or ethnic groups [26]–[29], and transmission chains rarely cross national borders [30]. While the global spatial distribution of HIV subtypes is not completely static, the diversification of the epidemic and shifts between subtypes occur very slowly in most regions [25]. Understanding the factors that set the time scale of HIV competition dynamics at the population level has great practical relevance. Subtypes differ in both transmissibility [31]–[33] and the rate of disease progression [34], [35], and further variation in these traits is bound to exist within the subtypes and in the vast diversity of unique recombinant forms (URFs) and unclassified basal lineages in Central Africa [36]–[38]. Virus variants that have higher transmission potential are likely to be spreading at the expense of less efficient strains, and epidemics may expand as the original variants are gradually replaced by “fitter” viral lineages. The risk and pace of these processes needs to be better characterized. We developed a simple model of sexually transmitted HIV epidemics that allowed us to monitor the competition dynamics of distinct virus strains with varying rates of transmission. In sexually transmitted epidemics, HIV is transmitted over the network of sexual contacts, which tends to include a very limited subset of all possible contacts, i.e. the host population is very far from “free mixing”. Our aim was to create an agent-based model of the sexual dynamics of a population and model the spreading of the virus over the emerging network. Since in Sub-Saharan Africa the primary way of infection is via heterosexual contact, we based the model on data from generalized heterosexual epidemics in Africa.

3.2 Our model

3.2.1 Basic model

The basis of the agent-based model is the network of sexual contacts, which consists of three types of nodes (individuals): males, (non sex worker) females and female

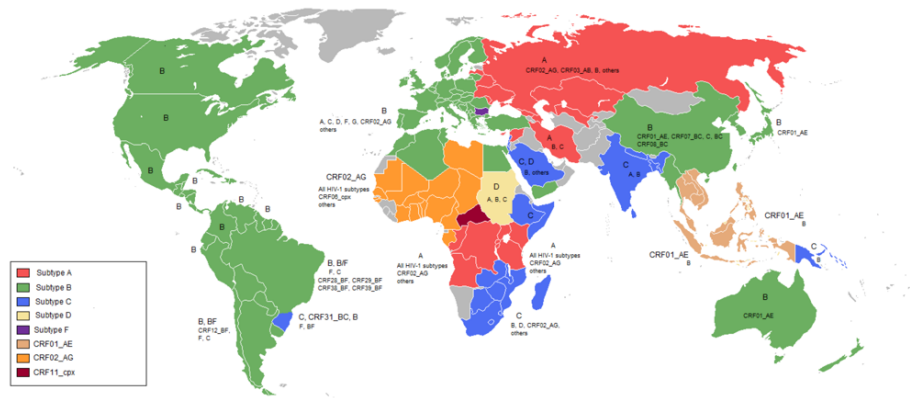


Figure 3.5: Worldwide prevalence of HIV-1 group M subtypes and CRF. Note, that usually very few subtypes are in one area, except for Africa. Figure taken from [39].

sex workers (FSW) and the links represent sexual contact. The model tracks the age and HIV status (stage of infection and the infecting virus type) of each individual, and for males and (non-FSW) females also a fixed quantifier of promiscuity (a preferred annual contact degree), and the number of distinct sexual partners in the last year (realized annual contact degree). Individuals enter the population at age 15 and are removed at the age of 50, to simulate dropping out of sexual activity. The preferred contact degree of each individual is drawn from an empirical distribution according to the type of the node and is kept constant for the lifetime of the individual. The promiscuity of males and (non-FSW) females are characterized by continuous power-law distributions of the form $P(x) \propto x^{-\gamma}$ (with different exponents for the two sexes, see Table 3.2) parametrized based on empirical data and censored at both a lower cut-off (one contact per year to ensure all nodes are active in the network) and an upper cut-off (this is a case where the upper limit given by the network size is unrealistic once it reaches a few thousand, since there is a physical limit for the human body). FSW have a fixed maximum number of one-time contacts per week, representing the businesslike organisation of their sex-life.

The simulations have a time step of one week, and each step consists of the following procedures:

- (a) generation of sexual acts along the links and virus transmission,
- (b) update of HIV status,
- (c) birth and death dynamics of individuals,
- (d) dissolution and formation of network links.

As the simplest assumption, the number of sexual acts in male-female links is drawn from a Poisson distribution (discarding zeros: no links were inactive); male-FSW links always involve a single sexual act. The probability of virus transmission to uninfected individuals is determined by the baseline transmission rate of the virus strain, amplified if the transmitting individual was in the acute stage of the infection. Newly infected individuals are immediately assigned a time to death from a uniform distribution between 3 – 20 years (consistent with recently estimated survival curves in cohorts not receiving antiretroviral treatment [40]), and for each infection event the following are recorded: the date of the event, the strain that was transmitted, the disease stage of the transmitter, and whether the transmission involved superinfection of an individual previously infected with the other virus type. For simplicity, the size of the population is kept constant (at 10,000 individuals of both sexes): all nodes who die of AIDS or leave the network at age 50 (whichever came first) are replaced with a new individual of age 15. The preferred annual contact degree of new nodes is drawn from the power-law distribution of the respective gender at entry to the population. The links between males and females are allowed to form and break up at each time step. The baseline probability of break-up is set to yield an average duration consistent with empirical estimates (see Table 3.2), and is scaled proportional to the average contact degree of the two nodes (such that more promiscuous individuals have shorter relationships [41]).

Link formation is implemented such that all non-FSW individuals will have a yearly number of sexual contacts approximately equivalent to their preferred annual contact degree, using a generalized random graph model. Although a generalized random graph model would allow for generating an exactly matching distribution, in our case only an aggregate (yearly) degree distribution was known, so we had to generate some links at each time step to add up to the preferred yearly contact degree. To do this, at each time step, the nodes are assigned a number of half-links generated randomly in proportion to their preferred contact degree, which was approximated by the preferred yearly contact degree divided by the number of weeks in a year (52). As we will see later, this method slightly increased the realized exponents, partially due to not accounting for links surviving longer than a year.

Because males have greater mean promiscuity than non-FSW females, the number of half-links for males exceed those of the females. New links are formed by first randomly connecting all female half-links to male half-links, then randomly distributing the remaining male half-links to the FSW. All simulation runs of the model

start with an initialization phase restricted to link formation and break-up until the sexual network settles to a steady state. FSWs have fixed promiscuity and are added one by one as long as there is a surplus of male half-links. The number of FSWs at steady-state is thus not pre-determined, but emerges to match and compensate the imbalance of male and (non-FSW) female links in each scenario.

Population level competition is simulated by implementing two virus types that are allowed to differ in their rate of transmissibility. The type of the infecting virus strain(s) is tracked for each infected individual. The first virus strain is introduced in a random sample of ten percent of all FSW after the initialization of the sexual network: this method allowed a reliable establishment of the "resident" epidemic with negligible risk of extinction. The second (invader) strain is also introduced in a sample of ten percent of all FSW (sampled from uninfected FSW) when the resident strain has attained a steady state in the population.

3.2.2 Mechanisms of interference

This simulation framework allowed us to investigate three potential mechanisms of interference between the resident and the invader strains. To do this, we defined four scenarios, a default scenario and three other scenarios that differs from the default one in a specific detail. In the following, we will introduce the default scenario and then present the supporting and counter arguments, which will also define our three other scenarios.

In the default scenario, superinfection can occur only by the replacement of the original strain with the superinfecting strain. In a sexual act between two individuals infected with different virus strains, both strains have a chance to be transmitted. Superinfection occurs if two check points are passed: initial transmission occurs according to the transmission rate of the infecting strain (modified by disease stage, if appropriate); then after successful initial transmission, the probability of superinfection is determined by the relative transmission rates ("fitness") of the two strains as follows: $P = \nu_2 / (\nu_1 + \nu_2)$, where ν_1 denotes the transmission rate of the virus infecting the potential recipient and ν_2 denotes the transmission rate of the strain infecting the potential transmitter. This means that at equal transmission rates its a 50-50 game. The "clock" of disease stage in the recipient is unaffected by superinfection in the default scenario; the stage of disease remains to be based on the age of infection defined by the date of the original first infection of the recipient. A new time to death is drawn randomly (from the 3 – 20 years range); however, it is used

only if the new date of death precedes the original date determined at the initial infection: superinfection could never extend the lifespan of an individual. Now that the default scenario is presented, let us investigate it in detail.

First, infection with one HIV strain may afford some protection against superinfection with another strain: both the depletion of target cells and the induction of anti-HIV immune responses are likely to create less favourable conditions for infection compared with an uninfected individual. Because the strength of such an effect is still subject to debate (see section 3.4), we used a conservative approach in the default scenario: if two infected individuals with different strains have a sexual act, both strains had a chance to be transmitted in a two-step procedure. The first step tested successful initial transmission, which had a probability based on the transmission rate of the given strain, equivalent to the first infection of an uninfected individual. Then in the second step the superinfecting virus replaced the original strain with a probability based on the relative transmission rates of the two strains. Thus in the default scenario, the first strain had neither advantage nor disadvantage at the within-host level, and the “inhibition effect” arose only from the assumption that the infection of each individual is dominated by a single virus strain, implying replacement rather than coexistence upon superinfection (which is a reasonable simplification for the modelling of population level spread; see Section 3.4). The default scenario model reduces the average probability of superinfection to 50% of that of initial infection, which is consistent with a recent prospective cohort study that estimated about two-fold lower hazard of superinfection compared with initial infection [42]. However, we also tested a “dual infection” scenario, in which superinfection was completely unhindered, and both strains were able to co-exist within one individual after superinfection occurred. In this scenario, in sexual acts between a dual infected and an uninfected individual both virus strains had an independent probability of being transmitted.

Second, we hypothesized that the peak of infectivity that characterizes acute infection [43], [44] may not occur again upon superinfection due to depleted target cell levels and the presence of anti-HIV immune responses. If this is indeed the case then the first virus strain to colonize a population may take advantage of a rapid early wave of expansion fuelled by a high relative frequency of efficient acute stage transmissions in a largely susceptible population. In contrast, any subsequent “invader” strain is limited to the lower rates of chronic transmission that characterize mature epidemics [45], and even successfully superinfected individuals represent a dimin-

ished resource if acute peak infectivity cannot be repeated. We implemented this possible mechanism by keeping track of disease stage independently of the identity of the infecting strain. If superinfection occurred after the end of acute infection, the individual was assumed to remain in chronic stage and the onward transmission of the superinfecting strain occurred according to its baseline (chronic) transmission rate. When superinfection occurred during the acute stage of the initial infection, then the superinfecting strain received the benefit of enhanced acute-stage transmission for the remaining time of the acute stage, timed from the initial infection of the individual. However, some evidence indicates that superinfection can generate a new temporary peak of viremia (when the virus can be found in the blood and is thus easily spreading elsewhere) at least in some of the cases [46]. We have therefore also tested a scenario where superinfection started a new window of enhanced acute-stage infectivity.

Third, we hypothesized that in the absence of broadly available antiretroviral treatment (ART), the first HIV epidemics may also have an impact by selectively infecting and killing highly promiscuous individuals who form the “hubs” of the network. Such individuals have been shown to be particularly important for the spread of sexually transmitted diseases [47], and they are likely to be infected preferentially due to their larger number of contacts and thus are also more likely to die of AIDS. To assess the strength of this effect, we also implemented a scenario in which all individuals who died of AIDS were replaced by an uninfected individual with the same promiscuity (preferred contact degree) as that of the deceased individual, which preserved the degree distribution of the contact network irrespective of the epidemics.

The parameters of the sexual network are based on contemporary surveys in Africa; HIV parameters are also based on available empirical data (Table 3.2). The high-prevalence setting was implemented by increasing (doubling) the baseline transmission rate, consistent with the recent finding that variation in prevalence among Sub-Saharan countries can largely be explained by differences in the rate of transmission in serodiscordant couples, i.e. in couples where only one member of the couple is infected [48].

symbol	description	value [reference]
N_m	Number of men in the population	10000
N_f	Number of women in the population	10000
γ_m	Exponent of male degree distribution	2.45 ^a [49]
γ_f	Exponent of female degree distribution	3.45 ^a [49]
K_c	Number of clients per FSW per year	400 ^b [50]–[52]
κ_{\min}	Lower cutoff of annual degree distribution	1
κ_{\max}	Upper cutoff of annual degree distribution	1000 ^c
p_b	Probability of link breakup per week	0.05 ^d [73]
λ	Poisson parameter for the number of sex acts per week	2 [53], [54]
ν_1	Strain 1 per-contact transmissibility in chronic stage	0.001 or 0.002 ^e [55]
ν_2	Strain 2 per-contact transmissibility in chronic stage	(1–1.5) ν_1
m_A	Transmission multiplier for acute infection	9 [56]
T_{acute}	Length of acute phase (weeks)	12 [43]
T_{age}	Duration of sexual activity (years)	35 (age 15–50)
T_{HIV}	Survival with HIV infection (range in years)	3–20 [57], [58]
T_{init}	Time steps (weeks) without virus	1000
T_{single}	Time steps (weeks) with only one virus	6000 or 4000 ^e

Table 3.2: Parameters used for the simulation of the HIV infection model.

- ^a Used to generate preferred annual contact degrees; for the exponents fitted to realized contact degrees, see Figures 3.6 and 3.7.
- ^b Middle value from 600 given in [50] and 150 calculated from [51], [52].
- ^c The maximum realized contact degree was lower in all simulations.
- ^d Baseline rate for links between individuals with degree 1.
- ^e Alternative values used to parameterize low- and high-prevalence settings.

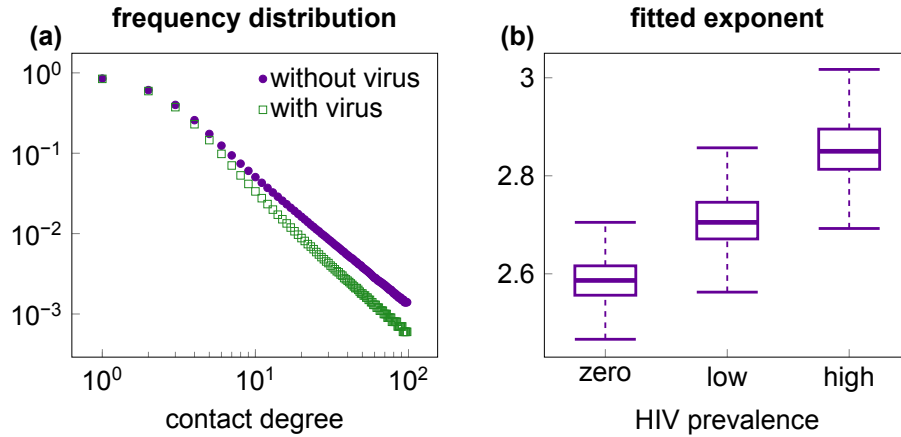


Figure 3.6: **Males:** (a) Frequency distribution of the annual number of sexual contacts (realized contact degree) of males in uninfected populations (purple dots) and in populations with high-prevalence epidemics (green squares), based on median data from 1000 simulation runs. Highly promiscuous individuals were selectively depleted in the presence of the virus. (b) Boxplot of the exponents of power-law distributions fitted to male individuals in batches of 1000 independent runs with no virus, low and high prevalence epidemics, respectively. Boxes depict interquartile range, median is indicated by horizontal lines within the boxes, and whiskers extend to the farthest values that are not more than 1.5 times the box width away from the box. Medians (and IQR) of the exponents were 2.59 (2.56–2.62), 2.70 (2.67–2.75) and 2.85 (2.81–2.90) in the absence of the virus and with low or high prevalence epidemics, respectively; all pairwise comparisons between the three scenarios were statistically significant ($p < 10^{-10}$; Wilcoxon rank sum test). Simulation parameters were set as in Table 3.2.

3.3 Results

3.3.1 Network properties with single strain infection

Before exploring the competition dynamics of our model we investigated how the system behaves without a virus, or with a single strain of virus.

First we validated the annual contact degree distribution of the resulting network for both males and females (see Figures 3.6 and 3.7). Power-law exponents of the realized annual contact degrees (based on the actual numbers of sexual contacts in the last year) were fitted as described in [59], estimating the lower cutoff with Kolmogorov-Smirnov statistics, using the implementation of [60]. The realized exponent of the annual contact degrees are slightly larger than the empirical, but are still very close.

One of the hypothesis on designing the basic scenario was that an individual will

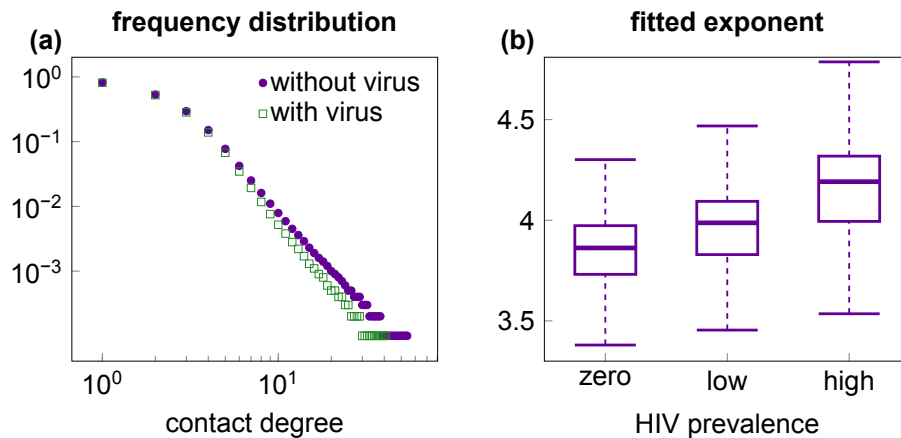


Figure 3.7: **Females:** (a) Frequency distribution of the annual number of sexual contacts (realized contact degree) of females in uninfected populations (purple dots) and in populations with high-prevalence epidemics (green squares), based on median data from 1000 simulation runs. Highly promiscuous individuals were selectively depleted in the presence of the virus. (b) Boxplot of the exponents of power-law distributions fitted to female individuals in batches of 1000 independent runs with no virus, low and high prevalence epidemics, respectively. Boxes depict interquartile range, median is indicated by horizontal lines within the boxes, and whiskers extend to the farthest values that are not more than 1.5 times the box width away from the box. Medians (and IQR) of the exponents were 3.73 (3.86 - 3.97), 3.83 (3.99 - 4.09) and 3.99 (4.19 - 4.32) in the absence of the virus and with low or high prevalence epidemics, respectively; all pairwise comparisons between the three scenarios were statistically significant ($p < 10^{-10}$; Wilcoxon rank sum test). Simulation parameters were set as in Table 3.2.

only have one acute phase, even in case of a superinfection. The importance of this is shown on Figure 3.8 A, where the relative contribution of acute stage transmissions in our simulations is depicted: after little over a decade, 80% of new infections originate from individuals in the chronic phase, lowering the overall ability to infect and thus hindering any subsequent infection from spreading.

Another factor that we hypothesised to negatively effect the spreading of any invader strain, is that the resident strain will deplete the highly connected hubs by selectively killing the highly promiscuous individuals. Indeed, in our simulations the probability of infection was strongly related to the promiscuity (preferred contact degree) of the individuals (Figure 3.8 b). Using collated data from 100 simulation runs, logistic regression against log transformed contact degree (controlling also for age and gender) estimated an effect size of 2.48 (95% CI: 2.46 - 2.50; $p < 10^{-10}$), implying that the odds of being infected increased by a factor of $\exp(2.48)$, i.e., about 12-fold

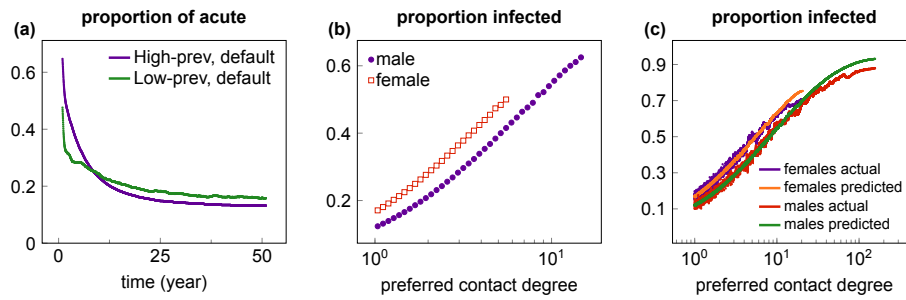


Figure 3.8: (a) The relative contribution of acute stage transmissions over the time course of single-strain epidemics. The proportion of transmissions originating from acute-stage transmitters decreases from high levels at the beginning of the epidemics to a steady-state around 0.15 and 0.13 in the low (purple dots) and high (green dots) prevalence epidemics, respectively, over a time scale of a few decades. Proportion data were calculated by combining transmission events recorded in 1000 simulation runs, then smoothed by averaging with a sliding window of 100 weeks length. (b) The ratio of infection among men (purple dots) and (non-FSW) women (red squares) increased with preferred contact degree (number of partners per year; plotted on logarithmic scale). The plot was created from 1000 independent simulation runs of single-strain epidemics of high prevalence, using logarithmic binning, right-censored at the top 1% of the male/female population (where rare classes result in strong stochastic variation). (c) The probability of infection as a function of the promiscuity (preferred contact degree) of the individuals: data and model fit. Using collated data from 100 simulation runs (2 million individuals total), we performed a logistic regression on the probability of infection in individuals using log transformed preferred contact degree, age and gender as explanatory variables. Purple and red lines show smoothed actual proportions of infected among females and males, respectively, calculated with a sliding window (moving along all individuals sorted according to contact degree; each point representing the frequency of infections among 1000 individuals). Predictions from the logistic regression (plotted as orange and green lines, using the same sliding window smoothing) provide an excellent fit to the data. Effect sizes (and 95% CI) for the three factors were estimated as follows: $\log_{10}(\text{degree})$: 2.48 (95% CI: 2.46–2.50), age: 0.0460 per year (95% CI: 0.0457–0.0464), female gender: 0.420 (95% CI: 0.413–0.428); all three effects were significant at $p < 10^{-10}$. Simulation parameters were set as in Table 3.2

for every order of magnitude increase in the preferred contact degree (Figure 3.8 c); the effect was robust also in regressions on individual simulation runs (effect size range in 100 simulations: 2.26–2.66; $p < 10^{-10}$ for all simulation runs). As a result, an established epidemic of the resident virus strain depleted highly connected nodes of the network preferentially: the power-law exponent of the contact degree distributions (fitted to the actual number of yearly partners) increased significantly compared with the pre-epidemic steady state ($p < 10^{-10}$, Wilcoxon rank sum test; Figures 3.6 and 3.7), which may also have put any invader strain at a disadvantage.

3.3.2 Default scenario

We simulated a simple scenario of competition between two strains of the virus. To assess the maximum potential for a “first comer advantage”, we started the simulations with one of the strains (the founder, or “resident” strain) and let the epidemics attain steady-state prevalence before introducing the second (“invader”) virus strain. The transmission rate of the invader strain was equal to or greater than that of the resident strain, and its chance and pace of growth was assessed in relation to its transmission advantage over the resident strain.

We hypothesized that the effect on the spread of the invader strain may depend on the prevalence of the resident strain, and have therefore considered two scenarios, where the steady-state prevalence of the resident strain was around 0.03 and 0.2, respectively. The two scenarios were set by changing the baseline rate of transmissibility (see Table 3.2); all other parameters were kept constant. Figure 3.9 shows the time course of multiple simulations for two selected cases where the invader virus had equal (Figure 3.9 a,c) or 25% greater (Figure 3.9 b,d) transmission rate compared with the resident strain in the high (Figure 3.9 a-b) or low (Figure 3.9 c-d) prevalence scenarios. The resident strain attains steady-state prevalence in about 84 and 74 years in the low- and high-prevalence scenario, respectively. With equal transmissibility, the invader strain shows no appreciable growth in a hundred years in the high-prevalence scenario (Figure 3.9 a), and grows, but remains in strong minority over the same time span in the majority of the simulations with the low-prevalence scenario (Figure 3.9 c). A 25% advantage in the transmission rate allowed the invader virus to outgrow the resident strain in both scenarios (Figure 3.9 b,d), but it still took a median of 60 and 104 years until the prevalence of the invader strain reached that of the resident strain in the low- and high-prevalence setting; due to its higher transmissibility, the invader strain was then able to attain higher steady-state prevalence compared with the initial steady state of the resident strain. Compared with the initial expansion of the resident strain, the expansion of the invader was much slower in all cases. In addition, 66.4 and 68.3 percent of the simulations with equal transmissibility of the invader resulted in the extinction of the invader virus in the low- and high-prevalence scenarios, respectively; extinction occurred in 2.4 and 1.2% of the cases when the invader had 25% transmission advantage. In contrast, with our settings the initial introduction of the resident virus was nearly always (in 998/1000 and 1000/1000 independent simulation runs of the low and high-prevalence settings, respectively) able to establish an epidemic that grew to steady state.

The timescales seen on Figure 3.9 are quite compatible with the known history of the HIV/AIDS pandemic. In our model it takes decades for the epidemic to stabilize in the population and any second strain also needs quite a few decades to become more prevalent, than the resident strain, which timescales are both congruent with the current epidemic.

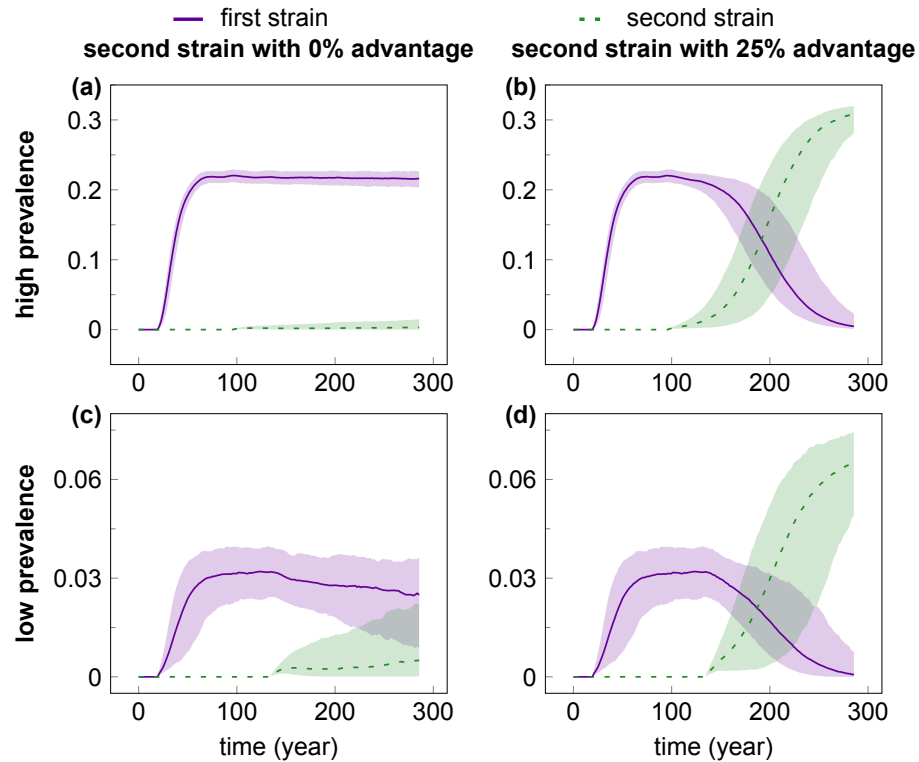


Figure 3.9: The invader virus had equal (a, c) or 25% greater (b, d) transmission rate compared with the resident strain in the high (a, b) or low (c, d) prevalence scenarios. The resident strain (solid purple line) was introduced in the population at Week 1000 (to allow the network to attain steady state); the invader strain (dashed green line) was introduced in the population when the first strain had already reached steady-state prevalence (at Week 5000 and 7000 for the high- and low-prevalence setting, respectively). Even with a 25% advantage in the transmission rate, it took the invader strain a median of 60 and 104 years to reach the prevalence of the resident strain in the low- and high-prevalence scenario, respectively. The lines show median prevalence from simulations where the invader strain did not go extinct (out of 1000 simulation runs); shading indicates the areas between the 5% and 95% quantiles. Simulation parameters were set as in 3.2.

Our strategy was thus to construct a default simulation scenario using settings that we deemed most plausible (partially inhibited superinfection, with strain replacement when superinfection is successful; one-time acute peak of infectiousness;

and emergent preferential depletion of highly connected individuals), then test the effect of switching off one mechanism at a time in a series of test scenarios: i) “dual infection” with possible co-existence of the two strains in the same individual and no inhibition of superinfection; ii) “multiple acute” with repeated episodes of enhanced acute-stage infectiousness upon each successful superinfection; and iii) “fixed degrees” in which the degree distribution of the contact network was preserved. This strategy allowed us to assess the relative impact of each mechanism on the population level competition dynamics, and served also as a sensitivity analysis for relaxing the assumptions of inhibited superinfection and one-time acute peak infectiousness.

3.3.3 Inhibition of superinfection dominates first comer advantage

We tested eight scenarios (default and three test cases, each in both low and high prevalence settings) with levels of relative transmission advantage for the invader strain ranging between 0–50%. The invader strain was introduced in the population when the resident virus had attained steady-state prevalence; all combinations of scenario and transmission advantage were tested in 1000 simulation runs. We extracted several statistics to quantify the probability and rate of the expansion of the invader virus (Figure 3.10).

When the transmission advantage of the invader strain was small, most simulations of the default scenario resulted in the extinction of the invader variant in both the high (Figure 3.10 a) and the low (Figure 3.10 d) prevalence settings. In contrast, the first (resident) strain was able to establish a stable epidemic in nearly all (>99%; dashed gray line) simulation runs when introduced into a fully susceptible population, which indicates a strong first comer advantage at the early stages of the spread of new strains. Preserving the degree distribution of the contact network (“fixed degrees”) had negligible effect compared with the default scenario; allowing multiple peaks of acute-stage infectiousness substantially reduced the probability of extinction in the high, but not in the low-prevalence setting. Finally, allowing for unhindered superinfection and coexistence (“dual infection”) reduced the probability of extinction to near zero even with no transmission advantage, illustrating that the inhibition of superinfection was the major factor in the heightened extinction risk of the invader strain. Greater relative advantage in the transmission rate reduced the

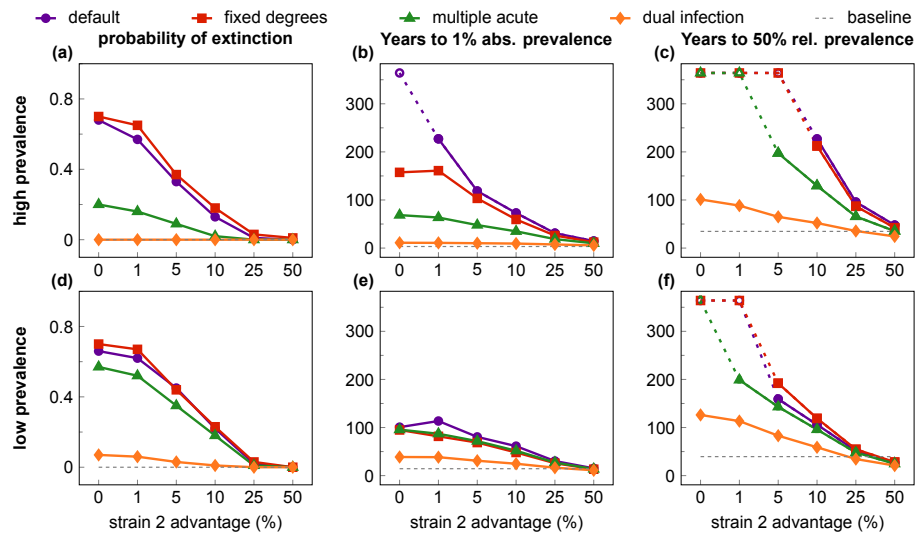


Figure 3.10: All quantifiers are plotted against the relative transmission rate advantage of the second (invader) strain, with alternative scenarios to test interference mechanisms. Rows show results from the high (top row) and low prevalence (bottom row) settings; columns depict three different quantifiers; scenarios are coded by symbols and colour. In the default scenario (purple lines and dots) the invader strain faced a high risk of extinction (a, d) and experienced very slow growth to 1% absolute prevalence (b, e) and to 50% relative prevalence (c, f) at low values of transmission rate advantage, compared with the initial growth of the resident virus (dashed gray lines). The effect was largely abrogated with unhindered superinfection and co-existence (dual infection scenario; orange lines and diamonds), and, in the high-prevalence setting, partially mitigated by allowing for repeated “acute stage” peak infectivity after superinfection (multiple acute scenario; green lines and triangles); fixing the degree distribution of the contact network (fixed degrees scenario; red lines and squares) had little effect compared with the default scenario. Increasing the relative transmission rate advantage of the invader strain also decreased the inhibition effects: values comparable to the single-strain baseline were observed around 25%–50% transmission advantage. Data in b-c and e-f depict medians from 1000 simulation runs (excluding those where the invader virus went extinct). Parameters are listed in Table 3.2; scenarios are described in detail in the main text. The maximum length of simulations was 19,000 weeks (365 years); empty symbols indicate where the invader strain did not reach the threshold prevalence by the end of the simulation in the majority of the cases.

risk of extinction in all scenarios, approaching zero extinction risk at around 25% advantage.

We defined two more quantifiers based on the time it took the invader strain to grow to selected threshold levels (in both cases we derived the statistics from the simulation runs where the invader strain did not go extinct). The time to one percent absolute prevalence (infecting one percent of the total population) was selected as a

low threshold that would allow for the detection of a new strain in a population (Figure 3.10 b,e). As a baseline comparison, we plotted also the median time until the resident strain attained one percent prevalence during its initial expansion (median of 14.4 and 3.3 years for the low and the high prevalence case; dashed gray lines). At small values of the transmission advantage, growing even to one percent prevalence can take a century or more in the default scenario (e.g. a median of 114 and 228 years with a transmission advantage of one percent, in the low and high-prevalence setting, respectively). The inhibition effect was stronger in the high-prevalence setting, and was gradually lost when the transmission advantage of the invader strain was increased to about 50%. The dominant mechanism of inhibition was again the inhibition of superinfection: allowing for dual infection abrogated most of the effect even at low values of the transmission advantage. The other two mechanisms of interference had negligible effect in the low-prevalence scenario (Figure 3.10 e), but had some partial effect in the high-prevalence scenario (Figure 3.10 b); multiple peaks of acute infectiousness had a stronger impact than fixed contact degrees also in this test case.

Finally, we also collected statistics on the time until the turning point when the invader strain accounted for 50% of the infections in the population (Figure 3.10 c,f). This time was extremely long (>300 years) when the invader strain had low transmission advantage in the default scenario, and a transmission advantage of 50 percent was needed to bring it down to a median of 27 and 48 years in the low and high-prevalence setting, respectively (in comparison, the resident strain reached 50% of its steady-state prevalence in a median of 35 and 40 years in the low and high-prevalence cases; dashed gray lines). Allowing for dual infection again had the strongest impact at lower transmission advantage, followed by allowing for multiple peaks of acute-stage infectiousness.

To understand why the impact of repeated acute-stage infectivity depended on the initial prevalence of the resident strain, we calculated the contribution of superinfection events and acute-stage transmissions to the spread of the invader strain in the various scenarios (Figure 3.11). As expected, the contribution of superinfection was very low (<5%) in the low-prevalence setting, where most individuals were uninfected at the introduction of the invader strain; in contrast, many more transmissions (20% initially) involved superinfection of carriers of the resident virus in the high-prevalence setting (Figure 3.11 a). Because multiple acute peaks of infectiousness take effect only when superinfection occurs, their impact on the frequency of acute

transmissions was much stronger in the high-prevalence setting (Figure 3.11 b–c), and the increased frequency of efficient acute transmissions explains the reduced risk of extinction and faster growth of the invader strain when multiple acute peaks of infectivity were allowed in the high-prevalence scenario. In the high-prevalence setting (Figure 3.11 a), the relative contribution of superinfection decreases faster in the multiple acute scenario compared with the default scenario: the reason for this difference is that multiple acute peaks of infectiousness can substantially accelerate the outgrowth of the invader strain in the high-prevalence scenario (see Figure 3.12), and the decline of the resident strain results in a decreasing probability that the invader (super)infects an individual who carries the resident strain.

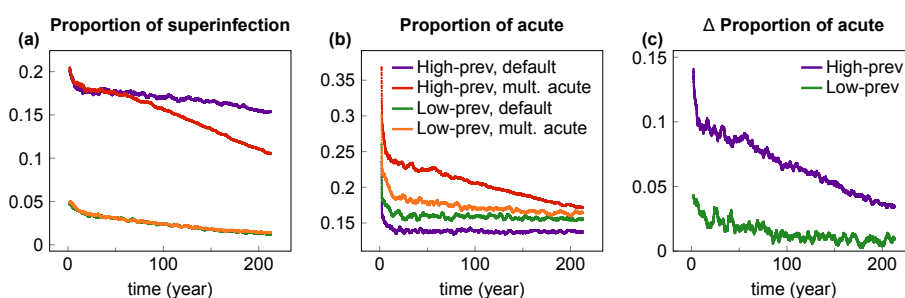


Figure 3.11: The contribution of superinfection events and acute-stage transmissions to the spread of the invader strain. (a) depicts the time course of the proportion of transmissions of the invader strain that involved superinfection of carriers of the resident virus. Coloured lines show smoothed proportion data for low and high prevalence epidemics using the default scenario, and the “multiple acute” scenario that allowed for repeated peaks of acute-stage infectiousness upon superinfection. In both scenarios, the contribution of superinfection was very low in the low-prevalence setting (green and orange lines), where most individuals were uninfected at the introduction of the invader strain; in contrast, many more transmissions involved superinfection in the high-prevalence setting (purple and red lines). (b) depicts the time course of the proportion of transmissions of the invader strain that originated from acute-stage transmitters in the four cases (colour coding is the same in a and b). (c) shows the difference in the proportion of acute-stage transmissions between the default and the multiple acute scenario for both prevalence settings (i.e. the distance between the red and purple, and between the green and yellow lines of Panel b). Allowing for multiple acute peaks of infectiousness greatly increased the proportion of acute-stage transmissions in the high-prevalence setting (purple line), but to a much lesser extent in the low-prevalence setting (green line). In all cases, time courses are plotted from the introduction of the invader strain into steady-state epidemics of the resident strain. Proportion data were calculated by combining transmission events recorded in 1000 simulation runs, then smoothed by averaging with a sliding window of length 100 weeks. Parameters were set as in Table 3.2; the transmission advantage of the invader strain was 5% in all cases.

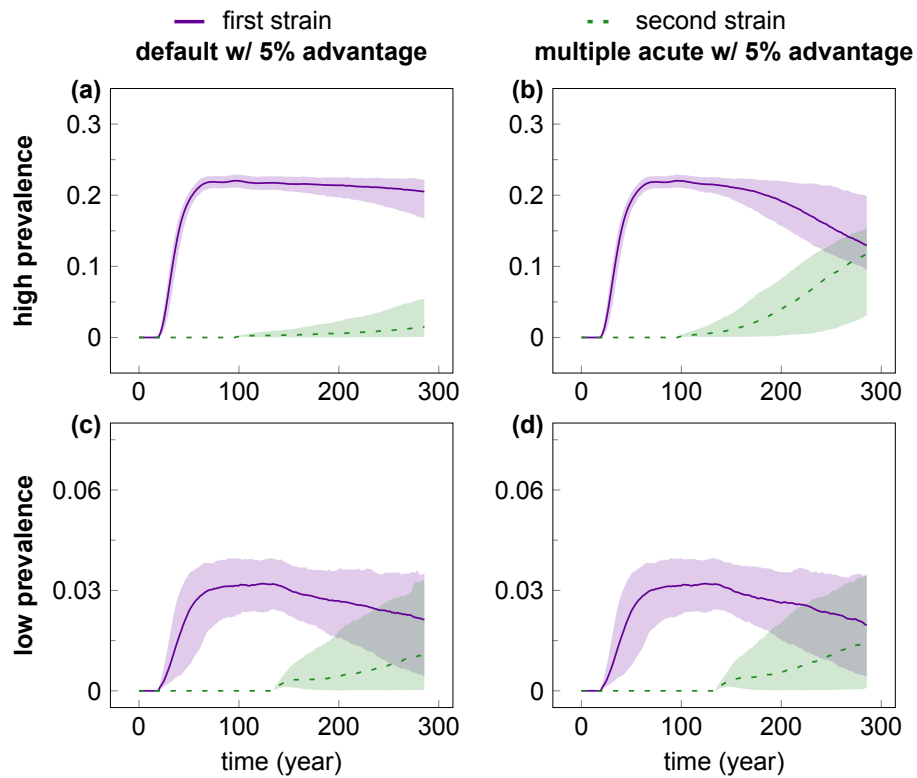


Figure 3.12: The effect of multiple acute infections on the competition of HIV strains. The figure compares the outgrowth of an invader virus with 5% transmission rate advantage in the high (top row) and low (bottom row) prevalence settings with default superinfection dynamics (left: a, c) or with repeated peaks of acute-stage infectiousness upon superinfection (right: b, d). The resident strain (solid purple line) was introduced in the population at Week 1000 (to allow the network to attain steady state); the invader strain (dashed green line) was introduced in the population when the first strain had already attained steady-state prevalence (at Week 5000 and 7000 for the high- and low-prevalence setting, respectively). Multiple acute peaks accelerate the outgrowth of the invader strain and the decline of the resident considerably in the high prevalence scenario (A vs. B), but not in the low prevalence scenario (c vs. d), where superinfection is rare. The lines show median prevalence from simulations where the invader strain did not go extinct (out of 1000 simulation runs); shading indicates the areas between the 5% and 95% quantiles. Simulation parameters were set as in Table 3.2; scenarios are described in detail in the main text.

3.3.4 Short head start or fast population turnover reduce first comer advantage

We next investigated what happens if the invader strain enters the population when the first strain is still in its growth phase and has not yet reached steady-state prevalence. We ran simulations where the invader was introduced when the resident

strain had attained 5%, 20% or 50% of its plateau prevalence level and compared the outcome to the previous default setting (Figure 3.13). As expected the first comer advantage was weaker when the second strain was introduced early in the growth phase of the first strain. However, the probability of extinction of the invader strain increased substantially already when the resident strain was at only 5% of its plateau level initially in the low-prevalence setting (3.13 d), or at 20% of plateau level in the high-prevalence setting (Figure 3.13 a). The time to 50% relative prevalence of the invader strain was strongly affected when the resident strain was initially at 5% of its plateau level in the high-prevalence setting (Figure 3.13 c), and at 20% of plateau level in the low-prevalence setting (Figure 3.13 f). We thus conclude that (depending on the prevalence setting) some aspects of the first comer advantage are established relatively early in the initial expansion of the first successful strain.

We also tested the effect of faster population turnover using a residence time of 20 years (as opposed to the default of 35 years) for uninfected individuals in the population. This scenario may apply to regions that experience intense population movements and/or high rates of non-AIDS mortality. Faster population turnover had little effect on the initial risk of extinction for the invader strain, but could substantially accelerate the rate of its growth in the simulation runs where it did not go extinct (Figure 3.14). The probability of extinction is influenced by the instantaneous availability of susceptible individuals, which is not affected by the rate of turnover (at a fixed population size); however, subsequent growth depends on the continuous supply of new susceptibles, which increases with the rate of population turnover.

3.3.5 Case study: The expansion of HIV-1 subtype A in Uganda

While the mechanisms of interference can slow down the invasion of new strains, the global pandemic is not static and major shifts between HIV lineages have been occurring in selected regions. The best-characterized example is the expansion of HIV-1 subtype A at the expense of subtype D in Eastern Africa [25], [61], [62], and we used the detailed data from Uganda [62] to derive a crude estimate for the transmission advantage required for the observed expansion. Between 1994 and 2002, the estimated prevalence of subtype D decreased from 11.9% to 8.1%, and the prevalence of subtype A increased from 2.8% to 3.0% in Uganda; the overall prevalence of HIV declined from 17% to 13% over the same period [62]. The overall decline probably reflects changes in risk behaviour and/or health interventions; with stable (17%) prevalence, the relative expansion of subtype A would roughly correspond to growing to

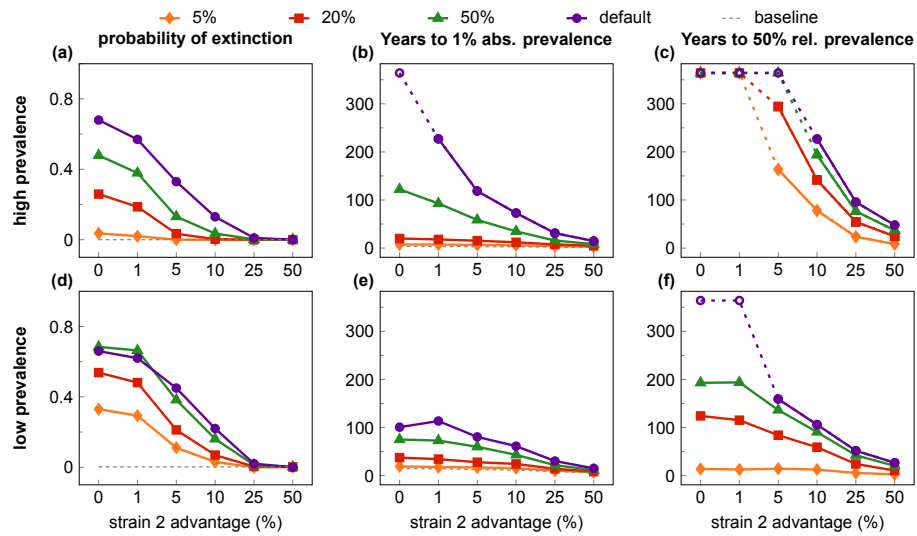


Figure 3.13: Quantifiers of the “first comer advantage” when the invader virus enters in the growth phase of the resident strain. Plotted are cases (coded by symbols and colour) where the invader was introduced when the resident strain had attained 5%, 20% or 50% of its plateau prevalence; in the default case the second virus was introduced at Week 7000/5000 in the low/high prevalence setting (as in Figure 3.10) when the resident strain had already reached a stable plateau in its prevalence. All quantifiers are plotted against the relative transmission rate advantage of the second (invader) strain. Rows show results from the high (top row) and low prevalence (bottom row) settings; columns depict three different quantifiers. First comer advantage is weaker when the invader enters at earlier stages of the growth of the initial strain. Dashed gray lines in a-b and d-e represent the growth of the resident virus without competition; with early introduction of the invader strain, 50% relative prevalence in C and F is attained well below plateau prevalence and therefore cannot be compared to the 50% point of single-virus epidemics as a baseline. Data in b-c and e-f depict medians from 1000 simulation runs (excluding those where the invader virus went extinct). Parameters are listed in Table 3.2; competition dynamics followed the default scenario in all cases. The maximum length of simulations was 19,000 weeks (365 years); empty symbols indicate where the invader strain did not reach the threshold prevalence by the end of the simulation in the majority of the cases.

3.9% (3.17/13) absolute prevalence, over a background prevalence comparable to that of our high-prevalence setting. Analyzing data from our high-prevalence default scenario, we found the closest match with the data when the transmission advantage of the invader strain was set to 25% (Figure 3.9 b), in which case the increase from 2.8% to 3.9% prevalence took 7.8 years on average (vs. 8 years in the empirical dataset). The rate of the relative expansion of subtype A observed in Uganda would thus require about 25% advantage over the resident subtype D strain, in a setting of stable overall prevalence in our simulations. Decreasing overall prevalence in the

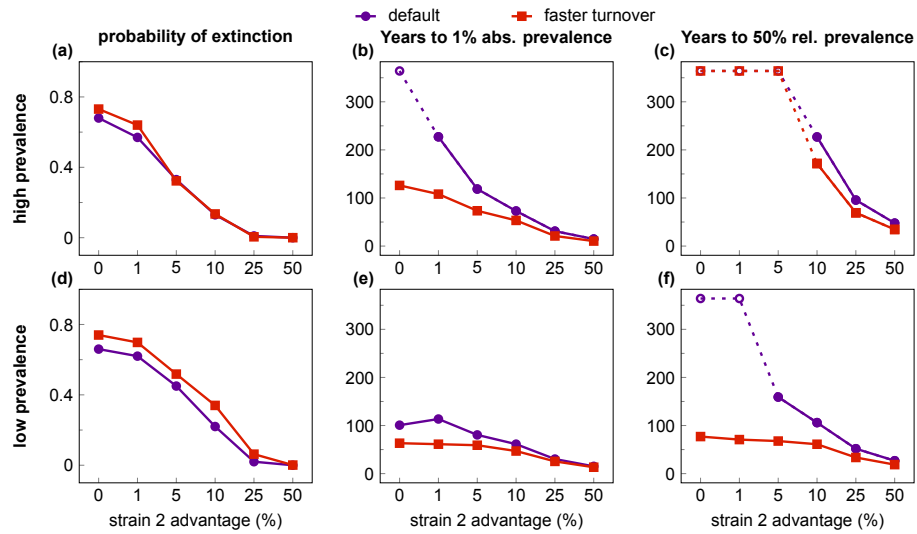


Figure 3.14: The effect of population turnover on the “first comer advantage”. All quantifiers are plotted against the relative transmission rate advantage of the second (invader) strain, for two levels of population turnover: 35 (default, purple dots) or 20 years (red squares) of uninfected (sexually active) lifespan, in the high (top row) and low (bottom row) prevalence settings. Faster turnover had little effect on the probability of extinction of the invader strain, but could have a pronounced effect on its rate of growth at low values of the transmission advantage. Data in b-c and e-f depict medians from 1000 simulation runs (excluding those where the invader virus went extinct). Parameters are listed in Table 3.2; superinfection and replacement dynamics followed the default scenario. The maximum length of simulations was 19,000 weeks (365 years); empty symbols indicate where the invader strain did not reach the threshold prevalence by the end of the simulation in the majority of the cases.

empirical data indicates a slowing turnover of infections, which requires a greater transmission advantage for the same tempo of strain replacement. This is roughly consistent with the independent empirical estimation that the overall (unadjusted) transmission rate of subtype A was 47% higher than that of subtype D in the same cohort [32].

3.4 Discussion

Both the probability and the rate of epidemic growth were strongly reduced for virus strains introduced into the steady state of a resident epidemic, when the default assumptions of partially inhibited superinfection and one-time acute peak of transmissibility were used in our simulations. To outgrow the resident strain over a few

decades (the time scale of human observations), the invader virus needed 25 percent or greater advantage in its rate of transmissibility over the resident strain. Of the three potential mechanisms of interference investigated, the direct inhibition of superinfection had the strongest effect in both prevalence settings, while one-time acute peak transmissibility had substantial effect only in the high-prevalence setting. The depletion of highly connected nodes in the network had little effect in most of the cases. In principle, a fourth mechanism of interference could also arise, because superinfected individuals (having progressed with their first infection) tend to have a shorter remaining lifespan, and therefore a shorter window of opportunity to transmit the superinfecting strain, compared with individuals who are infected for the first time. However, restarting the clock of disease progression upon superinfection had very little effect compared with the default scenario in a set of simulations (not shown); therefore, this mechanism does not seem to play an important role.

The reduction in the rate of growth of the invader strain was greater when the resident virus had higher initial prevalence, while the rate of extinction was insensitive to initial prevalence. The inhibition effect was weaker, but still considerable when the second strain was introduced while the first strain was still in the early phases of its growth, or if the (non-AIDS related) turnover of the population was faster.

Our results suggest that HIV competition dynamics is indeed characterized by a strong “first comer advantage” if the first strain to colonize a local transmission group expands to near plateau prevalence before further viral strains invade. This effect slows down the diversification of the epidemics and facilitates the persistence of founder effects. As far as we are aware, this is the first attempt to generally characterize the competition dynamics of different HIV strains over sexual networks, including multiple possible mechanisms of interference. The specific case of competition between HIV-1 and HIV-2 has been modelled in a similar framework [63], while another study looked at the competition of multiple evolving virus strains at the epidemic level without considering network structure [64]. Finally, Gross et al. [65] demonstrated that the inhibition of superinfection can preserve founder effects in the competition of equally transmissible virus strains, but have not considered network structure, alternative mechanisms of interference, or differential transmission.

The impact of the distinct mechanisms of interference may be modulated by factors that were not included in our simple model. First, heterogeneity may exist in the transmission rates across individuals and over time within the same partnership: in particular, per-contact transmission risk may decrease from the first exposures to

subsequent contacts within a serodiscordant partnership (independent of the effect of acute infection) [66], [67]. Such an effect can arise if the individuals highly susceptible to the virus of their partners tend to be rapidly infected, and the couples that remain serodiscordant become enriched in cases of low transmissibility over time (as reviewed in [68]). Similar effects are expected also if the partners of infected individuals can develop partially protective immunity to HIV in the exposures that do not result in transmission [69]–[71]. Irrespective of the mechanism, if time dependent variation in transmissibility is strain specific, then the invader virus has the advantage of being engaged in “first contact” with higher probability than the resident strain, which would decrease the first comer advantage of the latter. Second, if superinfection can generate a new “acute” temporary peak in viremia (and transmissibility) at least in some of the cases [46], then this mechanism of interference may also be weaker, which could reduce the first comer advantage (particularly in high-prevalence epidemics, according to our results). On the other hand, a detailed analysis of transmission risk in serodiscordant couples in Africa [43], and a recent phylodynamic analysis of a North American epidemic [44] have both estimated about 20-fold higher transmissibility during acute compared with chronic HIV infection. Using a 9-fold consensus estimate [56] we may thus have underestimated the interference effect if repeated “acute” peaks of transmissibility do not (or only rarely) occur after superinfection. Third, the observed partial inhibition of superinfection may not take effect until several months from the first infection [42], [72], e.g., if partially protective immune responses and/or a limiting depletion of target cells take a longer time to develop [42]. This would allow unhindered superinfection in the first few months after seroconversion, which would reduce the first comer advantage, especially if the second strain arrives while the first epidemic is still in its growth phase. Fourth, there is considerable debate on the strength of the (partial) protection from superinfection. Several studies have found zero or very low rates of superinfection [73], [74] (which would implicate strong protection against superinfection), while at the other extreme some studies have found rates of superinfection comparable to those of initial infection [72], [75], [76] (which would indicate little or no protection). The differences in the estimates may reflect genuine variation between the study populations, but also differences in study design, inclusion criteria and sensitivity of detection [46]. Importantly, deep sequencing methods allow the detection of superinfecting strains that grow only to low levels in the superinfected individuals (e.g., [75]), and may often be lost after a transient episode of superinfec-

tion [77]. Such low-level superinfection is likely to result in onward transmission of the minority variant with much lower probability compared with the baseline rate of transmission. In the context of population level spread and competition, superinfection is likely to be relevant only when the superinfecting strain grows to dominate the virus pool of the individual, which we approximated by allowing only strain replacement (and no co-existence) in the default scenario of our simulations. Relaxing this assumption and allowing for unhindered superinfection abrogated most of the first comer advantage in our results: we therefore conclude that the strong founder effects observed in the global phylogeography of HIV are more parsimoniously explained if superinfection is partially inhibited and the transmission of more than one strain from the same individual is rare.

Our generic modelling framework could not aim to account for all the (often population specific) complexities of human population dynamics and behaviour. For simplicity, population size was kept constant in our simulations, including instantaneous replacement of individuals who died of AIDS. With this implementation population turnover increased with HIV prevalence, e.g., the rate of death/replacement was about a third higher in the high-prevalence steady state compared with an uninfected population. Given that faster turnover reduces the first comer advantage, our results can be regarded as a conservative (under) estimation of the inhibition effect. Not replacing individuals who die of AIDS results in decreasing population size, which may further inhibit the expansion of invader strains by reducing the supply of susceptible individuals. In contrast, fast population growth or immigration may dilute the inhibition effect by increasing the influx of susceptible individuals. Migration may also play a role by introducing the same invading HIV strain repeatedly from a source population: this would eventually overcome the barrier of initial extinction, but would likely have little impact on the subsequent growth of the invader strain. Furthermore, an established HIV epidemic may also affect sexual behaviour: if high-risk sexual practices and/or promiscuity decrease in response to an ongoing epidemic, the spread of subsequent invader strains may be further inhibited. Finally, the complexities of the sexual network, e.g., assortative mating may further influence the strength of the inhibition effects.

Alternative or additional mechanisms may also contribute to the preservation of founder effects. If viral adaptation occurs to host traits that vary between human populations, then a locally adapted virus strain will enjoy a selection advantage against strains adapted to other host populations (as has been observed in some

model systems of host-parasite interactions [78], [79]). For example, the distribution of Human Leukocyte Antigen (HLA) alleles may differ between human populations, and local transmission may fix escape mutations against the locally frequent alleles that initially had a protective effect [80], particularly in populations with lower HLA diversity [81]; although this seems to be occurring slowly and to a limited extent where HLA diversity is high [82]–[84]. Location or population specific differences may exist in other host traits affecting HIV acquisition or transmission (e.g., in restriction factors [85], [86] or in other components of innate immunity [87]). Each locally adapted virus strain may therefore have a competitive advantage within its established host population, and a disadvantage in other populations—which would also slow down the global mixing of variants or could even result in the long term survival of several virus strains in different populations. We note, however, that long-term co-existence of several virus strains in the same epidemic (connected transmission group) is possible only if specific conditions are fulfilled, e.g., strain-specific immunity or therapy creates frequency-dependent selection that favours the rare type. Without such specific conditions, the strain with the highest transmission potential in a given host population drives all other strains extinct in the long run: this principle of competitive exclusion holds true from simple abstract mathematical models [88], [89] to complex simulations, including ours.

We parameterized our model based on data from generalized heterosexual epidemics in Africa, but it could easily be adapted to other routes of transmission and to concentrated epidemics. Furthermore, the results of our simulations can be applied not only to the competition of two distinct lineages (e.g., subtypes, or distinct clades of the same subtype [90]), but also to competition between virus variants that arise by local mutations. The general take-home message of our work posits that the expansion of the HIV pandemic to all susceptible populations across the world has made the conditions far less favourable for the spread of “novel” virus strains, irrespective of their origin.

Our results have important implications for understanding the past and for predicting the future of the HIV pandemic. The observed first comer advantage can delay evolution to “optimal virulence” [64], [91] that maximizes transmissibility, and can also delay the spread of drug resistance (by onward transmission [92]) in the face of increasing selection pressure from the broadening scope of ART. Widely available ART may affect resident and invader strains equally, effectively reducing the baseline rate of transmissions and transforming a high-prevalence setting towards lower

prevalence. Given that most aspects of the first comer advantage were strong in both low- and high-prevalence settings in our simulations, the broadening scope of ART may not affect this phenomenon strongly.

Because the mechanisms of first comer advantage do not operate at the front wave of an epidemic expanding into a susceptible population, we suggest that much of the (non-local) adaptation of HIV may have happened along these front waves, rather than in populations where prevalence has stabilized. Furthermore, considering that the currently dominant subtypes probably all expanded riding the wave of their first comer advantage, most or all of them may in fact possess suboptimal fitness and transmissibility. If the original founder strains of the early expansions were selected (at least partly) by “chance”, rather than due to high fitness, then even subsequent evolution may have constrained the subtypes to the local suboptima of the fitness landscape that were accessible from the initial sequence. This implies that the initial founder effects and the first comer advantage may have provided some benefit by preventing the fast global spread of the most transmissible HIV variants in the growth phase of the pandemic. However, the results also caution that the next stage of the pandemic may be characterized by a shift towards more transmissible strains over the slow time scales predicted by our model, and data from several regions indicate that this process has already started. HIV-1 subtype A is spreading at the expense of subtype D in Eastern Africa [25], [61], [62], and HIV-1 is expanding at the expense of HIV-2 in Western Africa [63], [93]. Our results suggest that these relatively fast replacements require a large selective advantage of the expanding strain. Indeed, subtype A is associated with higher transmissibility [32] and slower disease progression [34], [35] compared with subtype D, and HIV-2 has two orders of magnitude lower replicative capacity [94] and more than 3-fold lower per contact transmissibility [95] compared with HIV-1. In comparison, within individual patients the replicative fitness (a probable correlate of transmissibility) showed only about 10% variation between the fittest and the average viral genome in a study of untreated HIV-1 infected patients [96]. Our results indicate that variations of greater magnitude are needed to drive the relatively fast replacement dynamics of the few observed cases.

While differences are expected between the currently characterized subtypes, and those more efficient at transmission are slowly gaining ground at the expense of less transmissible subtypes, major innovations and potentially higher transmissibility may be more likely to arise from the complex diversity of HIV in Central Africa

and from the recombinant forms. CRFs probably emerged against the backdrop of established epidemics and their growth to detectable levels may indicate considerable selection advantage. The rapid growth of several CRFs in recent years [25], [97] is consistent with this concept and is therefore cause for concern for the future of the pandemic.

The interference mechanisms and first comer advantage demonstrated in this paper may also help explain why so few cross-species transmissions of SIV to humans were able to establish epidemic HIV lineages, and why no new major HIV types or groups have emerged since the middle of the 20th century [98]. It is possible that a successful reduction or elimination of the current HIV epidemic in Africa may, by eliminating the inhibiting competition effects, increase the risk for the emergence of new HIV lineages from novel cross-species transmissions.

Finally, we note that HIV may represent a rare combination of factors relevant for the observed first comer advantage: infection lasts and remains active for life; the inhibition of superinfection does not seem to be (strongly) strain specific [99] (as opposed to other infections with serotypes that elicit type specific immunity); and infected individuals remain in the contact network for many years. Taken together, these factors may imply that the first comer advantage, and its consequence of delayed global mixing, may be particularly strong for HIV and weaker for most other pathogens. For example, a persistent infection controlled by strain specific immunity would correspond approximately to our HIV scenario with no inhibition of superinfection, in which case most of the population level effect was lost in the simulations. Non-persistent infections would tip the balance further in favour of the novel strain, because individuals recovered from the initial infection would be susceptible to the novel strain while ceasing to transmit or be susceptible to the first strain.

In all, our results suggest that the interference mechanisms of competition, possibly aided by local adaptation, can slow down the adaptation of HIV at the population level, in spite of the huge evolutionary potential of the virus. These effects may explain why strong founder effects still persist several decades after the initial global expansion of the pandemic, and may hamper the ongoing adaptation of the virus to maximize its transmissibility and also slow down the spread of drug resistance.

3.5 Summary

Outside Africa, the global phylogeography of HIV is characterized by compartmentalized local epidemics that are typically dominated by a single subtype, which indicates strong founder effects. We hypothesized that the competition of viral strains at the epidemic level may involve an advantage of the resident strain that was the first to colonize a population. Such an effect would slow down the invasion of new strains and thus also the diversification of the epidemic.

We developed a stochastic agent-based modelling framework to simulate HIV epidemics over dynamic heterosexual contact networks. We simulated epidemics in which the second strain was introduced into a population where the first strain had established a steady-state epidemic, and assessed whether and on what time scale the second strain was able to spread in the population. Simulations were parameterized based on empirical data; we tested scenarios with varying levels of overall prevalence. The timescales of the framework were found to be congruent with the current HIV/AIDS epidemic.

The spread of the second strain occurred on a much slower time scale compared with the initial expansion of the first strain. With strains of equal transmission efficiency, the second strain was unable to invade on a time scale relevant for the history of the HIV pandemic. To become dominant over a time scale of decades, the second strain needed considerable (>25%) advantage in transmission efficiency over the resident strain. The inhibition effect was weaker if the second strain was introduced while the first strain was still in its growth phase. We also tested how possible mechanisms of interference (inhibition of superinfection, depletion of highly connected hubs in the network, one-time acute peak of infectiousness) contribute to the inhibition effect.

Our simulations confirmed a strong first comer advantage in the competition dynamics of HIV at the population level, which may explain the global phylogeography of the virus and may influence the future evolution of the pandemic.

4

Study 2: Collective motion of hierarchical herds

This chapter will present our study titled "Collective motion of groups of self-propelled particles following interactive leaders" [100] as an example of agent-based modelling. The study concerns itself with the modelling of the collective motion of hierarchical herds, that is herds that are made up from smaller groups of animals. In the next section we will overview the background literature needed to understand the different aspects of the problem and then present our specific motivation in creating the model. The rest of the sections of the chapter will present our work on the problem: the agent-based model we created, the results we obtained, and its discussion.

4.1 Background literature

4.1.1 Collective motion

Collective motion is the emergence of ordered motion in a system made up of many autonomous agents. Persistent motion is one of the hallmarks of animal life, yet recently several physical and chemical systems have been found which have self-propelled, interacting units. There are many questions we can ask about these systems. Are the observed phenomena unique to the particular systems, or are there some more general laws that these systems obey? Are these the same for physical, chemical and biological systems? How can we reproduce these motions? Can we build robots that exhibit collective motion or alter the behaviour of existing collective motion? Answering these questions promises advances in fields from animal husbandry to exploration. Collective motion is a subset of more general phenomena called collective behaviour, that has implications of the organisation of society, and as such, is of much interest.

4.1.2 The language of collective motion

The fundamental element of a collective motion system is the self-propelled particle (SPP) [101]. This is a point-like particle, that can change its velocity at will and has some internal energy reserve that allows for its movement. Since the SPP is a readily identifiable agent it is very straightforward to apply agent-based modelling to such a system and is indeed the more successful method, although there are works that go for continuous media approaches [102]. When modelling such systems, instead of physical forces different type of effective forces are taken into account, that often do not even have a force dimension. A system made up of such particles obviously will not conserve energy, momentum or angular momentum. Although an SPP model itself violates very basic physical laws, the systems they are modelling do not. Within a certain range of accelerations the model can be thought of as abstracting away from a unit's internal energy resources that it can use to propel itself and abstracting away from a unit transferring momentum and angular momentum to its environment during movement. Such as it is, most models do not take into account that very abrupt changes are simply not permitted by physical limitations even with the internal energy and the surrounding environment taken into account, but this is thought of as losing a bit of realism for greatly simplified models. Although details of the actual

environment is usually dropped, it is brought back through the introduction of some "thermal" noise acting on the particles.

Although SPP models are inherently non-equilibrium, they show some marked parallels with equilibrium statistical physics. In statistical physics the renormalization group method has shown that when a system undergoes a continuous phase transition, the particular details of the system in question become irrelevant and only a few relevant parameters remain. A system will have an order parameter, which measures the transition from one phase to the other and changes continuously, while the relevant parameters obey scaling laws at the point of transition. The values of the critical exponents with which these parameters scale allow for the classification of the different systems into universality classes. Remarkably, a very similar thing happens in SPP systems and both the order parameter and the scaling can be defined, implying that phase transitions in very different SPP systems should be very similar, as in equilibrium statistical physics [103].

4.1.3 Evidence

Collective motion has been observed from physical systems through cells to humans, but to quantitatively analyse and back up models with data each unit has to be tracked in space. This is a non-trivial task, since usually one must observe many units (up to the thousands in say starling flocks), which move rather fast in an open space and look very similar, although for example in bacteria, the space is confined and the observables slow, but on the other hand they are rather tiny.

Several techniques have been developed to record collective movement each suited for different scenarios. For cells, the particle image velocimetry method has been adapted (the method originally uses tracer particles added to a continuous media to track the velocity vector field of that media, based on the displacement of the particles). Bacteria have been tracked by using phase contrast microscopy to visualize them.

For larger animals, the unconfined space poses problems. For two dimensional movements, e.g. grazing herds aerial photography, or more recently flying drone based cameras were used to record the animal trajectories. In case of fish, which naturally move in three dimensions it is possible to build an aquarium that essentially forces them to move in two dimensions, making video tracking relatively easy. For three dimensional movement a single camera becomes rather problematic due to overlaps of individuals and in general the missing distance information. Fish are

more easily confined compared to birds, allowing for methods not viably for the latter. An early method for reconstructing the three dimensional movement of schools of fish was the shadow method, which used a grided background and the shadows of the fish on this background to determine positions of all the individuals. Later three orthogonally mounted video cameras were used to capture the trajectories of a school of fish.

For birds, such techniques are not possible, since most birds fly over much larger areas than is feasible to confine. To measure nearest neighbour distances in starlings stereoimaging techniques were used, although this did not make it possible to recover individual trajectories. The newest method, made possible by advances in the miniaturization of GPS and other animal-borne sensor technologies: each individual in a flock is supplied with a GPS receiver, which logs trajectories, although there are two shortcomings, first, the errors of the GPS signals are still quite large compared to bird-to-bird distances, especially in the vertical direction and that the time and resources needed to monitor a flock grows almost linearly with the size of the flock [103].

4.1.4 Simple two dimensional model of collective motion

The first quantitative treatise of collective motion was the Standard Vicsek Model (SVM), which first presented an SPP model described as a system would be in statistical physics [101]. The SVM describes a very simple system, that allows for two dimensional coherent motion to emerge from an initially disordered state and also shows phase transitions in two relevant parameters.

The system consists of N particles in a periodically bounded box of length L . The speed of the particles is constant and the same for all particles. The direction of the velocity is determined by the average velocity of other particles in their neighbourhood of radius r and a random noise. The velocities v_i and the positions x_i of the particles are updated simultaneously with the following equation

$$\mathbf{x}_i(t + \Delta t) = \mathbf{x}_i(t) + \mathbf{v}_i(t)\Delta t \quad (4.1)$$

where the speed of the velocity $v_i(t + \Delta t)$ is denoted by v and its direction is given by the formula

$$\vartheta_i(t + \Delta t) = \langle \vartheta(t) \rangle_r + \Delta \vartheta, \quad (4.2)$$

where $\langle \vartheta(t) \rangle_r$ is the average velocity of the particles within a radius r around the i^{th} particle and $\Delta\vartheta$ is a random noise drawn from the uniform distribution on the interval $[-\eta/2; \eta/2]$. Thus for a given L there are three independent parameters: η , v and the density $\rho = N/L^2$. The irrelevant parameters, which can be changed without the model exhibiting much change were set to fix values of $v = 0.03$, $\Delta t = 1$ and $r = 1$, and the initial condition was the random uniform distribution of particles in space and also the random uniform distribution of ϑ_i -s.

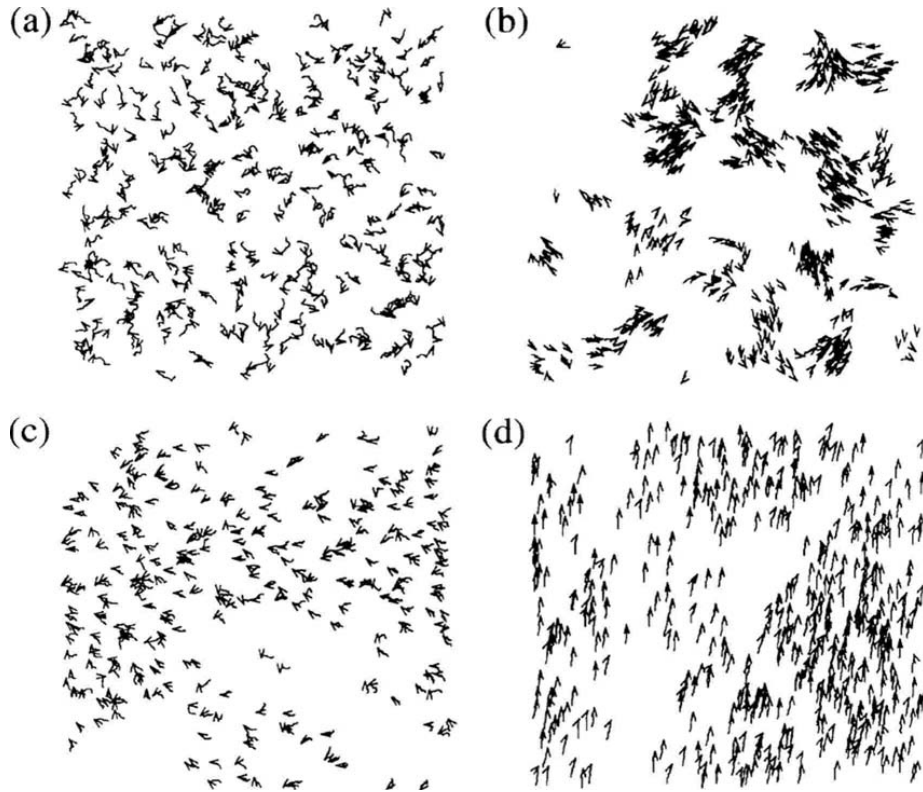


Figure 4.1: Trajectory segments of the SVM model for different values of ρ and η . (a) initial condition, (b) small ρ and η , (c) large ρ and η , (d) large ρ and small η (figure from [101]).

The model shows a continuous phase transition in ρ and η . The possible states are shown on Figure 4.1, where 20 steps of each particle's trajectory is plotted. We can see on a) the initial conditions, on b) that with low density and noise the particles form small groups, on c) that with large noise and density the particles basically move randomly, finally on d) that with large density and low noise all the particles go in the same direction.

The quantity

$$v_a = \frac{1}{Nv} \left| \sum_j \mathbf{v}_j \right| \quad (4.3)$$

serves as the order parameter since it is 0 when all particles are moving randomly, and is 1 when all particles are moving in the same direction. With this the critical exponents of the phase transition at $L \rightarrow \infty$ can be calculated given

$$v_a \sim (\eta_c(\rho) - \eta)^\beta \text{ and } v_a \sim (\rho - \rho_c(\eta))^\delta, \quad (4.4)$$

where $\rho_c(\eta)$ and $\eta_c(\rho)$ is the critical density and noise respectively, as $\beta = 0.45 \pm 0.07$ and $\delta = 0.35 \pm 0.06$.

As we can see, noise plays an important role in the SPP system, in that it can induce a phase transition from a disordered to an ordered state, in analogy with the temperature of equilibrium statistical physics. Moreover, in slightly more complicated systems noise can play an even more important part, as a certain level of noise can be a stabilizing factor for some system states. For example in [104] they found that adding attraction to the SPP model there are various motion patterns a group of SPP-s can produce, but some of these patterns are only stable when there is some noise in the system.

4.1.5 Collective motion of tissue cells

The study of Szabó et al. [105] is briefly introduced for two reasons, first, it is an example of trying to explicitly model an observed system and second, because it had a direct influence on our study. On Figure 4.2 we can see the observed system of tissue cells and their velocities. As predicted by the SVM, these cells undergo a phase transition from disordered movement to ordered collective movement as the density of the cells is increased.

Although the SVM predicts the behaviour the SVM's explicit averaging of the velocities of neighbouring cells would not be realistic, since cells very probably do not have receptors that would be able supply them with the necessary information to do the calculation. Instead, the collective motion must arise from the pairwise forces acting between the cells, thus in this model of cells each agent tries to align itself with the net forces acting on it.

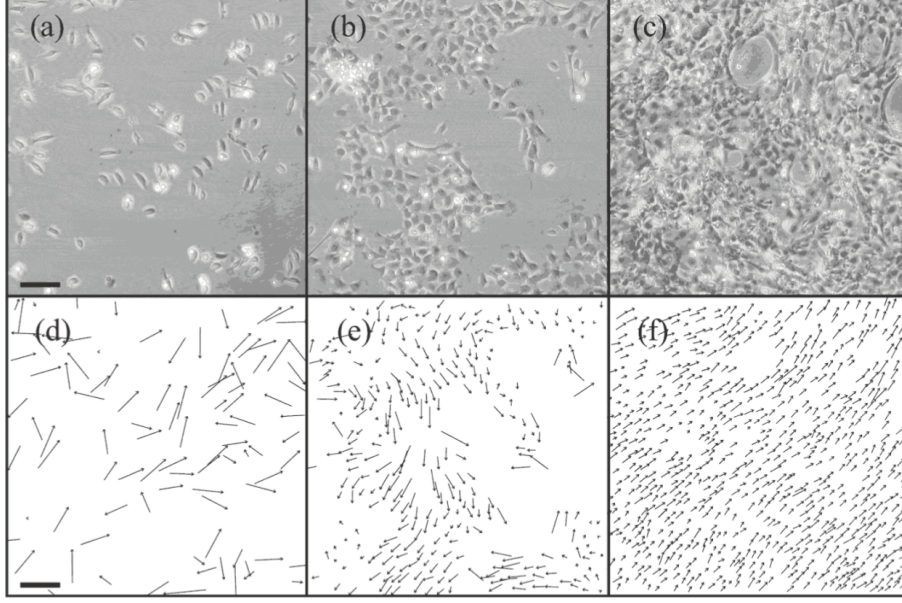


Figure 4.2: Phase contrast images showing the typical behaviour of cells for three different densities. (a) 1.8, (b) 5.3, (c) 14.7 cells/100x100 μm^2 . Observe that as cell density increases cell motility undergoes collective ordering. The speed of single cells is higher than that of cells moving in coherent groups. Scale bar: 200 μm . (d)-(f): Velocity of cells. Scale bar: 50 $\mu\text{m}/\text{min}$. Image and caption from [105].

The movement of the r_i cell is described by the overdamped dynamics:

$$\frac{d\mathbf{r}_i(t)}{dt} = v_0 \mathbf{n}_i(\theta_i(t)) + \sum_{j=1}^N \mathbf{F}(\mathbf{r}_i, \mathbf{r}_j), \quad (4.5)$$

thus each cell is trying to keep a self-propelled velocity (\mathbf{n}) of their own, while neighbouring cells exert forces on them. The self-propelled velocity slowly relaxes to the actual velocity thus:

$$\frac{d\theta_i^n(t)}{dt} = \frac{1}{\tau} \arcsin \left(\left[\mathbf{n}_i(t) \times \frac{\mathbf{v}_i(t)}{|\mathbf{v}_i(t)|} \right] \cdot \mathbf{e}_z \right) + \xi, \quad (4.6)$$

where ξ is a noise term and \mathbf{e}_z is a unit vector perpendicular to the plane of motion.

The pairwise forces are the most simple linear attractive and repulsive forces between defined by an equilibrium distance R_{eq} and a maximum interaction dis-

tance R_0 , while changing accordingly to the d_{ij} distances between cells:

$$\mathbf{F}(\mathbf{r}_i, \mathbf{r}_j) = \mathbf{e}_{ij} \times \begin{cases} F_{\text{rep.}} \frac{d_{ij} - R_{\text{eq.}}}{R_{\text{exteq.}}} & d_{ij} < R_{\text{eq.}}, \\ F_{\text{adh.}} \frac{d_{ij} - R_{\text{eq.}}}{R_0 - R_{\text{eq.}}} & R_{\text{eq.}} \leq d_{ij} \leq R_0, \\ 0 & R_0 < d_{ij}. \end{cases} \quad (4.7)$$

The critical behaviour of this system is very close to the SVM with $\beta = 0.44 \pm 0.08$ and $\delta = 0.38 \pm 0.07$ (cf. Equation (4.4)). This model adequately reproduces the observed behaviour of the cells, and also shows, that the explicit averaging of the SVM has very similar consequences as the gradual alignment to pairwise attraction and repulsion forces.

4.1.6 Coordinated stopping

In our previous study which is not part of the dissertation we have studied how a bias in the noise felt by the individual can enable coordinated stopping of SPP-s moving in a semi-2D system [106]. As we will later see, among our plans to continue research on the topic of this chapter is the stopping and starting of collective movement in herds, so we will briefly revisit our results on how the noise bias can be used to induce stopping.

The system is semi-2D in the sense that while it models the landing of birds, the movement in the horizontal plane is completely independent of vertical movements (bar actual landing), thus the landing can easily be interpreted as a stopping of some 2D motion.

The mechanism for the vertical motion (and subsequently, the landing) is as follows. The vertical position of a bird is updated as follows

$$z_i(t + \Delta t) = z_i(t) + v \frac{f_{z,i}^{\text{sum}}}{|f_{z,i}^{\text{sum}}|} \Delta t. \quad (4.8)$$

where the force $f_{z,i}^{\text{sum}}$ is the sum of the following parts: $f_{z,i}^a$ averaging over neighbouring birds' vertical velocities, $f_{z,i}^r$ repulsive force representing the empty space each animal keeps around itself, $f_{z,i}^h$ boundary which keeps the birds at a specified height and an $f_{z,i}^n$ noise.

The averaging is simply the mean of the vertical velocities over the birds in \mathcal{N}_i ,

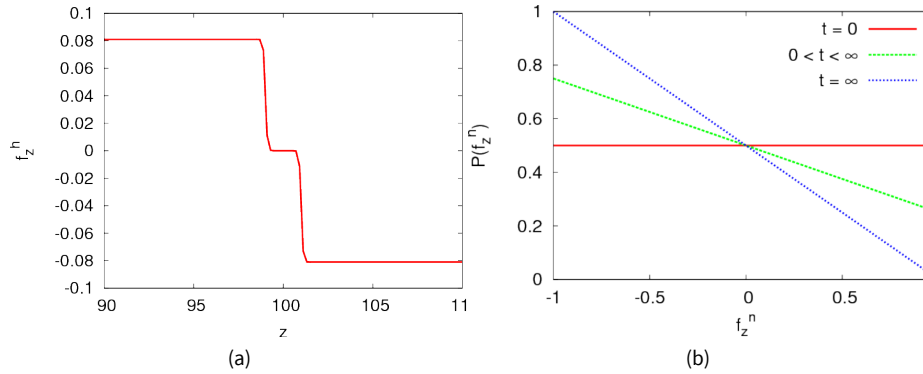


Figure 4.3: (a) The force f_z^h against z . The plot shows the small forceless regime around h and the fast strengthening of the force outside of that, quickly saturating to a constant. (b) The plot shows the time evolution of the probability distribution of f_z^n . Equation 4.12 is the explicit formula for generating values of this force. Figure from [106].

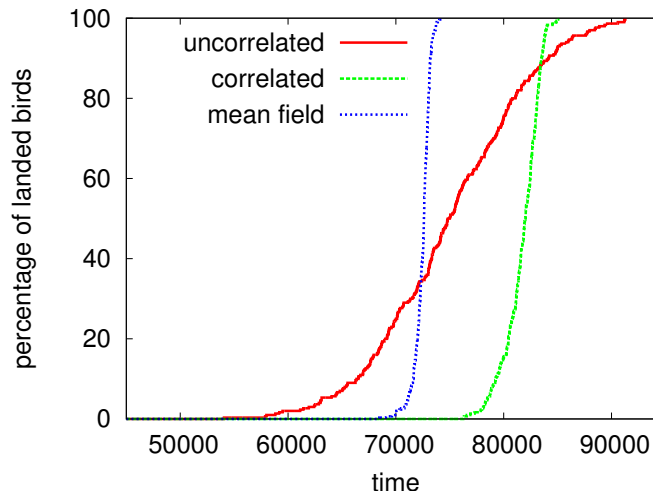


Figure 4.4: The percentage of landed birds as a function of time. The red curve corresponds to the case when coupling between the birds is absent, i.e., $f_z^a = 0$, the green one corresponds to the coupled case, while the blue curve is the mean field case, i.e., where the radius of \mathcal{N} is infinity instead of R . It is clearly seen that in the presence of coupling, the landing is much sharper *viz.* the synchronisation among the birds is much greater. It is also notable that increasing the radius of interaction to infinity does not make the landing process relevantly sharper, it merely decreases the time needed to make the decision to land. Figure from [106].

i.e. birds closer than a given distance measured in the horizontal plane.

$$f_{z,i}^a = \langle v_z \rangle_{\mathcal{N}_i} \quad (4.9)$$

The repulsive force represents the birds trying to keep a given minimal distance

$$f_{z,i}^r = \sum_{j=1}^N f_{z,ij}^r \quad (4.10)$$

where

$$f_{z,ij}^r = \left\{ \begin{array}{ll} A(d - |z_i - z_j|) & \text{if } 0 < |z_i - z_j| < d \\ 0 & \text{otherwise.} \end{array} \right\}. \quad (4.11)$$

The noise is given by the following formulas:

$$f_{z,i}^n(t) = \alpha \frac{1 - \sqrt{1 + 4\theta + 4\theta^2 - 8\xi_{z,i}(t)\theta}}{2\theta} \quad (4.12)$$

where

$$\theta = \frac{1}{2} \left\{ 1 + \exp\left(-\frac{t - t_i}{\tau}\right) \right\}. \quad (4.13)$$

In this each SPP is given a preferred stopping time t_i , which slowly biases the noise acting on them toward landing (see Figure 4.3). The force

$$f_{z,i}^h = -\frac{C}{20} \left[1 + \tanh \left\{ \frac{10}{R} \left(|z_i - h| - \frac{\Delta h}{2} \right) \right\} \right] \text{sign}(z_i - h), \quad (4.14)$$

keeps the SPP-s at a given height h . The bias, coupled through the averaging force is what creates the possibility of the SPP-s to overcome this force, creating the synchronisation effect. On Figure 4.4 we can see the effect of this synchronization, that is the landings of all the SPP-s happen over a much shorter period of time than it would without coupling and almost as fast, though later in time than it would for a mean field model (all SPP-s interacting with all other SPP-s). It is interesting to note, that in this model the inner states (t_i -s and θ -s), are not observable variables, only from their influence on actual behaviour allows other SPP-s to infer them.

4.1.7 Connection to network and control theory

Control theory concerns itself with the theory of influencing dynamical systems. If we imagine the flocking of some autonomous artificial agents (e.g. the more and

more popular drones), one can see the obvious problem. How to coordinate their movement? How to tell them to go left or right? Control theory is often expressed on networks with certain nodes effecting some other nodes and has extensively studied how the different network topologies influence the behaviours of systems. To apply such thinking to collective motion, we must induce a network topology, for which the most straightforward method is that each agent is a node and we draw edges between them, if the two agents interact. Obviously, this generates a time-dependent network, complicating matters, but nevertheless allows the harnessing of network and control theory in collective motion problems [103].

The above approach can be used to prove that consensus can be reached in a flocking scenario. Specifically if given a connected undirected graph (with an a_{ij} adjacency matrix) representing communication between agents of which each has a state x_i , the algorithm

$$\dot{x}_i(t) = \sum_{j \in N_i} a_{ij}(x_j(t) - x_i(t)) \quad (4.15)$$

asymptotically converges to an average consensus, i.e. to $x_1 = x_2 = \dots = x_N$, from any initial condition [107]. This means that as long as the flock can maintain a connected communication graph, they can reach consensus.

4.1.8 Leadership

In many species, individual recognition is most probably not possible, and collective motion seemingly arises on an egalitarian basis, since from the collective motion perspective, they are interchangeable, although even in these cases, leadership may arise from one or few individuals possessing some information not available to others. In other species, specifically in mammals, individual recognition is possible, and complex hierarchies emerge in their group structures. Although a natural assumption would be to point to the most dominant individual as a leader during collective motion, in many cases the identity and some inner state is responsible for leadership roles or leadership may be distributed among the group, with increased dominance levels giving increased influence during collective motion [103].

In ungulates leadership is often attributed to a single individual, yet a recent study [108] raises interesting questions about the validity of such a concept, based on observation of two groups of 12 and 6 Przewalski horses. Using different definitions of leadership (moving first, moving in front, or eliciting joining to move-

ment), no individuals that could be consistently classified as a leader were identified. Some limitations to that study are that several types of movements were not measured. In addition movements in the breeding season were also not measured; this was deemed problematic because in the breeding season the stallions directly elicit movements of their harems away from other stallions. Also, due to methodological reasons, only short periods of the day were observed. It has been shown in some cases that in the same group different type of leadership hierarchies might arise in different contexts [109], [110], and there are examples in nature where certain individuals in animal groups consistently act as leaders, for example in zebras and dolphins [111], [112]. Thus, although it is not very clear, how leadership works among these horses, the concept of a single leader can be valid for purposes of modelling.

It should be noted, that the concept of leadership, as we have just seen, is not exact. Leadership could mean starting movement, or leading movement, or for example leading from the back (although a common example of the alpha male wolf leading from the back of the pack is in fact not true [113]). Thus when reading the literature about leadership in actual systems attention must be paid to the exact type of leadership implied.

4.1.9 Motivation

Living in social structures with multiple levels of hierarchy is widespread in the animal kingdom [114], [115]. Examples range across several taxa, beginning with humans and primates [116], [117], through elephants [118], to whales [119], [120] and equids [121], [122]. There are numerous examples of subgroups forming around a single individual. For example groups may emerge around a matriarch from her descendants, like in african elephants [118], sperm whales [120], and killer whales [119]. Alternatively a reproductive unit may form around a breeding male with several breeding females and their young as in Przewalski horses [123] and plains zebras [122]. These breeding units can sometimes also include non-breeding males as well, like in hamadryas baboons [117] or geladas [124].

Our aim with the study presented in this chapter was to examine the way in which such a two-level hierarchy may spontaneously emerge in a group and what implications that hierarchy might have for the collective motion of the group. Our motivation and empirical basis was the collective motion of a Przewalski horse herd in light of group formation within the herd, aided by observations made in [125] at the Hor-

tobágy National Park in Hungary. As mentioned before, the Przewalski horse herd is split into harems, organized around a breeding male, with several breeding females and their young offspring. So-called bachelor groups, which consist of males that do not have their own harem are also present [126]. It should be noted, that although zebra harems form herds in the wild and have a very similar social structure to the Przewalski horse, the Przewalski herd at Hortobágy is only semi-wild as it lives in a bounded environment, which may force them into a herd. Although this has not been studied thoroughly, park officials reported, that the initial population did not form a herd, which only appeared after the growth of population density.

Both the collective motion of several different species of animals [103], and the emergence of hierarchy within the social system of the Przewalski horse [125] have already been modelled. Conversely, the collective motion of animals that are hierarchically organized into subgroups within a larger group have not been modelled. Thus, we aimed to construct a model of group formation and collective motion of a herd composed of sub-groups as a self-propelled particle model in two dimensions, where we identified leaders forming harems, and followers making up these harems. As we have discussed in subsection 4.1.8 that although attributing leadership to a single individual might not be applicable in all circumstances, it does have explanatory power in a wide range of scenarios. As such it stands to reason that conceptualizing the division between leaders and followers dichotomously helps simplify modelling at a minor cost. Simplifying modelling is helpful in the initial understanding of the type of collective movement of hierarchical herds as it abstractifies much of the ethological complications of a harem.

Herein we consider an earlier SPP model of collective cell movement introduced in Section 4.1.5 [105] and extend it with a two level hierarchy by introducing two distinct types of particles (i.e. leaders and followers) while simultaneously attempting to limit the increase in the number of parameters. In contrast with [125] the group formation is not driven by the environment of the herd, but by interactions dynamically evolving during the collective motion of the individuals. While formulating the model, we concentrated on mimicking the movements of Przewalski horses. While this specificity adds some complexity to our model, relative to what is usual in statistical physics, it is mostly related to nuances in movement and does not play a major factor in group formation, which was our main focus.

Our study could have potential implications for understanding how and why group formation occurs in nature, how group formation affects the system in which it

is happening and the rules governing collective motion in a two-level system. Inferring the universalities and the particulars of the different kind of mechanisms, could potentially be used to artificially control both living and human-made systems, such as domestically kept horse herds or flocks of drones.

4.2 Our model

The model is based on [105] in which a model was developed to depict the collective motion of cells. We modified this model to accommodate two types of SPP-s (leaders and followers), asymmetric interactions and group formation rules. While extending this model we aimed at minimizing the number of extra parameters. Compared with the usual SPP models the model of [105] gives smoother results due to intrinsic relaxation times. We choose parameters that allow the development of motion that resembles the movements of a herd made of harems as close as possible within the framework of the model. We provide a graphical overview of the model in Figure 4.5 and an introduction here.

The movements of the horses in the model are confined to a square area, large compared to the size of the herd, representing the herding area available to them (Figure 4.5 boundary). Periodic boundary conditions were not considered, first, because it is not realistic, and second, because it does not make sense in a co-moving herd to conceptualize that the front may interact with the rear. Also, we introduce a tendency for horses that stray too far from the herd to head back while still going in the general direction of the herd's (Figure 4.5 a)).

All horses may follow all other horses, but the strength of the interaction depends on the types and orientations of the SPP-s in question. Given, that it is plausible that leaders must also pay attention to followers, they will follow followers too, but to a much smaller extent than the other way around. Although the interactions taking place are based on metric distances, we introduce a directedness, meaning that a horse will follow the ones in front of it more than the ones behind it. Several types of interaction modes have been suggested in modelling collective motion. Early models used a simple metric distance, e.g., interacting with anybody nearer than a given distance [127]. Later topological distances were introduced, e.g., interacting with a fixed number of nearest neighbours [128]. Recently it has been proposed that the most biologically correct interaction ranges should be based on visual perception [129]. In our case, vision plays little part as equine vision is near 360° [130] and nei-

ther the distances within the herd nor the density of the herd imply that occlusion would have a major effect on interactions. As such, the effect of following the ones in front, rather than the ones behind is related more to the logic of not turning around if there are others heading in the same direction as oneself.

Leaders who acquire followers (i.e., a harem), will stay farther away from other leaders than if they were without followers (Figure 4.5 b) and c)). Harems are established based on spatial distance, but followers will gradually belong more and more to the leader they follow, making it easier for them to stay close, because of the stronger and slightly longer distance interactions with their leader than with another leader (Figure 4.5 d)).

Our model starts from randomized initial positions and velocities, without followers being assigned to any leader, thus all followers find groups and leaders at the same time. Our model forgoes the introduction of complex social rules by using only spatial interactions as described above and not taking into consideration that in reality, a new horse would be introduced to a herd already split into harems. On the other hand, taking the latter into consideration would not allow for the study of emergent group formation.

4.2.1 Formal model description

We have N_L number of leaders and N_F number of followers (the list of parameters can be found in Table 4.1). The 2-dimensional motion of the horse $i \in \{1, N = N_L + N_F\}$ is described by the overdamped dynamics

$$\frac{d\mathbf{r}_i(t)}{dt} = v_i^0 \mathbf{n}_i(\theta_i) + \sum_{\substack{j=1 \\ j \neq i}}^N \mathbf{F}_{\text{int}}(r_{ij}, \varphi_{ij}) + \mathbf{F}_{\text{com}}(\bar{\mathbf{r}} - \mathbf{r}_i, \bar{\mathbf{v}}) + \mathbf{F}_{\text{wall}}(\mathbf{r}_i, \mathbf{v}_i) + \boldsymbol{\xi} \quad (4.16)$$

where t is time, \mathbf{r}_i is the position of and \mathbf{v}_i is the velocity of horse i , v^0 is a preferred speed which differs for leaders and followers, \mathbf{n}_i is a unit vector characterized by the angle θ_i , \mathbf{F}_{int} is a pairwise interaction with $r_{ij} = |\mathbf{r}_i - \mathbf{r}_j|$ and φ_{ij} being the angle between $\mathbf{r}_i - \mathbf{r}_j$ and \mathbf{v}_i , \mathbf{F}_{com} is a global force dependant on the position ($\bar{\mathbf{r}}$) and the velocity ($\bar{\mathbf{v}}$) of the center of mass of the herd, \mathbf{F}_{wall} is the force acting at the boundaries and $\boldsymbol{\xi}$ is a vector whose components are delta-correlated white noise terms with zero mean.

The direction of the self-propelling velocity $\mathbf{n}_i(t)$, described by the angle $\theta_i(t)$, attempts to relax to $\mathbf{v}_i(t) = d\mathbf{r}_i(t)/dt$ with a relaxation time τ_i :

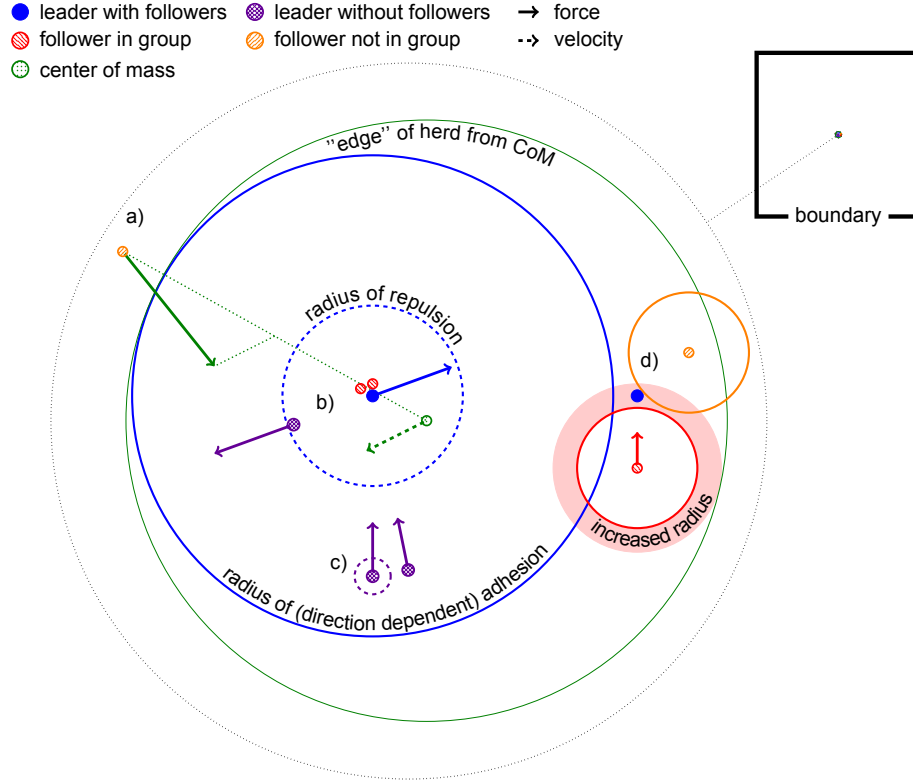


Figure 4.5: Graphical overview of the model depicting a small herd inside the boundary with various parts of $\mathbf{F}_{\text{int},r}(\mathbf{r}_i, \mathbf{r}_j)$ and \mathbf{F}_{com} shown. Radii are drawn to scale (cf. Table 4.1 for actual values), and the herd is magnified from within the boundary to show the forces. Solid arrows depict direction of forces, dashed arrows depict actual velocities. The following details are included: a) a horse farther from the center of mass than the given boundary (large green circle centred on the center of mass) will move towards the herd but also in the direction the herd is going, b) and c) leaders without groups can go closer to each other than to a leader with a group, while followers can go even closer to a leader, d) the attraction radius of the follower-leader interactions is generally smaller than that of the leader-leader interactions, but it is increased when interacting with the leader of the follower's group.

$$\frac{d\theta_i(t)}{dt} = \frac{1}{\tau_i} \arcsin \left[\left(\mathbf{n}_i(t) \times \frac{\mathbf{v}_i(t)}{|\mathbf{v}_i(t)|} \right) \cdot \mathbf{e}_z \right], \quad (4.17)$$

where \mathbf{e}_z is a unit vector orthogonal to the plane of motion, and τ_i differs for leaders and followers. This relaxation provides smooth transitions of the $\mathbf{n}_i(t)$ desired velocities. The value of τ was chosen larger for leaders than followers, implying that leaders are harder to "convince" than followers to change directions, but our results are not sensitive to changes in τ .

The $\mathbf{F}_{\text{int}}(r_{ij}, \varphi_{ij})$ force that carries the direct interaction between the horses can be split into the product of a spatial part ($\mathbf{F}_{\text{int},r}(r_{ij})$), and a coefficient part ($F_{\text{int},\varphi}(\varphi_{ij})$), the latter being dependent on the angle of the direction of horse j from horse i and the direction of the velocity of horse i . The spatial part consists of a pairwise, asymmetrical force, the direction of which lies on the line passing through the center of masses of the interacting horses and the magnitude of which is the function of the distance r_{ij} between the horses [105]. The actual form of the force depends on the type of horses involved:

$$\mathbf{F}_{\text{int},r}(r_{ij}) = \begin{cases} \mathbf{F}_{\text{LL}}(r_{ij}), & \text{if } i \text{ and } j \text{ are both leaders,} \\ \mathbf{F}_{\text{FL}}(r_{ij}), & \text{if } i \text{ is a follower and } j \text{ is leader,} \\ \mathbf{F}_{\text{LF}}(r_{ij}), & \text{if } i \text{ is a leader and } j \text{ is a follower,} \\ \mathbf{F}_{\text{FF}}(r_{ij}), & \text{if } i \text{ and } j \text{ are both followers.} \end{cases} \quad (4.18)$$

For all four cases there are two radii defined, R^{AT} which is the range of attraction, and a smaller radii R^{EX} , which is the range of repulsion, and also a distance L , which defines a distance inside R^{AT} but outside of R^{EX} , splitting the force into four parts depending on distance, namely a repulsive, an attractive and two non-interacting regimes, with different coefficients for all four types of interaction in both the interacting regimes (F^{AT} for the attractive and F^{EX} for the repulsive), thus having 8 radii with 8 coefficients and 4 distances. On the example of $\mathbf{F}_{\text{LF}}(r_{ij})$ the equations look like this (leader-leader and follower-leader interactions are slightly different):

$$\mathbf{F}_{\text{LF}}(\mathbf{r}_i, \mathbf{r}_j) = \mathbf{e}_{ij} \times \begin{cases} F_{\text{LF}}^{\text{EX}} \frac{r_{ij} - R_{\text{LF}}^{\text{EX}}}{R_{\text{LF}}^{\text{EX}}}, & r_{ij} < R_{\text{LF}}^{\text{EX}}, \\ 0, & R_{\text{LF}}^{\text{EX}} < r_{ij} < R_{\text{LF}}^{\text{EX}} + L_{\text{LF}}, \\ F_{\text{LF}}^{\text{AT}} \frac{r_{ij} - R_{\text{LF}}^{\text{EX}}}{R_{\text{LF}}^{\text{AT}} - R_{\text{LF}}^{\text{EX}} - L_{\text{LF}}}, & R_{\text{LF}}^{\text{EX}} + L_{\text{LF}} \leq r_{ij} \leq R_{\text{LF}}^{\text{AT}}, \\ 0, & R_{\text{LF}}^{\text{AT}} < r_{ij}, \end{cases} \quad (4.19)$$

where $\mathbf{e}_{ij} = (\mathbf{r}_i - \mathbf{r}_j)/r_{ij}$. The non-interacting part between R^{EX} and R^{AT} was chosen to be very small its only function being is to remove some "vibrations" that arise at such low densities, when a horse is on the edge of the attractive and repulsive regimes. The form of the force is one of the simplest ways to define gradually growing forces based on distances and the values of the specific parameters were chosen to imitate that leaders with harems wish to protect their followers from other lead-

ers, while bachelor leaders themselves can create groups.

In the cases of leader-leader (F_{LL}) and follower-leader (F_{FL}) interaction this picture is slightly changed due to the formation of groups. Followers will develop a certain amount of affinity to leaders who are close by, that increases in strength when they are close to the leader and decreases when they are farther away from the leader. Each follower keeps track of time spent near each leader with the quantities $D_{ij} \in [0, \infty]$, which follow the simple dynamics

$$\frac{dD_{ij}}{dt} = \begin{cases} +1, & r_{ij} \leq R_{LF}^{AT}, \\ -1, & r_{ij} > R_{LF}^{AT} \text{ and } D_{ij} > 0, \\ 0, & r_{ij} > R_{LF}^{AT} \text{ and } D_{ij} \leq 0. \end{cases} \quad (4.20)$$

This is then translated into an affinity

$$A_{ij} = 2A \left(\frac{1}{1 + \exp\left(\frac{-D_{ij}}{\tau_A}\right)} - 0.5 \right) + 1, \quad (4.21)$$

where τ_A is the characteristic time of affinity increase and A is a constant. The form of Equation (4.21) was chosen so that A_{ij} goes smoothly from $1 \rightarrow A+1$ as D_{ij} goes from $0 \rightarrow \infty$. This effectively changes the parameters in Equation (4.19) (but not in Equation (4.20)!) for the F_{FL} case from $F_{FL}^{AT} \rightarrow A_{ij}F_{FL}^{AT}$ and from $R_{LF}^{AT} \rightarrow A_{ij}R_{LF}^{AT}$. This allows a follower to split farther from the leader it belongs to, without leaving the harem, thus introducing more consistency into the group compositions.

The definition of groups is based on the values D_{ij} . Every follower is considered to be in the group of the leader for which the value of D_{ij} is largest for the given follower. The leader-leader interaction differs in one aspect if either of the participating leaders have a group, by effectively increasing the repulsive radius R_{LL}^{EX} of both leaders fivefold when interacting with each other. As such two leaders can be close to each other only if they don't each have their own groups. This is reminiscent of the distinction between bachelor groups, where males are close together and harems, where the males are farther apart.

The velocity dependent part is the same for both leaders and followers:

$$F_{int,\varphi}(\varphi_{ij}) = \frac{-1}{1 + \exp(-4(\varphi_{ij} - \frac{\pi}{2}))} + 1, \quad (4.22)$$

which effectively means, that a horse will pay more attention to horses that are in

front of it, rather than those that are behind it. The form was chosen because of the saturation properties. The total interaction is thus

$$\mathbf{F}_{\text{int}}(r_{ij}, \varphi_{ij}) = F_{\text{int},\varphi}(\varphi_{ij})\mathbf{F}_{\text{int},r}(r_{ij}). \quad (4.23)$$

The force \mathbf{F}_{com} keeps the herd roughly together, since if one strays farther than R_{com} from the center of mass of the herd it will experience the force

$$\mathbf{F}_{\text{com}}(\bar{\mathbf{r}} - \mathbf{r}_i, \bar{\mathbf{v}}) = F_{\text{com}} \frac{|\mathbf{r}_i - \bar{\mathbf{r}}| - R_{\text{com}}}{R_{\text{com}}} \left(\frac{\bar{\mathbf{r}} - \mathbf{r}_i}{|\bar{\mathbf{r}} - \mathbf{r}_i|} + \beta \frac{\bar{\mathbf{v}}}{|\bar{\mathbf{v}}|} \right), \quad (4.24)$$

where β is parameter that tunes how much the horse is guided in the direction the center of mass is heading and F_{com} is the overall strength of the force. Since R_{com} is relatively large this force is usually inactive, but will smoothly guide a lost horse back into the herd (adopted from [131], see Figure 4.6).

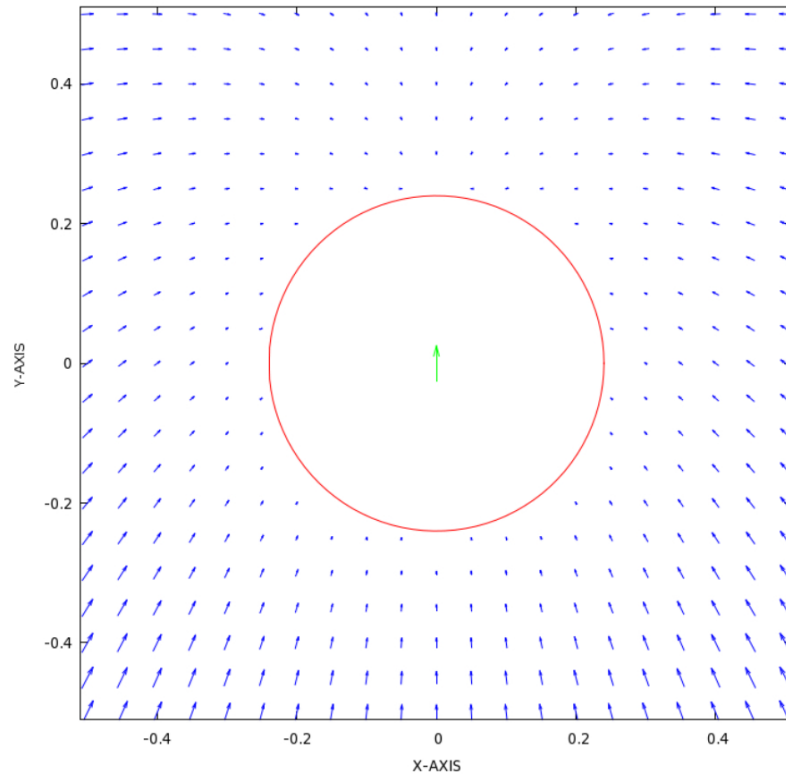


Figure 4.6: Snapshot of the force \mathbf{F}_{com} with $\beta = 0.75$ and the velocity of the center of mass of the flock pointing along Y axis. The force guides any stray members of the flock smoothly back with the forces growing proportionally away and back from the center of mass. Figure from [131].

The force \mathbf{F}_{wall} sets the boundary conditions. The herd is confined to a square area defined by the length D . This box is impenetrable and horses cannot leave it. For the herd to approach this hard boundary in a realistic way, there is a characteristic distance R_{wall} where the force \mathbf{F}_{wall} is turned on:

$$\mathbf{F}_{\text{wall}}(\mathbf{r}_i, \mathbf{v}_i) = \frac{F_{\text{wall}}}{2} \left(\sin \left[\pi \left(\frac{R_{\text{wall}} - d_{iw}}{R_{\text{wall}}} - \frac{1}{2} \right) \right] + 1 \right) \begin{pmatrix} \mathbf{v}_i \cdot \mathbf{n}_w \\ \mathbf{v}_i \cdot \mathbf{t}_w \end{pmatrix}, \quad (4.25)$$

where d_{iw} is the distance of the horse from the boundary, \mathbf{n}_w is the normal vector of the boundary and \mathbf{t}_w is the tangent vector of the boundary, driving the horses smoothly along the wall (adopted from [132] and [133]).

Initially both leaders and followers are evenly distributed over a square with a linear size of 500, with velocities also randomly distributed.

4.2.2 Parameters

Going, in a naïve way, from the one-type-particle model of [105] to the two-type-particle model would increase the number of required parameters from 14 to 30 (some parameters are doubled and some are increased fourfold given every possible combination of the particles). By considering that some of these are unnecessary to duplicate (or make four of) our model has 23 parameters. Of these only 7 are relevant in the sense that the formation of meaningful groups is sensitive to their value (parameters that would destroy cohesion even in a one-type-particle model were not taken into account), not considering the size of the herd. A parameter was considered relevant if an increase by twofold or a decrease by half resulted in 0.1% of followers not being in a group on average (this is less than one per a realization of the model). For a complete list of parameters see Table 4.1. Parameters were chosen so that cohesive movement occurs and that group formation happens. Except for cases where there was a reason to do otherwise, parameters that could be different for leaders and follower were kept the same. The distances were chosen based on observations, the coefficients of the various forces were chosen so that the phenomenology of the movements resembles that of a real herd. The leaders are slightly faster than followers so that they are able to stay in front of their harem. It must be noted, that in many cases, leaders in real-life examples may not be at the front of their group, but rather at the side or behind; we elected to use the leading-from-

front paradigm for the purpose of simplicity. Other choices pertaining to parameter value selection have been mentioned in the previous section describing the model.

4.3 Results

Our model, with the given parameters, produces a cohesive and ordered motion of the entire herd, while forming groups around leaders and also bachelor groups from group-less leaders. This is in qualitative agreement with the actual observed herd moving on an open plane and as an interesting extra phenomenon, our model also includes “fights” between leaders for followers. By “fights” we mean a situation where two or more leaders without groups get extremely close to one or more followers and after a short time, one of the leaders “wins”, i.e. a follower is ascribed to be in the leader’s group for long enough for it to chase away the other leaders (see video 1 on the CD supplement and Figure 4.10).

We found that the forming of groups within the herd causes cohesiveness to drop compared to a case without groups. We also found, that in accordance with but with a greater precision than the previous study, the group size distribution of the horses living in the Hortobágy National Park is lognormal. In contrast to this, the current model, based solely on spatial interactions, gives a normal distribution, which implies that spatial interactions alone are not enough to produce the observed group structure.

4.3.1 Cohesiveness of the herd

Starting from uniform random initial positions and velocities of the individuals, after sufficient time, the model develops ordered motion throughout the herd while forming groups and thus arriving at a structured and co-moving herd (see Figure 4.7 and video 2 on the CD supplement). We assumed that during collective migration the horses cannot stop, thus there are two phases of ordered movement: translational movement, and collective rotation about the – otherwise slowly moving – center of mass (see also Figure 4.9). Indeed, when it is not possible to stop (e.g. due to fear), but is not feasible or desirable to move the herd as a whole, herding mammals have been observed to rotate around a common point. To measure translational cohesiveness we use the following translational order parameter

variable	description	default value	approx. dimensions
relevant variables			
A	affinity of followers for leaders	1.3	1.3
τ_A	characteristic time of affinity	500	218 s
F_{FL}^{AT}	strength of F-L attraction	0.03	0.0125 m/s
R_{LL}^{AT}	radius of L-L attraction	200	36 m
R_{LL}^{EX}	radius of L-L repulsion	15	2.7 m
$R_{LL}^{EX}, 5R_{LL}^{EX}$	–	75	13.6 m
F_{LL}^{AT}, F_{LF}^{AT}	strength of L-L and L-F attraction	0.01	0.0042 m/s
N_L	number of leaders	25	25
N_F	number of followers	175	175
irrelevant variables			
F_{FF}^{AT}	strength of F-F attraction	0.0002	0.000083 m/s
F_{LL}^{EX}	strength of L-L repulsion	2	0.83 m/s
v_L^0	velocity of leaders	1	0.416 m/s
v_F^0	velocity of followers	0.9	0.375 m/s
τ_L	L velocity relaxation time	3	1.31 s
τ_F	F velocity relaxation time	1	0.44 s
ξ	strength of the noise	0.5	0.21 m/s
$L_{LL}, L_{LF}, L_{FL}, L_{FF}$	non-interaction distances	1	0.18 m
$R_{LF}^{AT}, R_{FL}^{AT}, R_{FF}^{AT}$	radii of attraction	50	9.1 m
$R_{LF}^{EX}, R_{FL}^{EX}, R_{FF}^{EX}$	radii of repulsion	5	0.9 m
$F_{LF}^{EX}, F_{FL}^{EX}, F_{FF}^{EX}$	strength of repulsion	5	2.08 m/s
R_{com}	radius of the cohesion force	250	45.5 m
F_{com}	strength of the cohesion force	2.5	1 m/s
β	cohesion force parameter	0.01	0.01
F_{wall}	strength of boundary repulsion	3	1.25 m/s
R_{wall}	distance of boundary repulsion	200	36.4 m
D	linear size of bounding box	10000	1800 m

Table 4.1: Table of the parameters of the model grouped according to relevancy in group formation. L and F abbreviate leader and follower respectively. The approximate proper dimensions are based on a comparison with observed horses, see Section 4.3.3 for details.

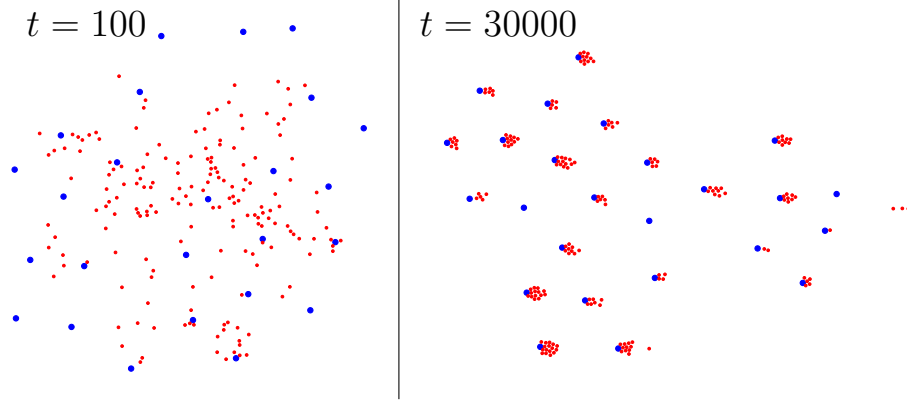


Figure 4.7: Starting from a uniform random distribution of positions and velocities (left side) the herd forms groups and exhibits ordered motion (right side). Blue dots represent leaders and red dots represent followers (see Supplementary video 2 for a video example).

$$\Phi_t = \frac{1}{N} \left| \sum_{i=1}^N \frac{\mathbf{v}_i}{|\mathbf{v}_i|} \right|, \quad (4.26)$$

and to measure the rotational cohesiveness we introduce the following rotational order parameter

$$\Phi_c = \frac{1}{N} \sum_{i=1}^N \mathcal{P} \left(\frac{\mathbf{v}_i}{|\mathbf{v}_i|} \right), \quad (4.27)$$

where \mathcal{P} denotes projection onto the normal of the line going through r_i and \bar{r} .

Going from a totally disordered translational movement to totally ordered translational movement Φ_t will grow from 0 to 1, while Φ_c will move from -1 to 1, as the system moves from a totally ordered rotation around the center of mass in one direction, through no collective rotation to totally ordered rotation in the other direction.

We found that the system, with parameters given in Table 4.1 switches between two modes, one of ordered rotation and one of ordered translational motion (see Figure 4.8 and video 3 on the CD supplement for an example of a transition from rotational to translational motion). Since the horses in the model do not have the capacity to stop, in an event of indecision about the direction to move they must rotate about a common axis, namely the center of mass. By averaging over the full length of 1000 runs in total, we found that the rotations have no specific direction, as expected (Mann-Whitney U-test, $p = 0.96$ on left-right similarity).

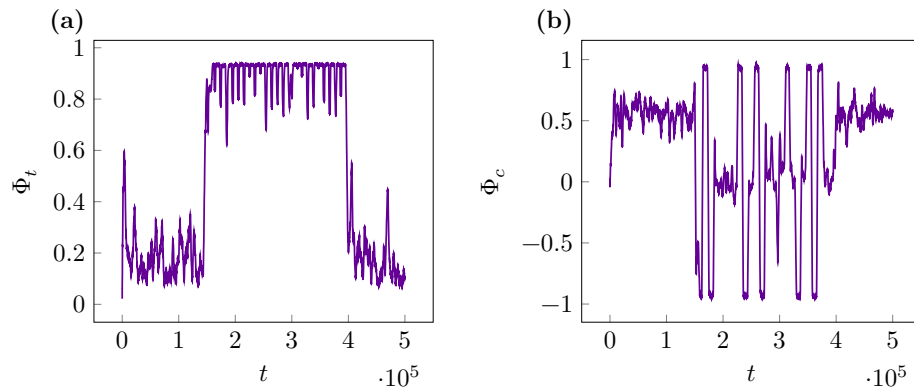


Figure 4.8: The herd as a whole either exhibits an ordered translational motion or rotates around a slowly drifting center of mass. These two different types of motions can be distinguished due to the values of the translational (a) and rotational (b) order parameters. The plots are from the same specific run of the model, with the curves smoothed by a window of $\Delta t = 1000$. The spikes during the translational phase are caused by the confining wall (see video 4 on the CD supplement for a sample of an interaction with the wall).

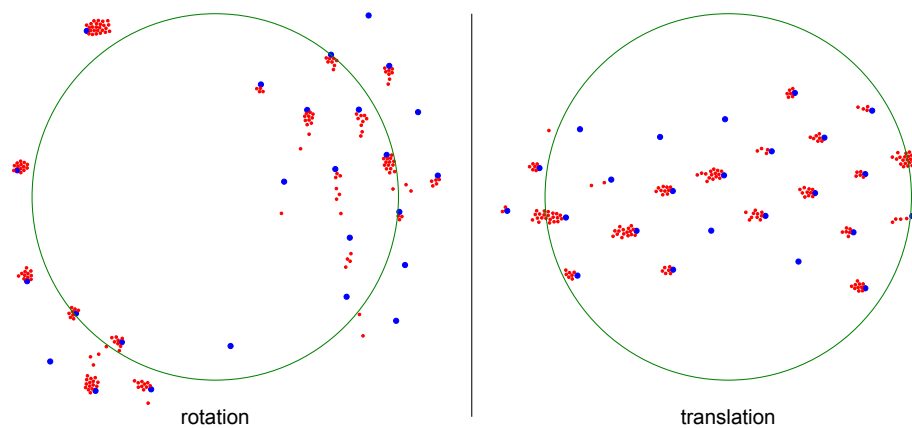


Figure 4.9: A rotational and a translational phase of two specific instances of the simulations with the boundary of the force \mathbf{F}_{com} (see Equation 4.24) shown in green. Large blue dots represent leaders and small red dots represent followers. During translation movement the main function of \mathbf{F}_{com} is to keep stragglers within the herd, while during rotation we see that while one part of the herd would go one way, the other part another, and the force keeps them together while the two groups otherwise do not interact too much.

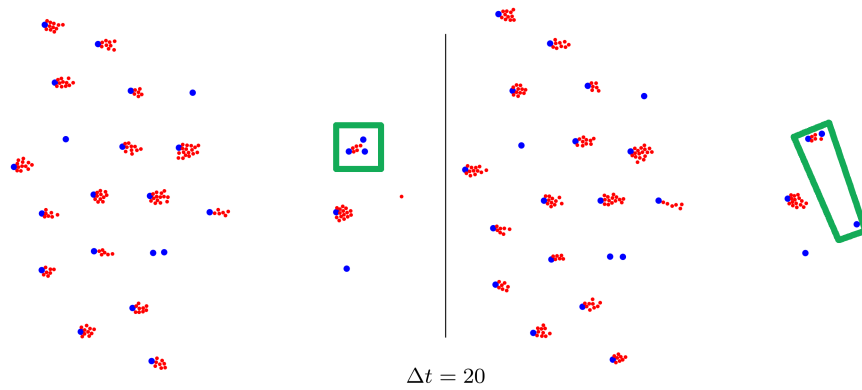


Figure 4.10: More than one leader without a follower may be drawn to followers. In this case one of them will ultimately succeed in gaining the follower in its "harem", while the losers are "fought" off to a distance. See the green bordered group with three leaders (large blue dots) crowding around some followers (small red dots), where one of them is driven off rather fast. Eventually, one of the remaining two will win. Time progresses from the left side of the image to the right side, in a specific instance of the simulations.

Calculating the pair-correlation function

$$\rho(\mathbf{r}) = \langle \delta(\mathbf{r} - \mathbf{r}_i) \rangle, \quad (4.28)$$

for the leaders in the normal scenario (i.e. where followers are present) and in the scenario where followers are missing, we find that the main structure of the herd is given by the leaders, and introducing followers only slightly loosens this (aside from the fact that it increases the distances between the leaders, see Figure 4.11). We also investigated the effect of introducing followers among the leaders on the order parameter of the translational movement. Comparing Φ_t (calculated using only the velocities of the leaders in two cases, one where there are only leaders and one where there are also followers) we find that order is decreased when allowing for followers and forming of groups (see Table 4.2). This loss in the efficiency of the movement of the herd as a whole points to benefits gained from social groupings outside the paradigm of simple locomotion.

4.3.2 Group size distribution

Starting from a uniform random spatial distribution and group-less state, the model, after sufficient time, will produce co-moving groups based on the relative positions of leaders and followers. The emerging group size distribution is normal, although

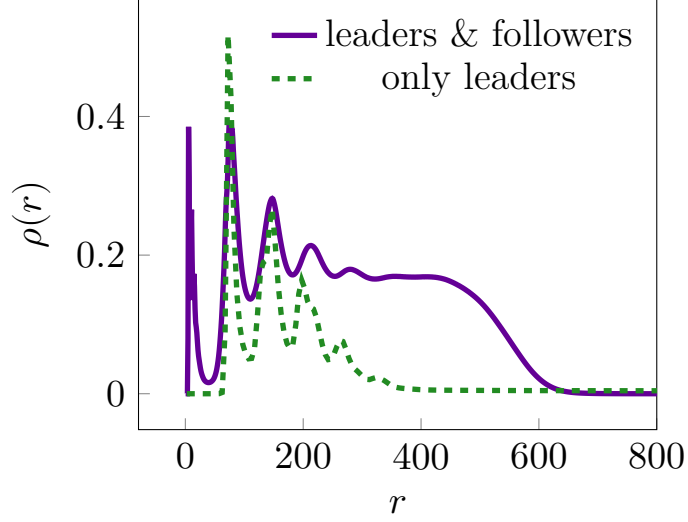


Figure 4.11: The pair-correlation for a herd composed of leaders and followers, but only calculated on the leaders (solid line), and in the case where only leaders are present (striped line). In the latter case the distances are scaled with R_{LL}^{*EX}/R_{LL}^{EX} , to compensate for the effect of no leader having a group (leaders without followers can be closer to each other than ones with followers). The main structure of the herd, even with followers, is set by the leaders, but the presence of followers slackens the rigidity of this structure.

	$\langle \Phi_t \rangle$	$\langle \Phi_t \rangle$ (only leaders)	$\langle \Phi_c \rangle$	$\langle \Phi_c \rangle$ (only leaders)
w/o followers	0.866 ± 0.016	-	-0.002 ± 0.011	-
with followers	0.608 ± 0.018	0.633 ± 0.017	0.025 ± 0.020	0.026 ± 0.021

Table 4.2: The translational and rotational order parameters averaged over 120 simulations with standard errors. The duration of the runs were many times longer than the stabilization of groups. The first row is from simulations where only leaders were present, the second row is the full model with followers. In this case the averages were calculated on the whole herd as well as on the leaders only. Adding followers and thus moving in groups decreases the order of translational movement, implying that group formation has benefits other than increased herd cohesion. Although the herd would rotate often, as expected, there is no specific direction of the rotation (Mann-Whitney U-test on 1000 runs, where the simulations was terminated at a time not long after stabilization of groups yields a $p = 0.96$ on left-rigth similarity).

some leaders and followers may not belong to a group. We define groups by the highest (non-zero) D_{ij} values of the followers, i.e a group consists of the leader and the followers with their highest D_{ij} rating corresponding to this leader. This effectively means that groups are formed by followers spending the most time with a specific

leader. The group size distribution rapidly reaches a close-to-final state and after some time relaxes to the final state (see Figure 4.12). We show the transition by creating a histogram of the group sizes at regular intervals during a simulation and taking the sum of the differences of each respective bin of the histogram in two consecutive measurements, averaged over 1000 independent simulations .

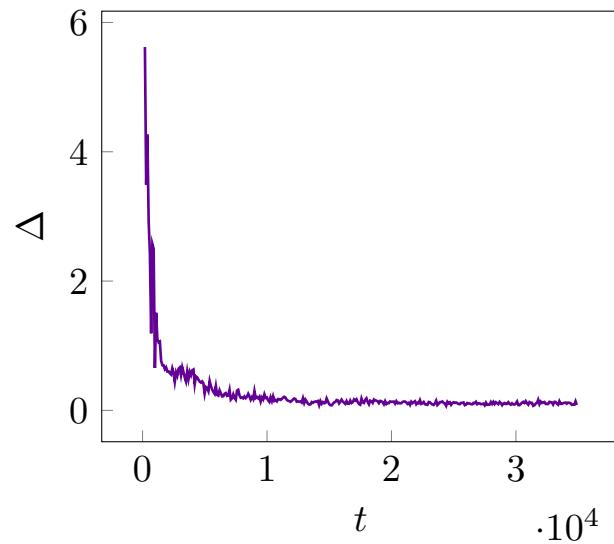


Figure 4.12: The group size distribution quickly stabilizes as it is shown by the plot of Δ . To calculate Δ we create a histogram of the group sizes at regular intervals during a simulation and take the sum of the differences of each respective bin of the histogram in two consecutive measurements. Each point is averaged over 1000 independent simulations.

On Figure 4.13 we show a comparison of the simulated distribution with real data obtained from a Przewalski horse herd (see [125] for details). Since harem sizes gradually change over time among the horses, the real data has been improved by taking into account historical harem size distributions, showing a more clear lognormal distribution than in the previous study of [125]. In this previous study a network model was formulated to account for the lognormal distribution of the group sizes, while the current model, based on purely spatial interactions was not able to reproduce this. This indicates that at this level of complexity, it is not possible to reduce social interactions to spatial interactions.

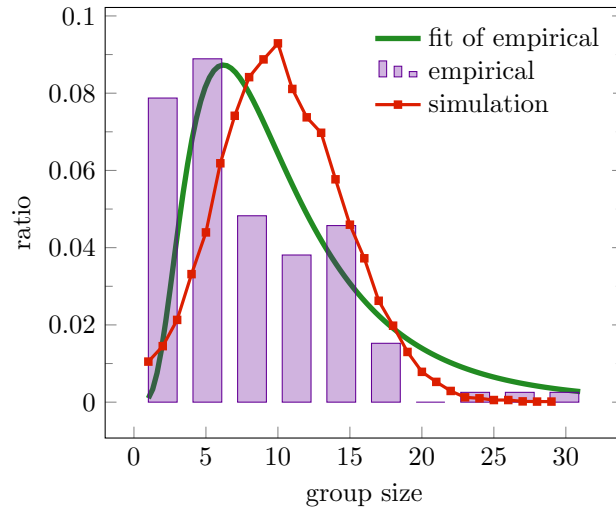


Figure 4.13: Comparison of the group size distribution in the model with an empirical one (the group size distribution of Przewalski horses living in the Hortobágy National Park). The empirical distribution follows a clearer lognormal distribution than in [125] due to the incorporation of historical data. The distribution obtained from the model is close to normal and is mean-fitted to the empirical distribution. We attribute the difference to the fact that the social interactions of horses are too complex to capture in purely spatial interactions.

4.3.3 Dimension scales

Horses usually travel by walking, which is roughly around 1.5 km/h based on our aerial observations averaged over several minutes. In this model v_L^0 is the corresponding parameter of the walking speed. To compare our model's length scale with that of reality we have calculated the pair-correlation function of the wild horses by using aerial pictures of the real herd and that of the herd in our model and compared the first peaks. This roughly equates the arbitrary length unit of our model to 0.18 m in reality (c.f. R_{LF}^{EX} in Table 4.1). From this we can calculate that the arbitrary time unit of our model is roughly equal to 0.44 s . This puts τ_L and τ_F at about reaction time ($0.5 - 1.5 \text{ s}$), τ_A to about 3 and a half minutes, and the emergence of a coherent collective motion, with stable harems to slightly less than 10 minutes. Since τ_L and τ_F both characterize a fast cognitive process it is not unrealistic that the characteristic times are on the scale of reaction times. Since in wild horses the groups do not form from randomly distributed individuals spontaneously, but rather evolve in an already laid down social context, the time needed for group formation is not readily comparable to that of the real herd. On the other hand, for a group

of 200 unfamiliar individuals, where leaders are already appointed and everybody is actually already moving, the 10 minutes seems like a reasonable time for group formation (the authors' personal experience with spontaneous group formation in human groups of comparable sizes would allow for even longer times).

4.4 Discussion

As the only truly wild horse in the world, the Przewalski horses, now mostly living in relatively easily accessible nature reserves, have drawn considerable attention. Both their collective movements [134] and the formation of their harems have attracted interest [125]. However, the unique collective motion displayed by this species, as a large herd consisting of cohesive harems moving together in a coordinated way, has not been modelled to date.

Our model, adapted from a model designed for cells, is able to qualitatively reproduce the motion of a wild horse herd moving on an open plain, along with formation of groups consisting of one leader and some followers and bachelor groups (group of leaders without followers), with a roughly adequate correspondence of dimension scales. During the analysis of the behaviour of the model we found three interesting phenomena, which we will address first, and then turn to some other aspects of the study.

First, the herd in our model will at times rotate around its center of mass. While we have not specifically observed the horses to circle, many animals do. That rotation occurs in our model is the direct effect of the fact, that within our framework the individuals are unable to stop. Indeed, animals that do rotate around a common axis are usually also unable to stop (e.g. flying animals) or is infeasible or dangerous for them to stop (or at least that is their observation on the matter). We are not aware of any scientific publication of observation of land mammals going around in circles, but we know of two videos on the internet showing the phenomena. The first example shows reindeer going in circles (https://www.youtube.com/watch?v=YJu_aUHeVL4, or see circling example 1 on the CD supplement). Note that although there is a fence, which obviously plays a role in the formation of the rotating movement the animals do not run along the fence, rather they rotate about a common point in an area much smaller than is available to them. The second example shows sheep doing much the same, although without any apparent confines (<https://www.youtube.com/watch?v=-PxbBWCQa1c> or see circling example 2 on

the CD supplement). On the other hand, since we have not observed horses doing this naturally, one could interpret rotation as an inability to decide which way to go, for which the more natural response would be to stop or slow down, until a decision is reached. Although some efforts have already been made to model the stopping of a group of animals [106], [131], we suggest further investigations into a model, that would allow for not only the stopping of, but also for the resuming of locomotion, along with possible data collection on the topic. A rather simple extension of our current model to allow stopping would be to take the circling as indication of motivation to stop and adding a factor that slows down the particles proportionally to their angular velocity, although if this achieves a natural looking stopping and restarting remains to be tested. Another appealing method to try would be to include a "tiredness" parameter as in [106] which would deplete on movement and replenish on standing still.

Second, the translational order parameter is decreased when we introduce followers among the leaders, thus the considered grouping process within the herd effectively reduces locomotion efficiency. In many systems the interactions during motion that give rise to collective motion is for the sake of more efficient locomotion of the group as a whole, but the harem formation within a herd is first and foremost due to reproductive reasons, which falls outside the realm of a collective motion study. It is not surprising that the reproductive benefits might outweigh the slight decrease in locomotive efficiency, while foraging or just changing locations. On the other hand this decreased locomotive efficiency may have a larger impact during the presence of predators. It would be interesting to model, how the presence of groups modify response to predation, and whether it has severe impact on the survivability of the individuals.

Third, the results obtained from our model are not in agreement with the observed group size distribution of the herd that motivated our work (the latter being a lognormal while the former being a normal distribution). Our simple model operates solely with interactions based on spatial distances, while group-forming processes in real societies have many complex attributes, thus deviations from the exact features of the empirical population is expected. On the other hand, the collective motion in many species can be described by purely distance-based interactions, making the exact nature of these deviations non-trivial. Consequently, we propose further investigations of collectively moving systems to find the properties that allow for the spatial formulation of interactions within the system. It can be supposed that in sys-

tems where individuals are interchangeable (in the meaning that individual recognition during the motion is not feasible), like a group of cells, ants or a flock of starlings, considering only distance-based interactions is enough to reproduce the observed collective motion pattern, but in animals living in structured social systems (and maintaining an individual recognition), like horses, social factors are much more important during interactions than actual distances, thus interchangeability might be one such property.

There are several questions that could be raised about the choices we made during model formation. One issue we have already mentioned is the question of mapping the individuals of a Przewalski herd to leaders and followers. Reality is quite complex compared to our model. Within the harem females, there is a hierarchy and the male actually quite often follows behind the group, while the young offspring probably further complicate the picture. Answering the question of who leads how in a Przewalski herd would require that we obtain detailed and continuous data on the movement of large groups of Przewalski horses. Unfortunately this is not an easy task, since we do not know of any herd, where attaching measurement devices to the animals is allowed by officials, thus one would have to use aerial observation. A substitute for real wild horses could be domestic and feral horses. The problem with the former is that even if a single institution has many horses, due to breeding issues and the safety of the stock (competing males will be aggressive with each other, and allowing them to freely copulate also risks injury) they lead a quite artificial lifestyle. Interestingly, both domestic and feral horses have been studied [135], [136] in terms of leadership, but the studies concentrate on movement initiation and not the collective motion itself, showing a somewhat different point-of-view in physicists and biologists. At the Department of Ethology we are currently working on a device for horses, that would not only provide long term recording of the positions of individual horses, but would also provide detailed information on the behaviour of the animal for the given point in time. Once ready we hope to be able to transfer it to enough animals to be able to obtain detailed enough data to answer questions about leadership in horses.

Another point of discussion is the necessity and form of Equation 4.24, which keeps the herd together. The rationale behind the form of the force is the following. A particle alone performs a sort of random walk. If we have two particles interacting, which for some reason become detached, i.e. the interaction between them ceases for a time, they become two independently random walking particles, meaning that

the chances of them coming into interaction again diminishes very fast, which obviously destroys any semblance of flocking. There are several ways to overcome this. One could add an interaction, which only goes to zero at infinity, like gravity, but that would be wholly unrealistic for animal interactions. One could enclose the particles in a boundary similar to what we used in our model, but small enough to force the particles into constant interaction, but this would severely limit the possibility of any collective translational movement. Thus the solution chosen by us comes very naturally, that the force responsible for the herd not losing any members during flocking only turns on sufficiently far from the center of mass of the herd so as not to interfere directly with flocking. On the other hand there is also another possibility, which is quite unrealistic for the flocking of animals where the density and the number of individuals is both low, but is widely used for bacteria and more theoretical oriented models: using periodic boundary conditions. This essentially bounds the particles in a sufficiently small space to keep them in continuous interaction, but introduces the possibility of a particles trailing after other particles to suddenly find themselves in front of those they have been following. Obviously, this is not a good choice for modelling animals where some are explicitly in front, but once the number of individuals reaches a level, where a randomly chosen unit will most likely be surrounded by other units, it becomes a viable approach. Although this is definitely not the case for the Przewalski's, it would be interesting to forgo Equation 4.24 and change the boundary conditions to periodic while increasing the number of particles to one or two magnitudes larger.

4.5 Summary

To keep their cohesiveness during locomotion, gregarious animals must make collective decisions. Many species boast complex societies with multiple levels of communities. A common case is when two dominant levels exist, one corresponding to leaders and the other consisting of followers. We studied, for the first time, the collective motion of such two-level assemblies of self-propelled particles, using terminology borrowed from wild horse herds, where the herd consists of smaller groups called harems.

We presented an agent-based model adapted from one originally proposed to describe the movement of cells resulting in a smoothly varying coherent motion. We studied the emergence (self-organization) of sub-groups within a herd during lo-

comotion by computer simulations and compared the resulting processes with our prior observations of a Przewalski horse herd (Hortobágy, Hungary) which we used from a published case study.

We found that the model reproduces key features of a herd composed of harems moving on open ground, including fights for followers between leaders and bachelor groups (group of leaders without followers). One of our findings, however, did not agree with the observations. While in our model the emerging group size distribution is normal, the group size distribution of the observed herd based on historical data have been found to follow lognormal distribution. We argued that this indicates that the formation (and the size) of the harems must involve a more complex social topology than simple spatial-distance based interactions.

5

Conclusion

In the previous two chapters I presented two studies wherein we investigated two systems. These systems are both complex, biologically relevant, and involve different types of agents. However, both the particulars of the systems and the questions asked were different. The first system was a sexual contact network of humans, wherein a sexually transmitted virus, HIV spreads. We asked how different strains of HIV would spread and compete in this network. The second system was a hierarchical herd of wild horses moving on an open plain. In essence asked whether a model of the collective movements of cells can be adapted to adequately explain the motion and group formation of the Przewalski horse. Following the goals set out in Chapter 1 I presented the relevant background of both topics to show in practice the methodology outlined in Chapter 2.

In Chapter 3 we built the network model based on empirical data available from Sub-Saharan Africa and observed that our model of HIV spreading is commensurate with the history of HIV. We showed that the first strain to infect a population will have considerable advantage over strains arriving later. Even if the later strain is stronger,

it needs at minimum decades to overcome the resident strain. This implies that without active prevention, strains of HIV, stronger than the current strains causing the epidemic, might start showing up in the not-too-distant future.

In the study presented in Chapter 4, we demonstrated that the modified cell-movement model produces results commensurate with wild horses moving on an open plain, but fails to capture all aspects of the horses' group structure. The model raised further questions about how it would be possible to include a mechanism for the stopping and restarting of movement in such a model and what exactly the properties of agents and their interactions are that allow for such a spatially-based modelling approach to work or fail.

This chapter also dealt in some detail with the concept of leadership in animals and in their collective motion models, specifically in horses. In short, the field lacks sufficient data to satisfactorily address questions regarding leadership since the observation of domesticated horses provides neither the needed group numbers nor the natural settings, while observation of wild horses is rather problematic due both to natural and legal causes. Observation of feral horses (domesticated horses living wild) may provide a solution to this issue.

In the future, I wish to continue with the research of collective motion and address the issues raised here in future works, but shift to not only doing theoretical work (modelling), but also data collection to underpin the models. I hope that the efforts at my current employment to develop an automated behaviour analysis for animals (currently dogs and horses) will pay off in this regard.

Publications

Publications included in theses

1. **Ferdinandy, B.**, Mones, E., Vicsek, T., Müller, V., “HIV competition dynamics over sexual networks: First comer advantage conserves founder effects,” *PLoS Comput Biol*, vol. 11, no. 2, e1004093, Feb. 2015.
2. **Ferdinandy, B.**, Ozogány, K., Vicsek, T., “Collective motion of groups of self-propelled particles following interacting leaders,” *Physica A: Statistical Mechanics and its Applications*, vol. 479, pp. 467–477, 2017.

Publications not included in theses

3. **Ferdinandy, B.**, Bhattacharya, K., Ábel, D., Vicsek, T., “Landing together: How flocks arrive at a coherent action in time and space in the presence of perturbations,” *Physica A: Statistical Mechanics and its Applications*, vol. 391, no. 4, pp. 1207–1215, 2012.
4. Abdai, J., **Ferdinandy, B.**, Terencio, C. B., Pogány, Á., Miklósi, Á., “Perception of animacy in dogs and humans,” *Biology Letters*, vol. 13, no. 6, 2017.
5. **Ferdinandy, B.**, Gerencsér, L., Corrieri, L., Csizmadia, G., Miklósi, Á., “Cross-species application of automated behaviour identification of dogs and wolves,” Under review.
6. Ábrám, D., Daróczy, B., **Ferdinandy, B.**, Gerencsér, L., Csizmadia, G., Benczúr, A., Miklósi, Á., “Novel machine learning algorithms in automated behaviour analysis,” In prep.

Bibliography

- [1] T. Vicsek, “Complexity: the bigger picture,” *Nature*, vol. 418, no. 6894, pp. 131–131, Jul. 2002.
- [2] S. Kauffman, *At home in the universe: The search for the laws of self-organization and complexity*. Oxford university press, 1996.
- [3] P. Érdi, *Complexity explained*. Springer, 2008, p. 397.
- [4] M. Gell-Mann, “What is complexity?” *Complexity*, vol. 1, no. 1, pp. 16–19, Sep. 1995.
- [5] P. M. Dickens, *Facilitating emergence: Complex, adaptive systems theory and the shape of change*. Antioch University, 2012.
- [6] S. E. Phelan, “What is complexity science, really?” *Emergence*, vol. 3, no. 1, pp. 120–136, 2001.
- [7] K. Richardson and C. Paul, Eds., *Emergence*, vol. 3, 1, 2001, *What is complexity science? What is complexity science?*
- [8] G. L. Levine and A. Rauch, *One culture: Essays in science and literature*. Univ of Wisconsin Press, 1987.
- [9] N. Perunov, R. A. Marsland, and J. L. England, “Statistical physics of adaptation,” *Physical Review X*, vol. 6, no. 2, p. 021 036, 2016.
- [10] N. Oreskes, K. Shrader-Frechette, and K. Belitz, “Verification, validation, and confirmation of numerical models in the earth sciences,” *Science*, vol. 263, no. 5147, pp. 641–646, 1994.
- [11] E. P. Wigner, “The unreasonable effectiveness of mathematics in the natural sciences. richard courant lecture in mathematical sciences delivered at new york university, may 11, 1959,” *Communications on pure and applied mathematics*, vol. 13, no. 1, pp. 1–14, 1960.

- [12] B. Ferdinandy, E. Mones, T. Vicsek, and V. Müller, "HIV competition dynamics over sexual networks: First comer advantage conserves founder effects," *PLoS Comput Biol*, vol. 11, no. 2, e1004093, Feb. 2015.
- [13] A. V. Alain Barrat Marc Barthelemy, *Dynamical Processes on Complex Networks*, 1st ed. 2008.
- [14] R. Albert and A.-L. Barabási, "Statistical mechanics of complex networks," *Reviews of modern physics*, vol. 74, no. 1, p. 47, 2002.
- [15] A. Barrat, M. Barthelemy, and A. Vespignani, *Dynamical processes on complex networks*. Cambridge university press, 2008.
- [16] D. J. Watts and S. H. Strogatz, "Collective dynamics of "small world" networks," *Nature*, vol. 393, pp. 440–442, 1998.
- [17] R. Pastor-Satorras and A. Vespignani, *Evolution and structure of the Internet: A statistical physics approach*. Cambridge University Press, 2007.
- [18] M. E. Newman, "The structure and function of complex networks," *SIAM review*, vol. 45, no. 2, pp. 167–256, 2003.
- [19] B. Korber, M. Muldoon, J. Theiler, F. Gao, R. Gupta, A. Lapedes, B. H. Hahn, S. Wolinsky, and T. Bhattacharya, "Timing the ancestor of the hiv-1 pandemic strains," *Science*, vol. 288, no. 5472, pp. 1789–1796, 2000.
- [20] M. Worobey, M. Gemmel, D. E. Teuwen, T. Haselkorn, K. Kunstman, M. Bunce, J.-J. Muyembe, J.-M. M. Kabongo, R. M. Kalengayi, E. Van Marck, *et al.*, "Direct evidence of extensive diversity of hiv-1 in kinshasa by 1960," *Nature*, vol. 455, no. 7213, pp. 661–664, 2008.
- [21] A. Rambaut, D. L. Robertson, O. G. Pybus, M. Peeters, and E. C. Holmes, "Human immunodeficiency virus: Phylogeny and the origin of hiv-1," *Nature*, vol. 410, no. 6832, pp. 1047–1048, 2001.
- [22] D. M. Tebit and E. J. Arts, "Tracking a century of global expansion and evolution of hiv to drive understanding and to combat disease," *The Lancet infectious diseases*, vol. 11, no. 1, pp. 45–56, 2011.
- [23] J. U. N. P. on HIV/AIDS (UNAIDS), *UNAIDS World Aids Day Report 2011*. UNAIDS, 2011.
- [24] M. Stevenson, "HIV-1 pathogenesis," *Nature Medicine*, vol. 9, no. 7, pp. 853–860, 2003.

- [25] J. Hemelaar, E. Gouws, P. D. Ghys, S. Osmanov, *et al.*, "Global trends in molecular epidemiology of hiv-1 during 2000–2007," *AIDS (London, England)*, vol. 25, no. 5, p. 679, 2011.
- [26] C.-Y. Ou, B. Weniger, C.-C. Luo, M. Kalish, H. Gayle, N. Young, G. Schochetman, Y. Takebe, S. Yamazaki, and W. Auwanit, "Independent introduction of two major hiv-1 genotypes into distinct high-risk populations in thailand," *The Lancet*, vol. 341, no. 8854, pp. 1171–1174, 1993.
- [27] V. V. Lukashov, M. T. Cornelissen, J. Goudsmit, M. N. Papuashvilli, P. G. Rytik, R. M. Khaitov, E. V. Karamov, and F. de Wolf, "Simultaneous introduction of distinct hiv-1 subtypes into different risk groups in russia, byelorussia and lithuania.," *Aids*, vol. 9, no. 5, 435–hyhen, 1995.
- [28] J. Van Harmelen, R. Wood, M. Lambrick, E. P. Rybicki, A.-L. Williamson, and C. Williamson, "An association between hiv-1 subtypes and mode of transmission in cape town, south africa," *Aids*, vol. 11, no. 1, pp. 81–87, 1997.
- [29] A. B. Abecasis, A. M. Wensing, D. Paraskevis, J. Vercauteren, K. Theys, D. A. Van de Vijver, J. Albert, B. Asjö, C. Balotta, D. Beshkov, *et al.*, "Hiv-1 subtype distribution and its demographic determinants in newly diagnosed patients in europe suggest highly compartmentalized epidemics," *Retrovirology*, vol. 10, no. 1, p. 1, 2013.
- [30] D. Frentz, A. M. Wensing, J. Albert, D. Paraskevis, A. B. Abecasis, O. Hamouda, L. B. Jørgensen, C. Kücherer, D. Struck, J.-C. Schmit, *et al.*, "Limited cross-border infections in patients newly diagnosed with hiv in europe," *Retrovirology*, vol. 10, no. 1, p. 1, 2013.
- [31] B. Renjifo, P. Gilbert, B. Chaplin, G. Msamanga, D. Mwakagile, W. Fawzi, M. Essex, T. Vitamin, H. S. Group, *et al.*, "Preferential in-utero transmission of hiv-1 subtype c as compared to hiv-1 subtype a or d," *Aids*, vol. 18, no. 12, pp. 1629–1636, 2004.
- [32] N. Kiwanuka, O. Laeyendecker, T. C. Quinn, M. J. Wawer, J. Shepherd, M. Robb, G. Kigozi, J. Kagaayi, D. Serwadda, F. E. Makumbi, *et al.*, "Hiv-1 subtypes and differences in heterosexual hiv transmission among hiv-discordant couples in rakai, uganda," *AIDS (London, England)*, vol. 23, no. 18, p. 2479, 2009.

- [33] B. L. Walter, A. E. Armitage, S. C. Graham, T. de Oliveira, P. Skinhøj, E. Y. Jones, D. I. Stuart, A. J. McMichael, B. Chesebro, and A. K. Iversen, "Functional characteristics of hiv-1 subtype-c compatible with increased heterosexual transmissibility," *AIDS (London, England)*, vol. 23, no. 9, p. 1047, 2009.
- [34] A. Vasan, B. Renjifo, E. Hertzmark, B. Chaplin, G. Msamanga, M. Essex, W. Fawzi, and D. Hunter, "Different rates of disease progression of hiv type 1 infection in tanzania based on infecting subtype," *Clinical Infectious Diseases*, vol. 42, no. 6, pp. 843–852, 2006.
- [35] J. M. Baeten, B. Chohan, L. Lavreys, V. Chohan, R. S. McClelland, L. Certain, K. Mandaliya, W. Jaoko, and O. Julie, "Hiv-1 subtype d infection is associated with faster disease progression than subtype a in spite of similar plasma hiv-1 loads," *Journal of Infectious Diseases*, vol. 195, no. 8, pp. 1177–1180, 2007.
- [36] N. Vidal, M. Peeters, C. Mulanga-Kabeya, N. Nzilambi, D. Robertson, W. Ilunga, H. Sema, K. Tshimanga, B. Bongo, and E. Delaporte, "Unprecedented degree of human immunodeficiency virus type 1 (hiv-1) group m genetic diversity in the democratic republic of congo suggests that the hiv-1 pandemic originated in central africa," *Journal of virology*, vol. 74, no. 22, pp. 10 498–10 507, 2000.
- [37] M. L. Kalish, K. E. Robbins, D. Pieniazek, A. Schaefer, N. Nzilambi, T. C. Quinn, M. E. St Louis, A. S. Youngpairaj, J. Phillips, H. W. Jaffe, *et al.*, "Recombinant viruses and early global hiv-1 epidemic," *Emerg Infect Dis*, vol. 10, no. 7, pp. 1227–1234, 2004.
- [38] N. Vidal, C. Mulanga, S. E. Bazepeo, J. K. Mwamba, J. Tshimpaka, M. Kashi, N. Mama, D. Valea, E. Delaporte, F. Lepira, *et al.*, "Hiv type 1 pol gene diversity and antiretroviral drug resistance mutations in the democratic republic of congo (drc)," *AIDS Research & Human Retroviruses*, vol. 22, no. 2, pp. 202–206, 2006.
- [39] A. F. Santos and M. A. Soares, "Hiv genetic diversity and drug resistance," *Viruses*, vol. 2, no. 2, pp. 503–531, Feb. 2010.
- [40] C. J. Murray, K. F. Ortblad, C. Guinovart, S. S. Lim, T. M. Wolock, D. A. Roberts, E. A. Dansereau, N. Graetz, R. M. Barber, J. C. Brown, *et al.*, "Global, regional, and national incidence and mortality for hiv, tuberculosis, and malaria during 1990–2013: A systematic analysis for the global burden of disease study 2013," *The Lancet*, vol. 384, no. 9947, pp. 1005–1070, 2014.

- [41] M. Moslonka-Lefebvre, S. Bonhoeffer, and S. Alizon, "Weighting for sex acts to understand the spread of sti on networks," *Journal of theoretical biology*, vol. 311, pp. 46–53, 2012.
- [42] K. Ronen, C. O. McCoy, F. A. Matsen, D. F. Boyd, S. Emery, K. Odem-Davis, W. Jaoko, K. Mandaliya, R. S. McClelland, B. A. Richardson, *et al.*, "Hiv-1 superinfection occurs less frequently than initial infection in a cohort of high-risk kenyan women," *PLoS Pathog*, vol. 9, no. 8, e1003593, 2013.
- [43] T. D. Hollingsworth, R. M. Anderson, and C. Fraser, "Hiv-1 transmission, by stage of infection," *Journal of Infectious Diseases*, vol. 198, no. 5, pp. 687–693, 2008.
- [44] D. A. Rasmussen, E. M. Volz, and K. Koelle, "Phylogenetic inference for structured epidemiological models," *PLoS Comput Biol*, vol. 10, no. 4, e1003570, 2014.
- [45] S. D. Pinkerton, "How many sexually-acquired hiv infections in the usa are due to acute-phase hiv transmission?" *AIDS (London, England)*, vol. 21, no. 12, p. 1625, 2007.
- [46] A. D. Redd, T. C. Quinn, and A. A. Tobian, "Frequency and implications of hiv superinfection," *The Lancet infectious diseases*, vol. 13, no. 7, pp. 622–628, 2013.
- [47] J. C. Thomas and M. J. Tucker, "The development and use of the concept of a sexually transmitted disease core," *Journal of Infectious Diseases*, vol. 174, no. Supplement 2, S134–S143, 1996.
- [48] H. Chemaitelly, S. F. Awad, and L. J. Abu-Raddad, "The risk of hiv transmission within hiv-1 sero-discordant couples appears to vary across sub-saharan africa," *Epidemics*, vol. 6, pp. 1–9, 2014.
- [49] V. Latora, A. Nyamba, J. Simporé, B. Sylvestre, S. Diane, B. Sylvestre, and S. Musumeci, "Network of sexual contacts and sexually transmitted hiv infection in burkina faso," *Journal of medical virology*, vol. 78, no. 6, pp. 724–729, 2006.
- [50] P. Roberts, K. Holmes, P. Piot, F. Plummer, L. D'Costa, M. Lightfoot, D. Koeh, J. Kreiss, A. Ronald, *et al.*, "Aids virus infection in nairobi prostitutes. spread of the epidemic to east africa.," 1986.

- [51] B. Ferry, M. Carael, A. Buve, B. Auvert, M. Laourou, L. Kanhonou, M. De Loenzien, E. Akam, J. Chege, F. Kaona, *et al.*, "Comparison of key parameters of sexual behaviour in four african urban populations with different levels of hiv infection," *Aids*, vol. 15, S41–S50, 2001.
- [52] A. Buvé, M. Caraël, R. J. Hayes, B. Auvert, B. Ferry, N. J. Robinson, S. Anagonou, L. Kanhonou, M. Laourou, S. Abega, *et al.*, "Multicentre study on factors determining differences in rate of spread of hiv in sub-saharan africa: Methods and prevalence of hiv infection," *Aids*, vol. 15, S5–S14, 2001.
- [53] A. Buvé, E. Lagarde, M. Caraël, N. Rutenberg, B. Ferry, J. Glynn, M. Laourou, E. Akam, J. Chege, T. Sukwa, *et al.*, "Interpreting sexual behaviour data: Validity issues in the multicentre study on factors determining the differential spread of hiv in four african cities," *Aids*, vol. 15, S117–S126, 2001.
- [54] M. J. Wawer, R. H. Gray, N. K. Sewankambo, D. Serwadda, X. Li, O. Laeyendecker, N. Kiwanuka, G. Kigozi, M. Kiddugavu, T. Lutalo, *et al.*, "Rates of hiv-1 transmission per coital act, by stage of hiv-1 infection, in rakai, uganda," *Journal of Infectious Diseases*, vol. 191, no. 9, pp. 1403–1409, 2005.
- [55] K. A. Powers, C. Poole, A. E. Pettifor, and M. S. Cohen, "Rethinking the heterosexual infectivity of hiv-1: A systematic review and meta-analysis," *The Lancet infectious diseases*, vol. 8, no. 9, pp. 553–563, 2008.
- [56] M.-C. Boily, R. F. Baggaley, L. Wang, B. Masse, R. G. White, R. J. Hayes, and M. Alary, "Heterosexual risk of hiv-1 infection per sexual act: Systematic review and meta-analysis of observational studies," *The Lancet infectious diseases*, vol. 9, no. 2, pp. 118–129, 2009.
- [57] S. P. Buchbinder, M. H. Katz, N. A. Hessel, P. M. O'Malley, and S. D. Holmberg, "Long-term hiv-1 infection without immunologic progression.," *Aids*, vol. 8, no. 8, pp. 1123–1128, 1994.
- [58] S. Abdel Babiker and D. Daniela De Angelis, "Kholoud porter. time from hiv-1 seroconversion to aids and death before widespread use of highly-active antiretroviral therapy: A collaborative re-analysis. collaborative group on aids incubation and hiv survival including the cascade eu concerted action. concerted action on seroconversion to aids and death in europe," *Lancet*, vol. 355, pp. 1131–1137, 2000.
- [59] A. Clauset, C. R. Shalizi, and M. E. Newman, "Power-law distributions in empirical data," *SIAM review*, vol. 51, no. 4, pp. 661–703, 2009.

- [60] J. Alstott, E. Bullmore, and D. Plenz, "Powerlaw: A python package for analysis of heavy-tailed distributions," *PloS one*, vol. 9, no. 1, e85777, 2014.
- [61] S. Rainwater, S. DeVange, M. Sagar, J. Ndinya-Achola, K. Mandaliya, J. K. Kreiss, and J. Overbaugh, "No evidence for rapid subtype c spread within an epidemic in which multiple subtypes and intersubtype recombinants circulate," *AIDS Research & Human Retroviruses*, vol. 21, no. 12, pp. 1060–1065, 2005.
- [62] S. A. Conroy, O. Laeyendecker, A. D. Redd, A. Collinson-Streng, X. Kong, F. Makumbi, T. Lutalo, N. Sewankambo, N. Kiwanuka, R. H. Gray, *et al.*, "Changes in the distribution of hiv type 1 subtypes d and a in rakai district, uganda between 1994 and 2002," *AIDS research and human retroviruses*, vol. 26, no. 10, pp. 1087–1091, 2010.
- [63] W.-P. Schmidt, M. S. Van Der Loeff, P. Aaby, H. Whittle, R. Bakker, M. Buckner, F. Dias, and R. White, "Behaviour change and competitive exclusion can explain the diverging hiv-1 and hiv-2 prevalence trends in guinea-bissau," *Epidemiology and infection*, vol. 136, no. 04, pp. 551–561, 2008.
- [64] G. Shirreff, L. Pellis, O. Laeyendecker, and C. Fraser, "Transmission selects for hiv-1 strains of intermediate virulence: A modelling approach," *PLoS Comput Biol*, vol. 7, no. 10, e1002185, 2011.
- [65] K. L. Gross, T. C. Porco, and R. M. Grant, "Hiv-1 superinfection and viral diversity," *Aids*, vol. 18, no. 11, pp. 1513–1520, 2004.
- [66] A. Downs and I. De Vincenzi, "Probability of heterosexual transmission of hiv: Relationship to the number of unprotected sexual contacts. european study group in heterosexual transmission of hiv.," *J Acquir Immune Defic Syndr Hum Retrovirol.*, vol. 11, no. 4, pp. 388–395, 1996.
- [67] B. Leynaert, A. Downs, and I. De Vincenzi, "Heterosexual transmission of human immunodeficiency virus: Variability of infectivity throughout the course of infection. european study group on heterosexual transmission of hiv.," *Am J Epidemiol*, vol. 148, pp. 88–96, 1998.
- [68] N. J. Nagelkerke, P. Arora, P. Jha, B. Williams, L. McKinnon, and S. J. de Vlas, "The rise and fall of hiv in high-prevalence countries: A challenge for mathematical modeling," *PLoS Comput Biol*, vol. 10, no. 3, e1003459, 2014.

- [69] R. Kaul, F. A. Plummer, J. Kimani, T. Dong, P. Kiama, T. Rostron, E. Njagi, K. S. MacDonald, J. J. Bwayo, A. J. McMichael, *et al.*, "Hiv-1-specific mucosal cd8+ lymphocyte responses in the cervix of hiv-1-resistant prostitutes in nairobi," *The Journal of Immunology*, vol. 164, no. 3, pp. 1602–1611, 2000.
- [70] E. Nicastrì, L. Ercoli, L. Sarmati, G. d’Ettorre, P. Iudicone, P. Massetti, V. Vullo, and M. Andreoni, "Human immunodeficiency virus-1 specific and natural cellular immunity in hiv seronegative subjects with multiple sexual exposures to virus," *Journal of medical virology*, vol. 64, no. 3, pp. 232–237, 2001.
- [71] N. Promadej, C. Costello, M. M. Wernett, P. S. Kulkarni, V. A. Robison, K. E. Nelson, T. W. Hodge, V. Suriyanon, A. Duerr, and J. M. McNicholl, "Broad human immunodeficiency virus (hiv)–specific t cell responses to conserved hiv proteins in hiv-seronegative women highly exposed to a single hiv-infected partner," *Journal of Infectious Diseases*, vol. 187, no. 7, pp. 1053–1063, 2003.
- [72] C. S. Kraft, D. Basu, P. A. Hawkins, P. T. Hraber, E. Chomba, J. Mulenga, W. Kilembe, N. H. Khu, C. A. Derdeyn, S. A. Allen, *et al.*, "Timing and source of subtype-c hiv-1 superinfection in the newly infected partner of zambian couples with disparate viruses," *Retrovirology*, vol. 9, no. 1, p. 1, 2012.
- [73] M. J. Gonzales, E. Delwart, S.-Y. Rhee, R. Tsui, A. R. Zolopa, J. Taylor, and R. W. Shafer, "Lack of detectable human immunodeficiency virus type 1 superinfection during 1072 person-years of observation," *Journal of Infectious Diseases*, vol. 188, no. 3, pp. 397–405, 2003.
- [74] R. Tsui, B. L. Herring, J. D. Barbour, R. M. Grant, P. Bacchetti, A. Kral, B. R. Edlin, and E. L. Delwart, "Human immunodeficiency virus type 1 superinfection was not detected following 215 years of injection drug user exposure," *Journal of virology*, vol. 78, no. 1, pp. 94–103, 2004.
- [75] A. D. Redd, A. Collinson-Streng, C. Martens, S. Ricklefs, C. E. Mullis, J. Manucci, A. A. Tobian, E. J. Selig, O. Laeyendecker, N. Sewankambo, *et al.*, "Identification of hiv superinfection in seroconcordant couples in rakai, uganda, by use of next-generation deep sequencing," *Journal of clinical microbiology*, vol. 49, no. 8, pp. 2859–2867, 2011.
- [76] A. Piantadosi, M. O. Ngayo, B. Chohan, and J. Overbaugh, "Examination of a second region of the hiv type 1 genome reveals additional cases of superinfection," *AIDS research and human retroviruses*, vol. 24, no. 9, pp. 1221–1224, 2008.

- [77] A. R. Templeton, M. G. Kramer, J. Jarvis, J. Kowalski, S. Gange, M. F. Schneider, Q. Shao, G. W. Zhang, M.-F. Yeh, H.-L. Tsai, *et al.*, "Multiple-infection and recombination in hiv-1 within a longitudinal cohort of women," *Retrovirology*, vol. 6, no. 1, p. 1, 2009.
- [78] D. Ebert *et al.*, "Virulence and local adaptation of a horizontally transmitted parasite," *SCIENCE-NEW YORK THEN WASHINGTON-*, pp. 1084–1084, 1994.
- [79] C. M. Lively and M. F. Dybdahl, "Parasite adaptation to locally common host genotypes," *Nature*, vol. 405, no. 6787, pp. 679–681, 2000.
- [80] Y. Kawashima, K. Pfafferoth, J. Frater, P. Matthews, R. Payne, M. Addo, H. Gatanaga, M. Fujiwara, A. Hachiya, H. Koizumi, *et al.*, "Adaptation of hiv-1 to human leukocyte antigen class i," *Nature*, vol. 458, no. 7238, pp. 641–645, 2009.
- [81] T. Furutsuki, N. Hosoya, A. Kawana-Tachikawa, M. Tomizawa, T. Odawara, M. Goto, Y. Kitamura, T. Nakamura, A. D. Kelleher, D. A. Cooper, *et al.*, "Frequent transmission of cytotoxic-t-lymphocyte escape mutants of human immunodeficiency virus type 1 in the highly hla-a24-positive japanese population," *Journal of virology*, vol. 78, no. 16, pp. 8437–8445, 2004.
- [82] B. Schmid, C. Keşmir, and R. J. de Boer, "The specificity and polymorphism of the mhc class i prevents the global adaptation of hiv-1 to the monomorphic proteasome and tap," *PLoS One*, vol. 3, no. 10, e3525, 2008.
- [83] M. John, D. Heckerman, I. James, L. P. Park, J. M. Carlson, A. Chopra, S. Gaudieri, D. Nolan, D. W. Haas, S. A. Riddler, *et al.*, "Adaptive interactions between hla and hiv-1: Highly divergent selection imposed by hla class i molecules with common supertype motifs," *The Journal of Immunology*, vol. 184, no. 8, pp. 4368–4377, 2010.
- [84] L. A. Cotton, X. T. Kuang, A. Q. Le, J. M. Carlson, B. Chan, D. R. Chopera, C. J. Brumme, T. J. Markle, E. Martin, A. Shahid, *et al.*, "Genotypic and functional impact of hiv-1 adaptation to its host population during the north american epidemic," *PLoS Genet*, vol. 10, no. 4, e1004295, 2014.
- [85] M. H. Malim and P. D. Bieniasz, "Hiv restriction factors and mechanisms of evasion," *Cold Spring Harbor perspectives in medicine*, vol. 2, no. 5, a006940, 2012.

- [86] K. Zhao, Y. Ishida, T. K. Oleksyk, C. A. Winkler, and A. L. Roca, "Evidence for selection at hiv host susceptibility genes in a west central african human population," *BMC evolutionary biology*, vol. 12, no. 1, p. 1, 2012.
- [87] M. J.-Y. Ploquin, B. Jacquelin, S. P. Jochems, F. Barré-Sinoussi, and M. C. Müller-Trutwin, "Innate immunity in the control of hiv/aids: Recent advances and open questions," *Aids*, vol. 26, no. 10, pp. 1269–1279, 2012.
- [88] H. J. Bremermann and H. Thieme, "A competitive exclusion principle for pathogen virulence," *Journal of mathematical biology*, vol. 27, no. 2, pp. 179–190, 1989.
- [89] C. Castillo-Chavez, W. Huang, and J. Li, "Competitive exclusion in gonorrhea models and other sexually transmitted diseases," *SIAM Journal on Applied Mathematics*, vol. 56, no. 2, pp. 494–508, 1996.
- [90] S. Hué, D. Pillay, J. P. Clewley, and O. G. Pybus, "Genetic analysis reveals the complex structure of hiv-1 transmission within defined risk groups," *Proceedings of the National Academy of Sciences of the United States of America*, vol. 102, no. 12, pp. 4425–4429, 2005.
- [91] C. Fraser, T. D. Hollingsworth, R. Chapman, F. de Wolf, and W. P. Hanage, "Variation in hiv-1 set-point viral load: Epidemiological analysis and an evolutionary hypothesis," *Proceedings of the National Academy of Sciences*, vol. 104, no. 44, pp. 17 441–17 446, 2007.
- [92] I. Bartha, M. Assel, P. M. Sloot, M. Zazzi, C. Torti, E. Schülter, A. De Luca, A. Sönnernborg, A. B. Abecasis, K. Van Laethem, *et al.*, "Superinfection with drug-resistant hiv is rare and does not contribute substantially to therapy failure in a large european cohort," *BMC infectious diseases*, vol. 13, no. 1, p. 1, 2013.
- [93] T. I. de Silva, C. van Tienen, C. Onyango, A. Jabang, T. Vincent, M. F. S. van der Loeff, R. A. Coutinho, A. Jaye, S. Rowland-Jones, H. Whittle, *et al.*, "Population dynamics of hiv-2 in rural west africa: Comparison with hiv-1 and ongoing transmission at the heart of the epidemic," *Aids*, vol. 27, no. 1, pp. 125–134, 2013.
- [94] K. K. Ariën, A. Abraha, M. E. Quinones-Mateu, L. Kestens, G. Vanham, and E. J. Arts, "The replicative fitness of primary human immunodeficiency virus type 1 (hiv-1) group m, hiv-1 group o, and hiv-2 isolates," *Journal of virology*, vol. 79, no. 14, pp. 8979–8990, 2005.

- [95] P. B. Gilbert, I. W. McKeague, G. Eisen, C. Mullins, A. Guéye-NDiaye, S. Mboup, and P. J. Kanki, "Comparison of hiv-1 and hiv-2 infectivity from a prospective cohort study in senegal," *Statistics in medicine*, vol. 22, no. 4, pp. 573–593, 2003.
- [96] R. Batorsky, M. F. Kearney, S. E. Palmer, F. Maldarelli, I. M. Rouzine, and J. M. Coffin, "Estimate of effective recombination rate and average selection coefficient for hiv in chronic infection," *Proceedings of the National Academy of Sciences*, vol. 108, no. 14, pp. 5661–5666, 2011.
- [97] M. Zhang, B. Foley, A.-K. Schultz, J. P. Macke, I. Bulla, M. Stanke, B. Morgenstern, B. Korber, and T. Leitner, "The role of recombination in the emergence of a complex and dynamic hiv epidemic," *Retrovirology*, vol. 7, no. 1, p. 1, 2010.
- [98] J. D. Sousa, V. Müller, P. Lemey, and A.-M. Vandamme, "High gud incidence in the early 20th century created a particularly permissive time window for the origin and initial spread of epidemic hiv strains," *PLoS One*, vol. 5, no. 4, 2010.
- [99] A. Piantadosi, B. Chohan, V. Chohan, R. S. McClelland, and J. Overbaugh, "Chronic hiv-1 infection frequently fails to protect against superinfection," *PLoS Pathog*, vol. 3, no. 11, e177, 2007.
- [100] B. Ferdinandy, K. Ozogány, and T. Vicsek, "Collective motion of groups of self-propelled particles following interacting leaders," *Physica A: Statistical Mechanics and its Applications*, vol. 479, pp. 467–477, 2017.
- [101] T. Vicsek, A. Czirók, E. Ben-Jacob, I. Cohen, and O. Shochet, "Novel type of phase transition in a system of self-driven particles," *Phys. Rev. Lett.*, vol. 75, no. 6, pp. 1226–1229, 1995.
- [102] C. Castellano, S. Fortunato, and V. Loreto, "Statistical physics of social dynamics," *Rev. Mod. Phys.*, vol. 81, no. 2, pp. 591–646, 2009.
- [103] T. Vicsek and A. Zafeiris, "Collective motion," *Physics Reports*, vol. 517, no. 3–4, pp. 71–140, 2012, Collective motion.
- [104] D. Strömbom, "Collective motion from local attraction," *Journal of Theoretical Biology*, vol. 283, no. 1, pp. 145–151, Aug. 2011.
- [105] B. Szabó, G. J. Szöllösi, B. Gönci, Z. Jurányi, D. Selmeczi, and T. Vicsek, "Phase transition in the collective migration of tissue cells: Experiment and model," *Phys. Rev. E*, vol. 74, p. 061 908, 6 Dec. 2006.

- [106] B. Ferdinandy, K. Bhattacharya, D. Ábel, and T. Vicsek, "Landing together: How flocks arrive at a coherent action in time and space in the presence of perturbations," *Physica A: Statistical Mechanics and its Applications*, vol. 391, no. 4, pp. 1207–1215, 2012.
- [107] R. Olfati-Saber, J. A. Fax, and R. M. Murray, "Consensus and cooperation in networked multi-agent systems," *Proceedings of the IEEE*, vol. 95, no. 1, pp. 215–233, Jan. 2007.
- [108] M. Bourjade, B. Thierry, M. Hausberger, and O. Petit, "Is leadership a reliable concept in animals? an empirical study in the horse," *PLoS ONE*, vol. 10, no. 5, pp. 1–14, May 2015.
- [109] I. Watts, B. Pettit, M. Nagy, T. B. de Perera, and D. Biro, "Lack of experience-based stratification in homing pigeon leadership hierarchies," *Royal Society Open Science*, vol. 3, no. 1, 2016.
- [110] M. Nagy, G. Vásárhelyi, B. Pettit, I. Roberts-Mariani, T. Vicsek, and D. Biro, "Context-dependent hierarchies in pigeons," *Proceedings of the National Academy of Sciences*, vol. 110, no. 32, pp. 13 049–13 054, 2013.
- [111] L. C. David Lusseau, "The emergence of unshared consensus decisions in bottlenose dolphins," *Behavioral Ecology and Sociobiology*, vol. 63, no. 7, pp. 1067–1077, 2009.
- [112] I. R. Fischhoff, S. R. Sundaresan, J. Cordingley, H. M. Larkin, M.-J. Sellier, and D. I. Rubenstein, "Social relationships and reproductive state influence leadership roles in movements of plains zebra, *Equus burchellii*," *Animal Behaviour*, vol. 73, no. 5, pp. 825–831, 2007.
- [113] L. D. Mech, "Alpha status, dominance, and division of labor in wolf packs," *Canadian Journal of Zoology*, vol. 77, no. 8, pp. 1196–1203, 1999.
- [114] C. C. Grueter, B. Chapais, and D. Zinner, "Evolution of multilevel social systems in nonhuman primates and humans," *Int J Primatol*, vol. 33, no. 5, pp. 1002–1037, Oct. 2012.
- [115] C. C. Grueter, I. Matsuda, P. Zhang, and D. Zinner, "Multilevel societies in primates and other mammals: Introduction to the special issue," *Int J Primatol*, vol. 33, no. 5, pp. 993–1001, Oct. 2012.
- [116] J. Abegglen, *On Socialization in Hamadryas Baboons: A field study*. Bucknell University Press, Lewisburg, 1984.

- [117] H. Kummer, *Social Organisation of Hamdryas Baboons. A Field Study*. University of Chicago Press, Chicago, 1968.
- [118] G. Wittemyer, I. Douglas-Hamilton, and W. Getz, "The socioecology of elephants: Analysis of the processes creating multitiered social structures," *Animal Behaviour*, vol. 69, no. 6, pp. 1357–1371, 2005.
- [119] R. Baird, "The killer whale: Foraging specializations and group hunting.," in *Cetacean Societies*, J. Mann, R. Connor, P. Tyack, and H. Whitehead, Eds., University of Chicago Press, Chicago, 2000, pp. 127–153.
- [120] H. Whitehead, R. Antunes, S. Gero, S. Wong, D. Engelhaupt, and L. Rendell, "Multilevel societies of female sperm whales (*physeter macrocephalus*) in the atlantic and pacific: Why are they so different?" *International Journal of Primatology*, vol. 33, no. 5, pp. 1142–1164, 2012.
- [121] C. Feh, B. Munkhtuya, S. Enkhbold, and T. Sukhbaatar, "Ecology and social structure of the gobi khulan equus hemionus subsp. in the gobi b national park, mongolia," *Biological Conservation*, vol. 101, no. 1, pp. 51–61, 2001.
- [122] D. Rubenstein and M. Hack, "Natural and sexual selection and the evolution of multi-level societies: Insights from zebras with comparisons to primates.," in *Sexual Selection in Primates: New and Comparative Perspectives*, P. Kappler and C. van Schaik, Eds., Cambridge University Press, New York, 2004, pp. 266–279.
- [123] L. Boyd and K. Houpt, *Przewalski's Horses*. State University of New York Press, New York, 1994.
- [124] R. Dunbar and P. Dunbar, "Social dynamics of gelada baboons.," *Contrib Primatol*, vol. 6, pp. 1–157, 1975.
- [125] K. Ozogány and T. Vicsek, "Modeling the emergence of modular leadership hierarchy during the collective motion of herds made of harems," *Journal of Statistical Physics*, pp. 1–19, 2014.
- [126] E. Hartmann, E. Søndergaard, and L. J. Keeling, "Keeping horses in groups: A review," *Applied Animal Behaviour Science*, vol. 136, no. 2–4, pp. 77–87, 2012.
- [127] T. Vicsek, A. Czirók, E. Ben-Jacob, I. Cohen, and O. Shochet, "Novel type of phase transition in a system of self-driven particles," *Physical review letters*, vol. 75, no. 6, p. 1226, 1995.

- [128] M. Ballerini, N. Cabibbo, R. Candelier, A. Cavagna, E. Cisbani, I. Giardina, V. Lecomte, A. Orlandi, G. Parisi, A. Procaccini, *et al.*, “Interaction ruling animal collective behavior depends on topological rather than metric distance: Evidence from a field study,” *Proceedings of the national academy of sciences*, vol. 105, no. 4, pp. 1232–1237, 2008.
- [129] A. Strandburg-Peshkin, C. R. Twomey, N. W. Bode, A. B. Kao, Y. Katz, C. C. Ioannou, S. B. Rosenthal, C. J. Torney, H. S. Wu, S. A. Levin, *et al.*, “Visual sensory networks and effective information transfer in animal groups,” *Current Biology*, vol. 23, no. 17, R709–R711, 2013.
- [130] D. E. Brooks and A. Matthews, “Equine ophthalmology,” *Veterinary ophthalmology*, vol. 2, pp. 1165–1274, 1999.
- [131] K. Bhattacharya and T. Vicsek, “Collective decision making in cohesive flocks,” *NEW JOURNAL OF PHYSICS*, vol. 12, Sep. 2010.
- [132] C. Virágh, G. Vásárhelyi, N. Tarcai, T. Szörényi, G. Somorjai, T. Nepusz, and T. Vicsek, “Flocking algorithm for autonomous flying robots,” *Bioinspiration & Biomimetics*, vol. 9, no. 2, p. 025 012, 2014.
- [133] C. Virágh, G. Vásárhelyi, N. Tarcai, T. Szörényi, G. Somorjai, T. Nepusz, and T. Vicsek, “Corrigendum: Flocking algorithm for autonomous flying robots (2014 bioinspir. biomim. 9 025012),” *Bioinspiration and Biomimetics*, vol. 9, no. 4, 2014.
- [134] M. Bourjade, B. Thierry, M. Maumy, and O. Petit, “Decision-making in przewalski horses (*equus ferus przewalskii*) is driven by the ecological contexts of collective movements,” *Ethology*, vol. 115, no. 4, pp. 321–330, 2009.
- [135] L. Briard, C. Dorn, and O. Petit, “Personality and affinities play a key role in the organisation of collective movements in a group of domestic horses,” *Ethology*, vol. 121, no. 9, pp. 888–902, 2015.
- [136] K. Krueger, B. Flauger, K. Farmer, and C. Hemelrijk, “Movement initiation in groups of feral horses,” *Behavioural Processes*, vol. 103, pp. 91–101, 2014.

Realistic modelling of complex systems of biological agents: epidemiology of HIV on complex sexual networks and collective motion of hierarchical herds

– Summary –

Bence Ferdinandy

The study of complex systems – systems comprised of many units, the interactions of which give rise to unique global phenomena – has gained momentum with the rise of computational power and significantly increasing data availability on a variety of systems. In the dissertation I review the methods of modelling complex systems and discuss the relevant practical and epistemological issues. The focus is on agent-based modelling, since complex systems, in general, are well suited for the method, and biological systems are even more so.

I present two studies, carried out with my co-authors, concerning the modelling of two systems. Both systems are complex, biologically relevant, and involve different types of agents. However, both the particulars of the systems and the questions asked were different. The first system was a sexual contact network of humans, wherein a sexually transmitted virus, HIV spreads. We asked how different strains of HIV would spread and compete in this network. The second system was a hierarchical herd of wild horses moving on an open plain. In essence, asked whether a model of the collective movements of cells can be adapted to adequately explain the motion and group formation of the Przewalski wild horse.

In the first study we built the network model based on empirical data available from Sub-Saharan Africa and observed that our model of HIV spreading is commensurate with the history of HIV. We showed that the first strain to infect a population will have considerable advantage over strains arriving later. Even if the later strain is stronger, it needs at minimum decades to overcome the resident strain. This implies that without active prevention, strains of HIV stronger than the current strains causing the epidemic, might start showing up in the not-too-distant future.

In the second study, we demonstrated that the modified cell-movement model produces results commensurate with wild horses moving on an open plain, but fails to capture all aspects of the horses' group structure. The model raised further questions about how it would be possible to include a mechanism for the stopping and restarting of movement in such a model and what exactly the properties of agents and their interactions are that allow for such a spatially-based modelling approach to work or fail.

Both studies address relevant questions in their respective fields, while showcasing the diverse applicability of agent-based modelling of complex systems.

Biológiai ágensek komplex rendszerének realisztikus modellezése: a HIV epidemiológiája komplex szexuális hálózatokon és hierarchikus csordák kollektív mozgása

– Összefoglaló –

Ferdinandy Bence

A komplex rendszerek – olyan, sok egységből álló rendszerek, amelyekben az egységek kölcsönhatásai nyomán új, globális jelenségek keletkeznek – tanulmányozása a folyamatosan növekvő számítási kapacitásnak és a különböző rendszerekről jelentősen megnőtt adatmennyiségnek köszönhetően virágkorát éli. A disszertációban összefoglalom a komplex rendszerek modellezési módszereit, érintve a releváns gyakorlati és episztemológiai kérdéseket. A fókuszban az ágens-alapú modellezés van, tekintettel arra, hogy általában a komplex rendszerek, de különösen a biológiai rendszerek modellezésére rendkívül alkalmas.

Két rendszer modellezéséről szóló tanulmányt mutatok be, amelyeket szerzőtársaimmal készítettünk. Mindkét rendszer komplex, biológiai ihletésű és több típusú ágensből áll, azonban a rendszerek részleteikben, valamint a róluk feltett kérdésekben eltérnek egymástól. Az első rendszer emberek szexuális kapcsolatainak hálózata, amelyen a szexuális úton terjedő HIV fertőző. Arra kerestük a választ, hogy a HIV különböző törzsei miképpen terjednek és versengenek ezen a hálózaton. A második rendszer egy nyílt terepen mozgó hierarchikus vadló csorda, amely esetében a kérdésünk lényegében az volt, hogy egy, a sejtek kollektív mozgására kitalált modell módosítható-e úgy, hogy elfogadható módon magyarázza a Przewalski vadlovak mozgását és csoportjaiknak kialakulását.

Az első tanulmányban a hálózati modellt szubszaharai Afrikából származó empirikus adatok alapján építettük, és azt találtuk, hogy a HIV terjedési modellünk a HIV történelmével összevethető eredményeket produkál. Megmutattuk, hogy a populációt fertőző első HIV törzs jelentős előnyt szerez a később érkező törzsekkel szemben. A később érkező törzsnek még akkor is legalább évtizedekre van szüksége arra, hogy felülkerekedjen a korábbi törzsön, ha lényegesen fertőzőképesebb. Ez arra utal, hogy aktív prevenció nélkül a mostani járványt okozó törzsnél fertőzőképesebb törzsek jelenhetnek meg a nem túl távoli jövőben.

A második tanulmányban bemutattuk, hogy a módosított sejtmozgás-modell képes a nyílt terepen közlekedő vadlovakéval összevethető mozgást produkálni, de nem tudja megragadni alovak csoportstruktúrájának minden elemét. A modellünk további kérdéseket vet fel: hogyan lehetne egy olyan mechanizmust beépíteni, amittől a csorda időnként megáll, majd elindul, valamint, hogy melyek az ágensek és interakcióik azon tulajdonságai, amelyek alkalmassá vagy alkalmatlanná tesznek egy hasonló, távolság alapú modellt a rendszer leírására.

Mindkét tanulmány a saját területén releváns kérdésekkel foglalkozik, miközben szemlélteti, hogy a komplex rendszerek ágens-alapú modellezése széles körben alkalmazható módszer.

a doktori értekezés nyilvánosságra hozatalához

I. A doktori értekezés adatai

A szerző neve: Ferdinandy Bence

MTMT-azonosító: 10028021

A doktori értekezés címe és alcíme:

Realistic modeling of complex systems of biological agents: epidemiology of HIV on complex sexual networks and collective motion of hierarchical herds

DOI-azonosító³⁹: 10.15476/ELTE.

A doktori iskola neve: Fizika Doktori Iskola

A doktori iskolán belüli doktori program neve: Statisztikus Fizika, Biológiai Fizika és Kvantumrendszerek Fizikája

A témavezető neve és tudományos fokozata: Dr. Vicsek Tamás, az MTA rendes tagja

A témavezető munkahelye: Eötvös Loránd Tudományegyetem, Biológiai Fizika Tanszék

II. Nyilatkozatok

A doktori értekezés szerzőjeként⁴⁰

a) hozzájárok, hogy a doktori fokozat megszerzését követően a doktori értekezésem és a tézisek nyilvánosságra kerüljenek az ELTE Digitális Intézményi Tudástárban. Felhatalmazom a Természettudományi Kar Dékáni Hivatalának Doktori, Habilitációs és Nemzetközi Ügyek Csoportja ügyintézőjét, hogy az értekezést és a téziseket feltöltse az ELTE Digitális Intézményi Tudástárba, és ennek során kitöltse a feltöltéshez szükséges nyilatkozatokat.

b) kérem, hogy a mellékelt kérelemben részletezett szabadalmi, illetőleg oltalmi bejelentés közzétételéig a doktori értekezést ne bocsássák nyilvánosságra az Egyetemi Könyvtárban és az ELTE Digitális Intézményi Tudástárban;⁴¹

c) kérem, hogy a nemzetbiztonsági okból minősített adatot tartalmazó doktori értekezést a minősítés (*dátum*)-ig tartó időtartama alatt ne bocsássák nyilvánosságra az Egyetemi Könyvtárban és az ELTE Digitális Intézményi Tudástárban;⁴²

d) kérem, hogy a mű kiadására vonatkozó mellékelt kiadó szerződésre tekintettel a doktori értekezést a könyv megjelenéséig ne bocsássák nyilvánosságra az Egyetemi Könyvtárban, és az ELTE Digitális Intézményi Tudástárban csak a könyv bibliográfiai adatait tegyék közzé. Ha a könyv a fokozatszerzést követően egy évig nem jelenik meg, hozzájárulok, hogy a doktori értekezésem és a tézisek nyilvánosságra kerüljenek az Egyetemi Könyvtárban és az ELTE Digitális Intézményi Tudástárban.⁴³

2. A doktori értekezés szerzőjeként kijelentem, hogy

a) az ELTE Digitális Intézményi Tudástárba feltöltendő doktori értekezés és a tézisek saját eredeti, önálló szellemi munkám és legjobb tudomásom szerint nem sértem vele senki szerzői jogait;

b) a doktori értekezés és a tézisek nyomtatott változatai és az elektronikus adathordozón benyújtott tartalmak (szöveg és ábrák) mindenben megegyeznek.

3. A doktori értekezés szerzőjeként hozzájárulok a doktori értekezés és a tézisek szövegének plágiumkereső adatbázisba helyezéséhez és plágiumellenőrző vizsgálatok lefuttatásához.

Kelt: 2017. szeptember 6.

.....
a doktori értekezés szerzőjének aláírása